RADC-TR-79-166
Final Technical Report
June 1979

A MODEL FOR SPACE RADAR CLUTTER

Decision-Science Applications, Inc.

P. G. Tomlinson

ROME AIR DEVELOPMENT CENTER
Air Force Systems Command
Griffiss Air Force Base, New York 13441

This report has been reviewed by the RADC Information Office (OI) and is releasable to the National Technical Information Service (NTIS). At NTIS it will be releasable to the general public, including foreign nations.

RADC-TR-79-166 has been reviewed and is approved for publication.

APPROVED: Robert G. Polce

ROBERT G. POLCE
Project Engineer

APPROVED:

OWEN R. LAWTER
Colonel, USAF
Chief, Surveillance Division

FOR THE COMMANDER: John P. Huss

JOHN P. HUSS
Acting Chief, Plans Office

If your address has changed or if you wish to be removed from the RADC mailing list, or if the addressee is no longer employed by your organization, please notify RADC (RBRM), Griffiss AFB NY 13441. This will assist us in maintaining a current mailing list.

Do not return this copy. Retain or destroy.

UNCLASSIFIED

SECURITY CLASSIFICATION OF THIS PAGE *(When Data Entered)*

(19) REPORT DOCUMENTATION PAGE		READ INSTRUCTIONS BEFORE COMPLETING FORM
(18) 1. REPORT NUMBER RADC-TR-79-166	2. GOVT ACCESSION NO.	3. RECIPIENT'S CATALOG NUMBER
(6) 4. TITLE *(and Subtitle)* A MODEL FOR SPACE RADAR CLUTTER		(9) 5. TYPE OF REPORT & PERIOD COVERED Final Technical Report, 15 Feb 78 - 15 Feb 79
		6. PERFORMING ORG. REPORT NUMBER DSA Report 116
(10) 7. AUTHOR(s) P. G. Tomlinson		(15) 8. CONTRACT OR GRANT NUMBER(s) F30602-78-C-0129 new
9. PERFORMING ORGANIZATION NAME AND ADDRESS Decision-Science Applications, Inc. 1500 Wilson Blvd, Suite 810 Arlington VA 22209		10. PROGRAM ELEMENT, PROJECT, TASK AREA & WORK UNIT NUMBERS (16) 62702F 45061433 (17) 14
11. CONTROLLING OFFICE NAME AND ADDRESS Rome Air Development Center (RBRM) Griffiss AFB NY 13441		(11) 12. REPORT DATE June 1979 13. NUMBER OF PAGES 107
14. MONITORING AGENCY NAME & ADDRESS *(if different from Controlling Office)* Same (12) 107 pp		15. SECURITY CLASS. *(of this report)* UNCLASSIFIED
		15a. DECLASSIFICATION/DOWNGRADING SCHEDULE N/A

16. DISTRIBUTION STATEMENT *(of this Report)*

Approved for public release; distribution unlimited.

17. DISTRIBUTION STATEMENT *(of the abstract entered in Block 20, if different from Report)*

Same (14) DSA-116

18. SUPPLEMENTARY NOTES

RADC Project Engineer: Robert G. Polce (OCSA)

19. KEY WORDS *(Continue on reverse side if necessary and identify by block number)*

Ground clutter
Backscatter coefficient
Space radar

20. ABSTRACT *(Continue on reverse side if necessary and identify by block number)*

A model for radar clutter as encountered from a space-based platform is developed. Included in the model are land, sea and airborne clutter with emphasis on land clutter. Parametric fits to existing reflectivity data are performed for seven generic terrain types: desert, forest, mountain, rural, urban, snow and ice and sea. The fits are parametric in frequency and grazing angle and, in the case of sea clutter, polarization. In addition to the mean values of clutter reflectivity, the variation about the mean is emphasized.

(Cont'd)

DD FORM 1 JAN 73 1473

UNCLASSIFIED

SECURITY CLASSIFICATION OF THIS PAGE *(When Data Entered)*

393 157

The underlying causes of clutter variability nonhomogeneous terrain type, terrain undulation, etc., are discussed. Quantitative estimates of their effects are presented. A theory of probability density function of clutter based on the resolution cell size, correlation lengths, and underlying statistics of individual scatterers, is presented. Examples are worked out for five terrain types and a large resolution cell. The results are threshold settings required for given false alarm probabilities. Clutter spectra are discussed briefly. Finally, requirements and computer simulations are examined with particular attention to the advantages and disadvantages of three candidate measurement programs.

EVALUATION

This report summarizes the development of an analytical model of the clutter environment encountered by space-based microwave radars. The model provides a unique tool for describing clutter as it affects the performance and design of space-based radar systems. It is intended that this model be utilized for the analysis and design of space-based radar systems. The information generated in this report is in direct support of technical program objective (TPO) R1C, Indications and Warning, Surveillance Sensor Technology.

Robert G. Polce

ROBERT G. POLCE
Project Engineer

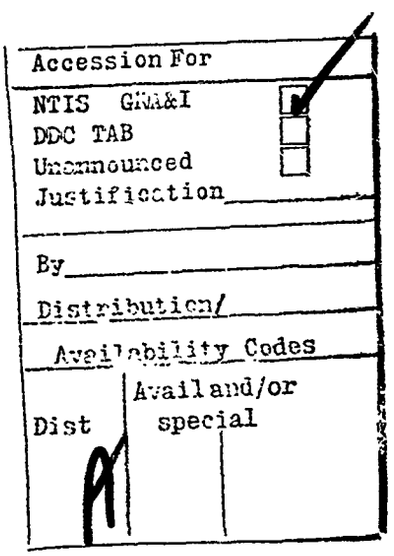

CONTENTS

FIGURES

FIGURES (Cont.)

FIGURES (Cont.)

TABLES

1.0 INTRODUCTION

This is the final report prepared by Decision-Science Applications, Inc., (DSA) under contract number F30602-78-C-0129, Space Radar Clutter Characterization, sponsored by Rome Air Development Center. The contents of this report comprise a model for the description of radar clutter as it is involved in space-based radars (SBR). It is expected to be of value in modeling, analysis, and design of future SBR systems.

With this purpose in mind, the clutter model was designed to be as simple and easy to use as possible while providing an adequate description of clutter as it is expected to be encountered in SBR. The present data base, based on measured ground clutter, was organized into seven generic terrain types. Variation of the mean backscatter coefficient was obtained by regression analysis as a function frequency and grazing angle for each terrain type. In addition, the statistics of variation about the mean were explored. Experimental data was used to infer a probability density function (pdf) (sometimes referred to as a distribution) and a correlation length for several of the terrain types. Using a theory of scattering for a number of independent scatterers, we have developed a method for deriving the pdf as a function of resolution cell size. The method was used on five terrain types to determine threshold settings to give a specified false alarm rate.

This report is organized into six sections. Following this introduction is a section which discusses the general problem of clutter for look-down radar, pointing out the special considerations for the SBR case. Immediately following are sections which present in order: parametric regression analysis of σ°, statistics of variation from the mean, clutter spectra, and finally recommendations for further measurement and analysis. Also included is an appendix describing the DSA computer program which simulates clutter signals based on a microscopic description of clutter. This was developed for the purpose of evaluating signal processing algorithms for realistic clutter scenarios and was partially supported under this contract.

2.0 GENERAL DISCUSSION OF CLUTTER

Before examining the quantitative details of the model, a qualitative overview is in order. This section describes the attributes of clutter with emphasis on its likely impact on SBR systems. Figure 1 shows a typical look-down scenario, graphically illustrating how reflections from background clutter interfere with targets. Within the radar footprint, there is distributed clutter such as vegetation, discretes such as buildings and vehicles, and airborne clutter like birds, weather, and chaff. Some are stationary, while others may be moving.

In the missions which must detect air vehicles against the earth's background, the space radar is confronted with the traditional look-down radar problem of suppressing ground clutter. The space radar problem is quite different from the airborne radar because of the broad extent of clutter in the range/range-rate domain, larger resolution cells, and range/Doppler ambiguous returns.

2.1 MAJOR CLUTTER SOURCES AND THEIR IMPACT ON SYSTEM PERFORMANCE

Before one can accurately assess the adequacy of the clutter suppression approach, one must be able to quantify the various attributes of the clutter background. This section presents a short review of radar clutter sources. Those aspects of clutter which most impact system design are presented in order of importance.

The basic clutter cross section determines the amount of clutter suppression necessary through the following equation.

$$I = \frac{(S/C)\sigma_c}{\sigma_t} \tag{2-1}$$

where I is the required AMTI improvement factor required, S/C is the necessary signal-to-clutter ratio, σ_c is the clutter radar cross section (RCS), and σ_t is the target RCS.

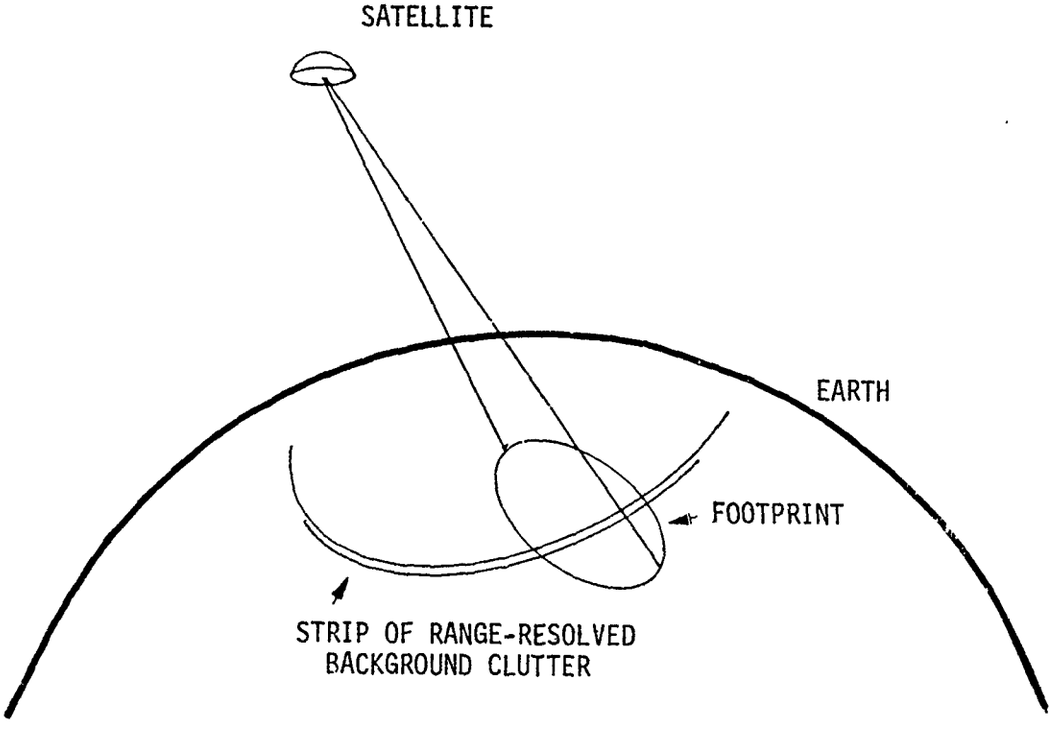

Figure 1. Schematic of Spaceborne Look-Down Radar

For land and sea clutter σ_c is determined by the product of the backscatter coefficient, σ°, and the area of the illuminated resolution cell, taking into account the additional clutter from range and Doppler ambiguities. In general, σ° is dependent upon terrain type, grazing angle, frequency, and polarization. In addition, it is sensitive to such factors as moisture content, season, time of day, etc. Sea clutter is very sensitive to wind speed and direction and wave height as well. Figure 2 shows some typical values of σ° as a function of terrain type. Most SBR clutter is of the extended type, however, some discrete scatterers will be present. They lie entirely within a resolution cell; hence their radar cross section is sufficient to describe their impact.

For volume distributed clutter sources such as aurora, weather, birds and chaff, the parameter of interest is the RCS density per unit volume η. The clutter RCS is given by the product of η and the resolved clutter cell volume. As a general rule, these sources are much weaker than land clutter but can appear at finite velocities with respect to the ground. Figure 3 summarizes the magnitudes and velocities of common clutter sources.

2.2 GROUND CLUTTER DESCRIPTION

In addition to the expected value of clutter RCS, the probability distribution about the mean value is important. The probability distribution impacts the required S/C. For most clutter sources, the distribution is similar to a Rayleigh function. However, land clutter at low grazing angles and high-resolution sea clutter has been shown experimentally to exhibit a lognormal distribution of large variance. The impact of lognormal clutter on threshold setting for detection is shown in Figure 4. It is speculated that the distribution approaches Rayleigh as the resolution cell size increases for all types of clutter. This has been demonstrated to a certain extent by SKYLAB X-band data.[1]

[1] K. Soofi, Clutter Model for Land, Forest, Snow, Seaice, and Ocean, Remote Sensing Laboratory, University of Kansas Technical Dept. No. TR-2923-2, July 1978.

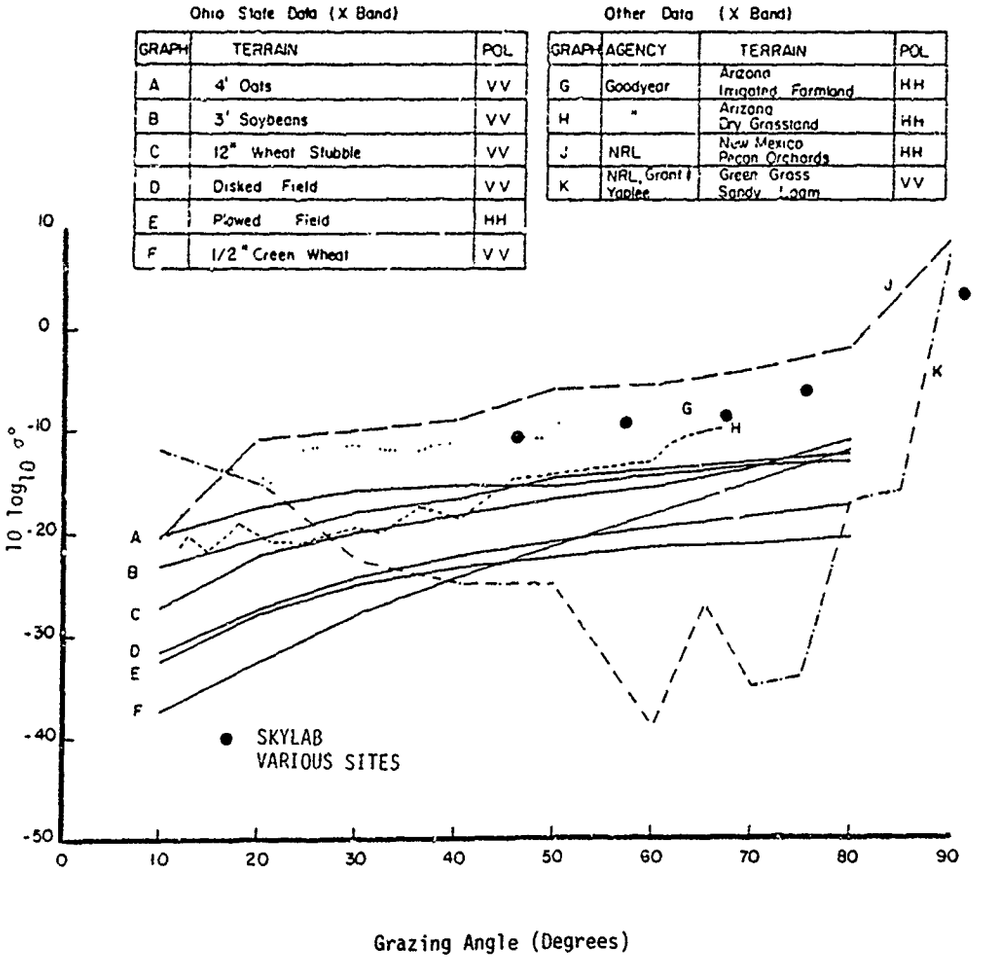

From L.J. Greenstein, et al., IIT (1969).

Figure 2. Farmland Clutter Cross Section Measurements of Various Investigators

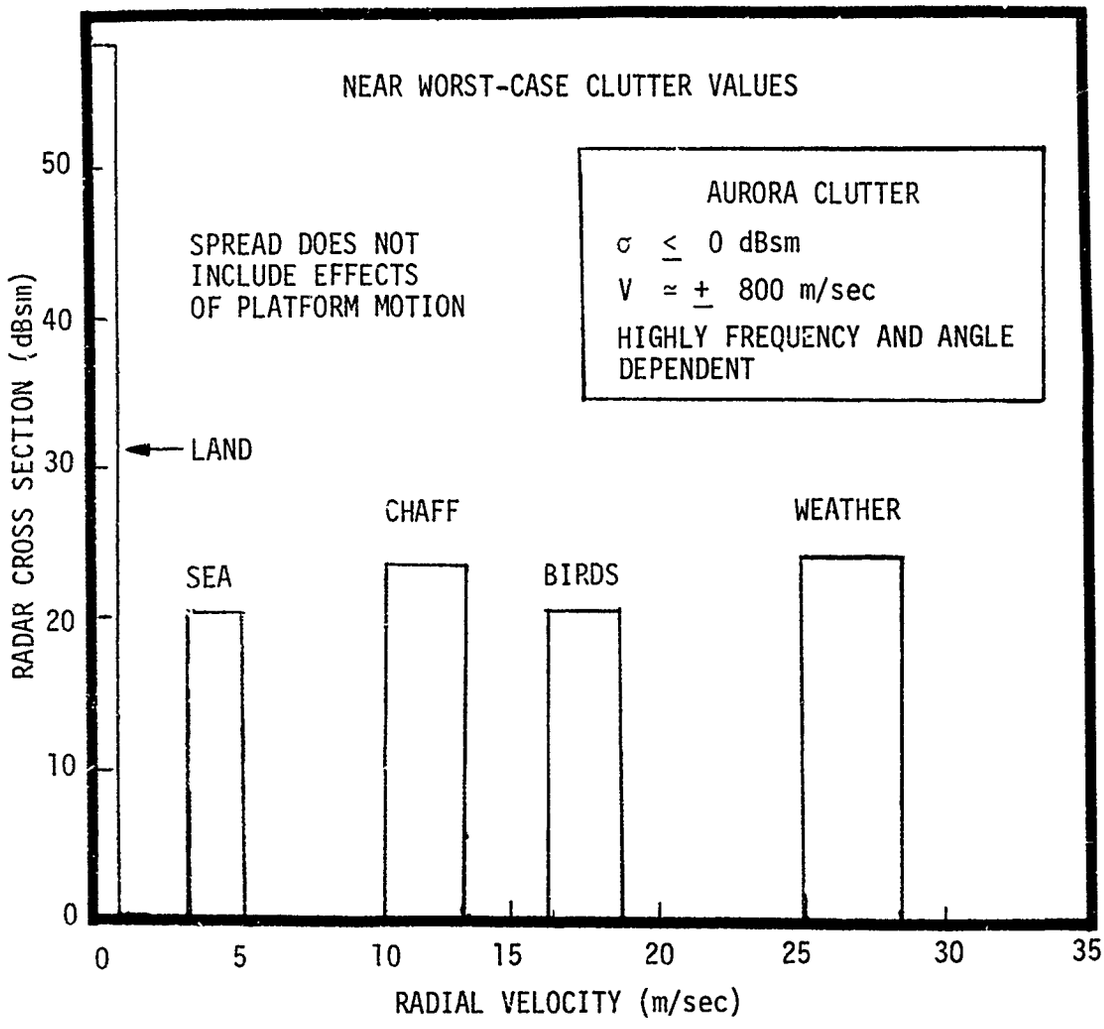

Figure 3. Comparisons of Cross Sections and Velocity Spreads

- CONSTANT TARGET RCS
- PROBABILITY OF FALSE ALARM = 10^{-6}
- N = NUMBER OF INDEPENDENT OBSERVATIONS

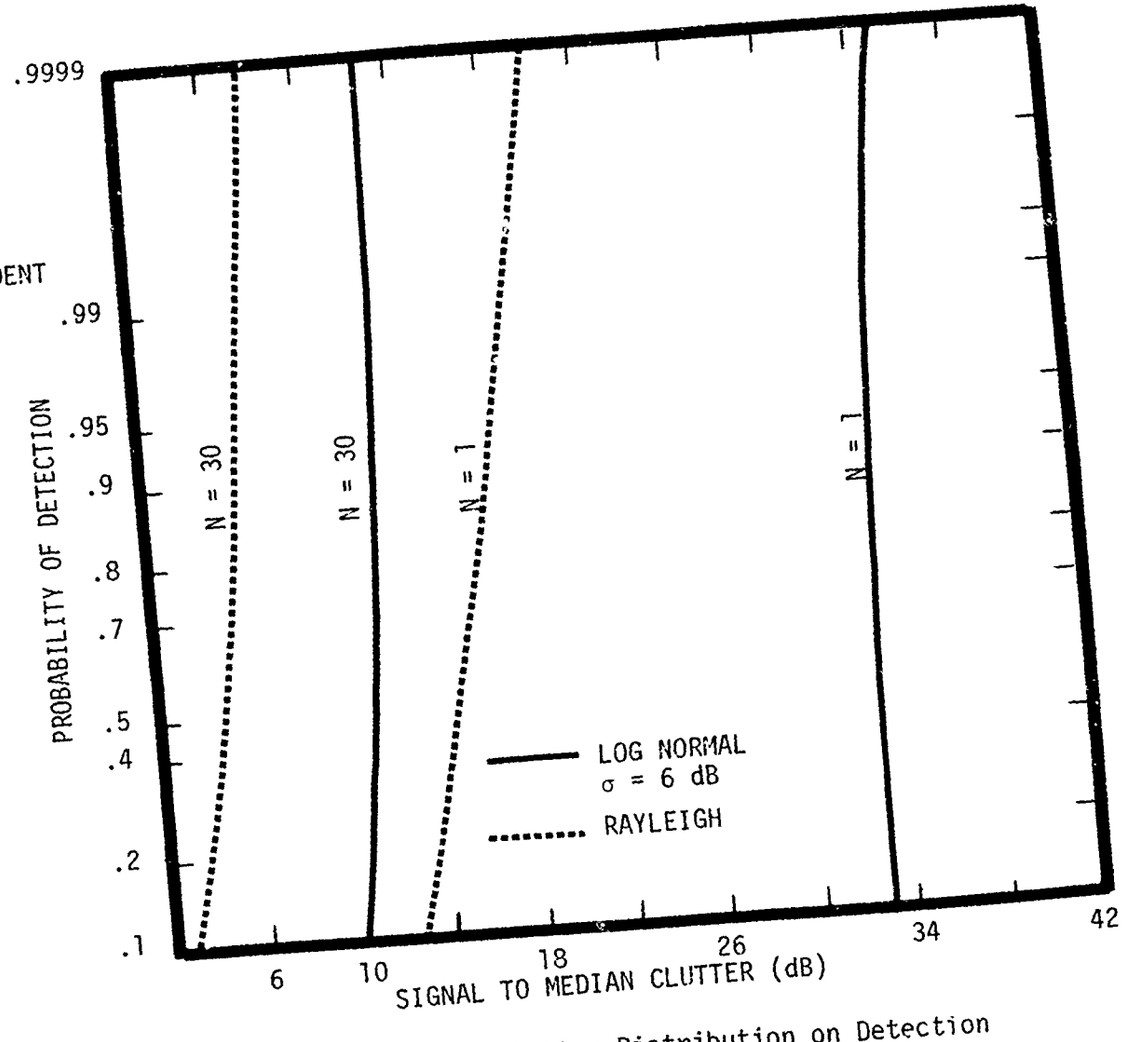

Figure 4. Impact of Statistical Clutter Distribution on Detection

Of interest also is the correlation of clutter. This spatial correlation is a measure of the distance between independent areas of clutter. Spatial correlation is important in evaluating the tracking performance and in design of constant-false-alarm rate detectors. Temporal correlations or spectra are another way of expressing the velocity spread of clutter important for moving target indication (MTI). For SBR applications, this is usually dominated by the spread induced by platform motion. However, the inherent internal motion can be important in some cases.

2.3 CLUTTER AS VIEWED BY SPACE-BASED RADAR

Those aspects of clutter which are peculiar to space-based radar are summarized below. They require special care in modeling since the data base for SBR clutter is limited.

2.3.1 Large Resolution Cells

Due to the long ranges involved, typical footprints measure ten to twenty miles by as much as one hundred miles. The geometry is such that this results in strips which extend the width of the footprint in cross range and approximately C/2BW in range, where C is the speed of light and BW is the modulation bandwidth. When a pulse-burst waveform is used, there are ambiguities in range-Doppler space. When Doppler ambiguities are spaced wide enough apart to prevent blind speeds, range ambiguities occur in the mainbeam footprint. These range ambiguities cause clutter foldover in range, adding to the effective clutter per resolution cell. These ambiguities are independent in amplitude and phase, a fact which reflects itself in the resulting pdf.

2.3.2 Discretes

Because of the large resolution cells encountered in SBR, it is almost inconceivable (although theoretically possible), for a single discrete scatterer to add a significant contribution to the whole. We believe, since our model is based on data from actual terrains (not set up in a laboratory), that the proper contribution of discrete scatterers is taken into consideration. This is true for parametric regression analysis,

variability statistics, and spatial correlations. For these reasons we saw no need to focus explicitly on discretes.

This is not to say that discretes will never be a problem for SBR. If they are moving at velocities which overlap the range of possible target velocities and have an RCS comparable to targets of interest, they will look like targets. These may have to be acquisitioned and tracked and eventually rejected based on a higher order detection logic. Evaluation of the impact of objects of this sort is straightforward but not well defined enough to be within the scope of this project.

2.3.3 Sidelobe Clutter

Sidelobe clutter is a major problem for SBR as it is for airborne radars. In both cases, the earth is illuminated by sidelobes of the antenna pattern as well as the mainlobe. For airborne radars, parts of the earth illuminated by sidelobes can be at ranges much shorter than that of the target and mainlobe clutter. The R^4 term in the radar equation can significantly increase sidelobe clutter. The broad velocity spectrum of the sidelobe clutter compounds the difficulty.

However, for SBR, the range differences are not so great. DSA has the capability to evaluate sidelobe clutter parametrically or for a specific antenna pattern. An example of parametric results is shown in Figure 5. A good rule of thumb is that sidelobe levels 80 dB (two-way power) below the peak are sufficient for sidelobe clutter suppression for bomber-type targets. Also, sidelobe levels required for desirable antijamming properties are usually much lower than this. For smaller targets, the sidelobe clutter can become a more severe problem than mainlobe clutter. Accurate estimates of sidelobe clutter can be derived from the model if they become the dominant clutter source.

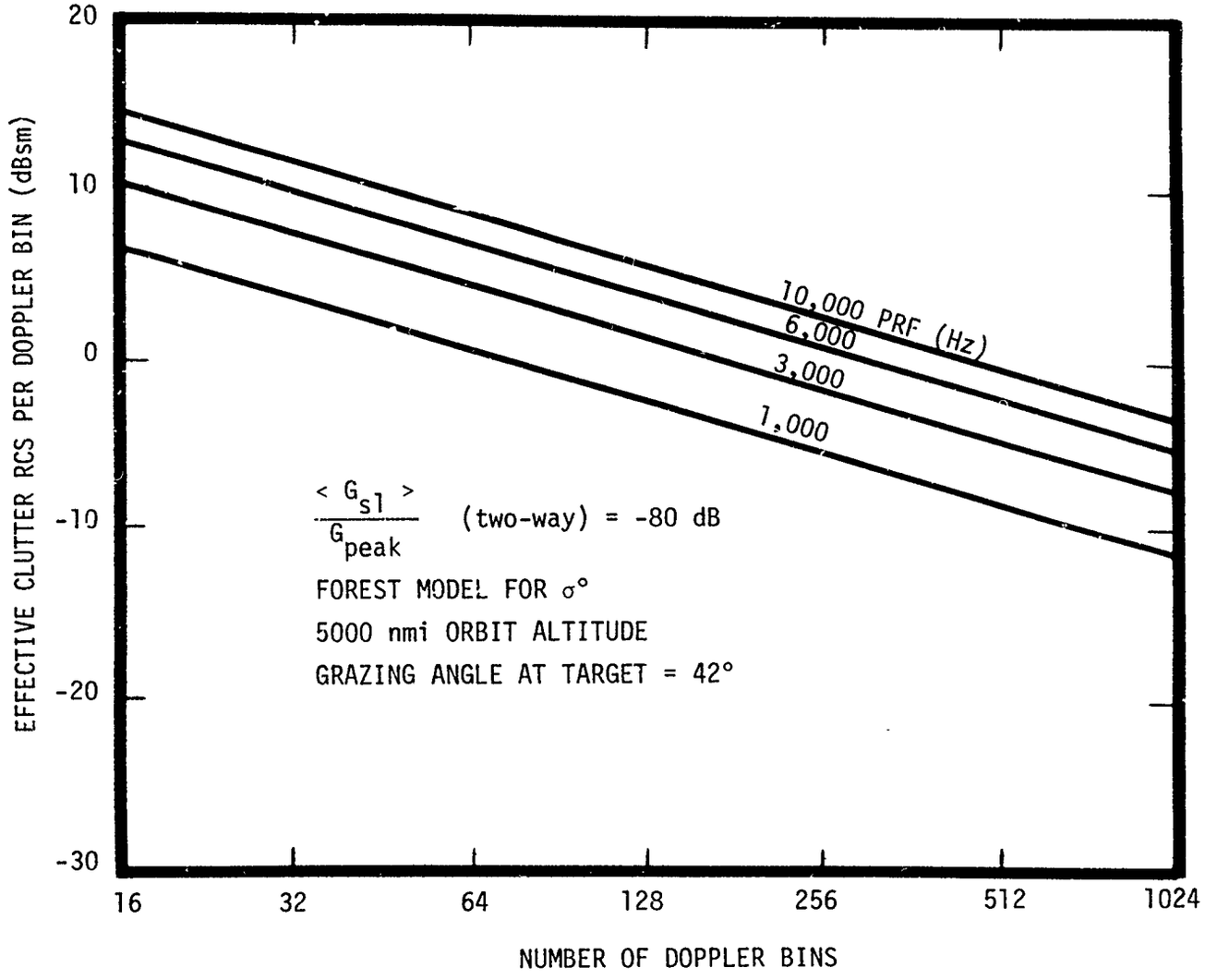

Figure 5. Effective Clutter for -80 dB Sidelobe Level as a Function of Number of Doppler Bins.

3.0 MODEL FOR EXTENDED CLUTTER

3.1 GENERAL

This section deals with a parametric description of the backscattering properties of extended clutter. In particular, the backscatter coefficient σ° is modeled as analytic expressions whose coefficients are determined by best fits to measured physical data.

The goal is to derive a model which will be useful for describing clutter as it affects the performance and design of spaceborne radar systems. Although a secondary result of this effort is certain to be a better basic understanding of the scattering properties of land and sea, that was not the purpose of this study. Therefore, wherever possible, a wide variety of terrains were included within each generic terrain type, and data were included from a variety of sources. The alternative was to choose a single experiment or source upon which to base the model. We feel that the former approach, although it may not provide a tightly controlled data base, provides a better representation of the radar community's collective understanding of clutter. This also was the approach selected by IIT in the Overland Radar Technology program.[1]

An essential requirement is that the resulting model be simple. That is, in order to be useful, it is necessary that as little as possible need be specified a priori. The essence of the physical data must be distilled into a few equations. With this in mind, the world was broken down into seven terrain types:

1. Desert
2. Rural (fields, orchards, etc.)
3. Forest (forest, woods, heavy vegetation)
4. Mountains
5. Snow and ice
6. Urban (cities and urban areas)
7. Sea

---

[1] L. J. Greenstein, et al., A Comprehensive Ground Clutter Model for Airborne Radars, IIT Research Institute, Final Report Under Contract No. F33615-69-C-1387.

There appeared to be little if any consistent variation in σ° between horizontal and vertical polarization for land clutter, and for this reason polarization was not included as a model parameter. Thus, grazing angle and frequency were the only parameters other than terrain type. For the case of sea clutter, fits were also made to cross polarized data (HV and VH). Also, sea data were separated into categories on the basis of wind speed. Specifically they were separated into two groups, less than or equal to 15 kt and greater than 15 kt, and fit separately.

The fitting was made easier by developing a simple computerized data entry and data base retrieval system. The data and the system will be retained after the completion of this project.

3.2 RESULTS

The process of arriving at an analytical model for distributed clutter involved the following steps:

1. Select and organize a data base.
2. Preview the data to isolate the most important parameters.
3. Select analytic forms which appear to be likely candidates for providing good fits.
4. Select the best fits by experimentation.
5. Eliminate data which deviates too much from the norm.
6. Perform the final fits to determine the adjustable coefficients.
7. Repeat steps 1 through 6 if necessary.

The analytic form which was most successful in fitting the land data was as follows:

$$\bar{\sigma}^\circ = A + B\theta + (C + D\theta) \log F \qquad (3\text{-}1)$$

where we have adopted the notation $\bar{\sigma}^\circ$ which is σ° expressed in decibels (dB) ($\bar{\sigma}^\circ = 10 \log_{10} \sigma^\circ$), and where θ is the grazing angle in degrees and F is the

frequency in GHz. Forms involving terms proportional to F, log θ, and sin θ, were tried and found to be less suitable. For sea clutter, on the other hand, $\bar{\sigma}^\circ$ falls off sharply at low grazing angles and it was discovered that the grazing angle dependence was better expressed by a term proportional to log θ. Hence

$$\bar{\sigma}^\circ = A + B(\log \theta) + C(\log F) + D(\log \theta \log F) \tag{3-2}$$

The method of least squares or regression analysis is well suited to these expressions. The result is an analytic expression $\bar{\sigma}^\circ(\theta, F)$ such that the sum of the squares of the error terms for N data points

$$S = \sum_{i=1}^{N} [\bar{\sigma}^\circ(\theta_i, F_i) - \bar{\sigma}_i^\circ]^2 \tag{3-3}$$

is minimized. This of course does not imply that the sum of the squares of the error terms is minimized if σ° is not expressed in decibels. In fact, one might argue that a least squares fit to $\bar{\sigma}^\circ$ is always biased slightly low for this reason. Therefore, we compute for each fit an adjustment factor, which we recommend be added.

$$\bar{\sigma}_+^\circ = \bar{\sigma}^\circ + \delta$$

where $\delta = 0.115(S/N)^2$ where δ is given by Equa. 3-3. In short, this correction is arrived at by assuming that the variation of the data about the fit is Gaussian (in dB). The correction term, δ, is the difference in dB between the mean σ° and the mean $\bar{\sigma}^\circ$.

The remaining details of the results and the procedures through which they are arrived are discussed below, separately by terrain type.

3.2.1 Desert

The types of terrain included under the broad category of "desert" ranged from "sandy desert" to "dry lake bed." The data as a whole were very well described by the fit below, the square root of the mean squared error being 3.2 dB.

$$\bar{\sigma}^\circ = -34.15 + 0.163\theta + (8.69 + 0.0093\theta) \log F \qquad (3\text{-}4)$$

with

$$\delta = 1.16 \text{ dB}$$

Figures 6a and 6b show plots of this formula versus θ and versus F, with and without data superimposed.

3.2.2 Rural

Of all the data gathered on the radar reflection from land clutter the vast majority is based on crops and farmland. Some data included initially had to be excluded because it deviated too much from the norm and adversely affected the fits. Examples of excluded data were bare plowed fields and Arizona farms. In the end, a fit based on data from five experiments yielded a fit which was a fair description of rural clutter data. This was

$$\bar{\sigma}^\circ = -23.61 + 0.994\theta + (3.53 + 0.091\theta) \log F$$

$$\delta = 0.79 \qquad (3\text{-}5)$$

Plots are shown in Fig. 7a,b. The root mean square (rms) deviation from the fit was 2.62 dB.

3.2.3 Forest (Heavy Vegetation)

Unlike the previous case, there is relatively little data available on forest clutter. Nevertheless, data was found sufficient to cover the frequencies and grazing angles of interest.

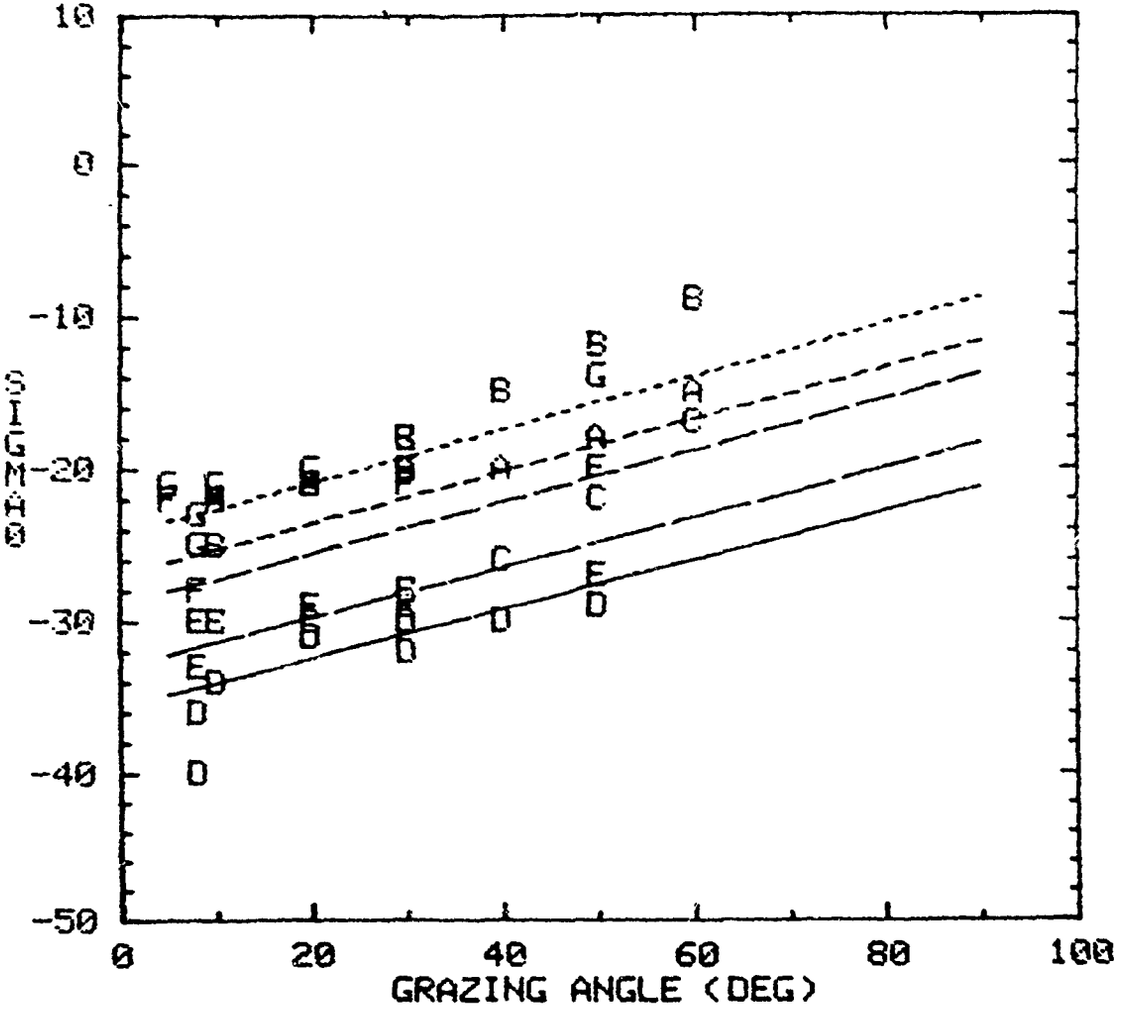

	DESCRIPTION	FREQ.	ANGLE
A	BROKEN DESERT	10.0	10.0
B	DRY LAKE BED	10.0	10.0
C	SANDY DESERT	10.0	10.0
D	ARIZONA DESERT	10.0	0.5
E	ARIZONA DESERT	10.0	1.5
F	ARIZONA DESERT	5.0	6.0
G	ARIZONA DESERT	5.0	10.0

LINE CODE	FREQUENCY (GHz)
————	0.5
—— —— —	1.0
— — — — —	3.0
- - - - - - -	5.0
----------	10.0

Figure 6a. Desert Terrain, $\bar{\sigma}°$ versus Grazing Angle

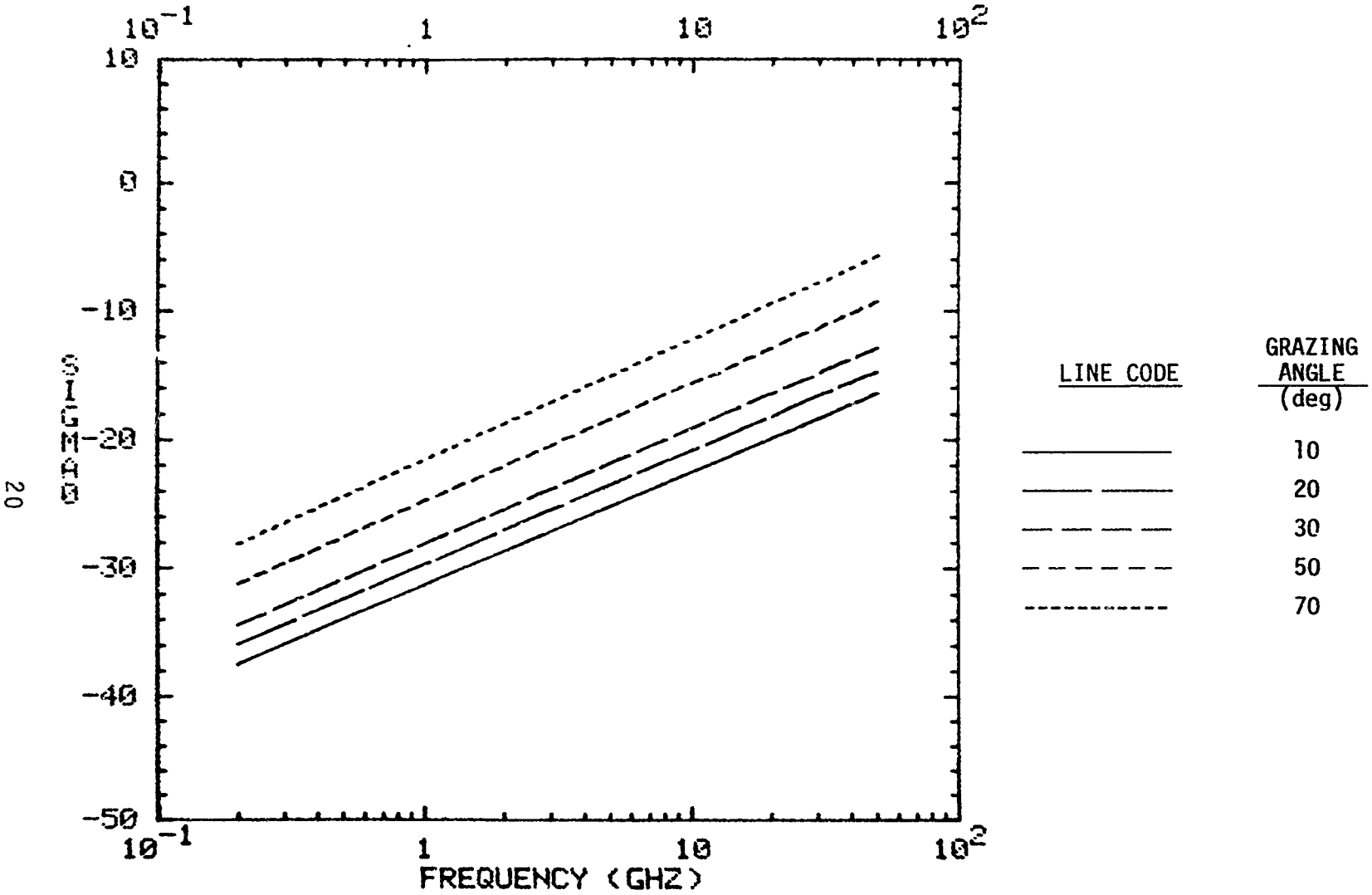

Figure 6b. Desert Terrain, $\bar{\sigma}^{\circ}$ versus Frequency

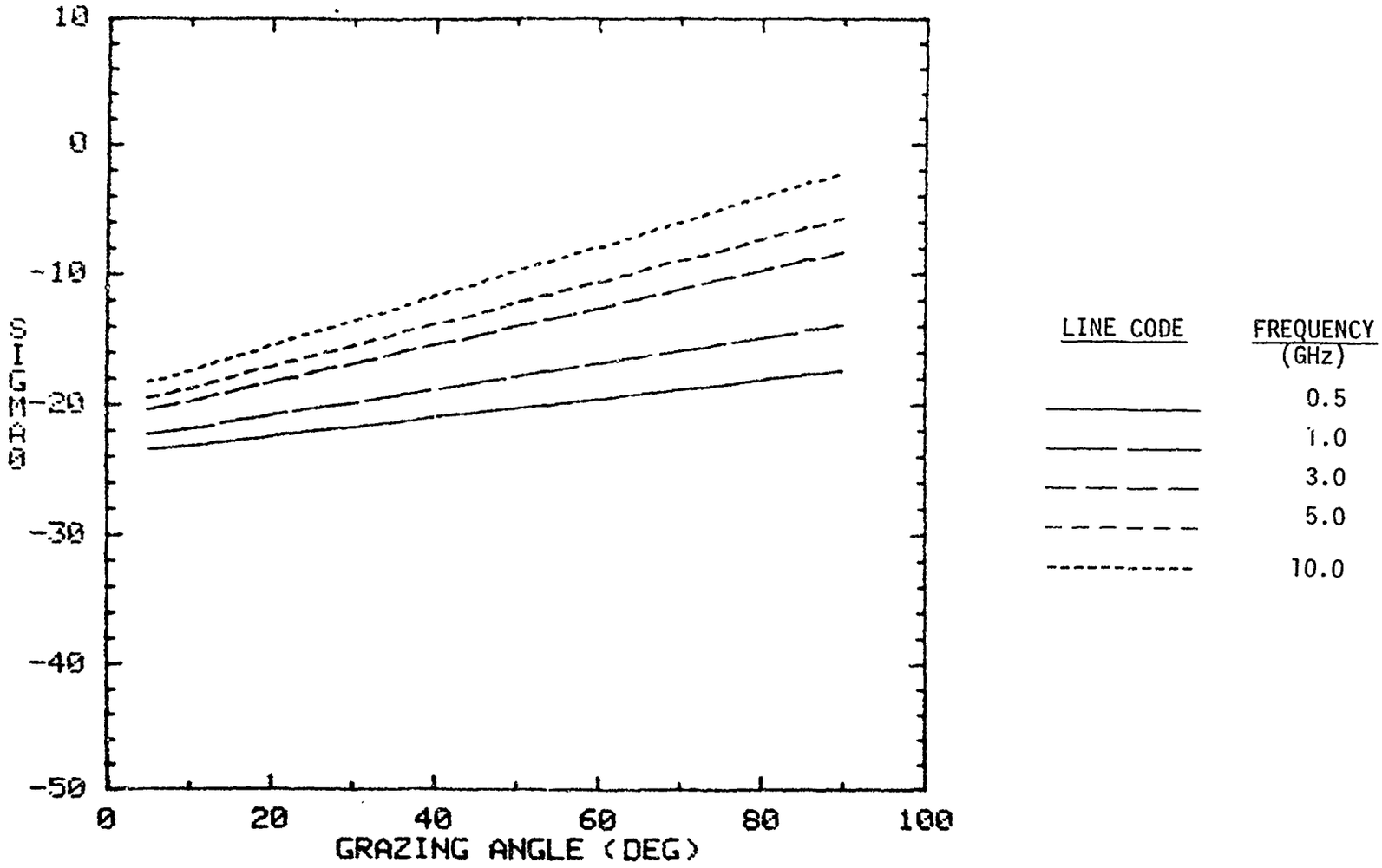

Figure 7a. Rural, $\bar{\sigma}^{\circ}$ versus Grazing Angle

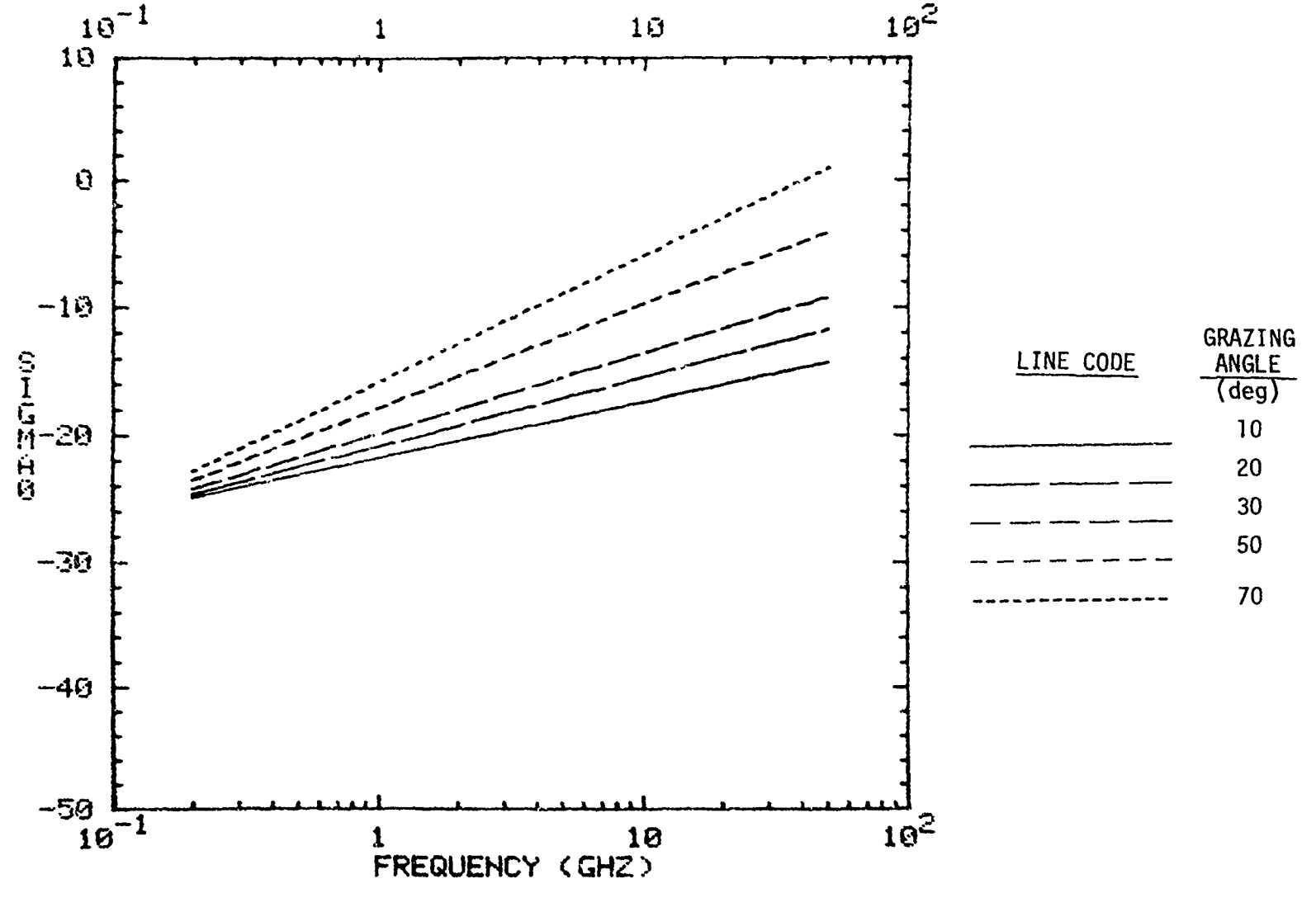

Figure 7b. Rural, $\bar{\sigma}^c$ versus Frequency

Much of the data used in the fit comes from the University of Kansas Remote Sensor Laboratory (RSL),[1] who performed a separate curve to fit their data. Their fit does not predict so low a $\bar{\sigma}°$ at low frequencies and low grazing angles (-22.9 dB at θ = 10°, F = 0.5 GHz). However, their fit was linear in F, not log F and it noticeably deviates from the observed data at low frequency and low grazing angles.

The chosen analytical form fits the data quite well with an rms difference = 2.81 dB. The result was

$$\bar{\sigma}° = -42.36 + 0.52\theta + (24.93 - 0.358\theta) \log F$$

$$\delta = 0.91 \text{ dB} \qquad (3\text{-}6)$$

This is plotted in Fig. 8a,b. Note that in the region of low grazing angles and low frequencies a very low $\bar{\sigma}°$ is predicted. At frequencies below 1 GHz there was no data for grazing angles below 60°. Therefore, this result should be treated with caution.

3.2.4 Mountains

Understandably, there is not a great deal of mountain data available. Also there is a great variability in the radar reflection from mountains due to the variability in the slope and composition of the terrain, making parametric analysis difficult. Mountains, nevertheless, are of great interest to SBR analysis due to the possibility of large specular returns from facets normal to the incident radiation.

Most of the data were of Arizona mountains taken by Naval Research Laboratory (NRL).[2] There were a few measurements taken by the Environmental Institute of Michigan (ERIM),[3] from L-band calibrated SAR data. Again the data were fairly true to form and the rms deviation from the fit was 2.98 dB. The fitted parameters are

---

[1] R. K. Soofi, ibid.

[2] J. C. Daley, NRL Terrain Clutter Study, Phase II, NRL Report No. 6749, Oct 1968.

[3] A. Maffatt et al., L-Band Radar Clutter Statistics for Terrain and Ice, ERIM Report No. 128900-9-F, (I), January 1978.

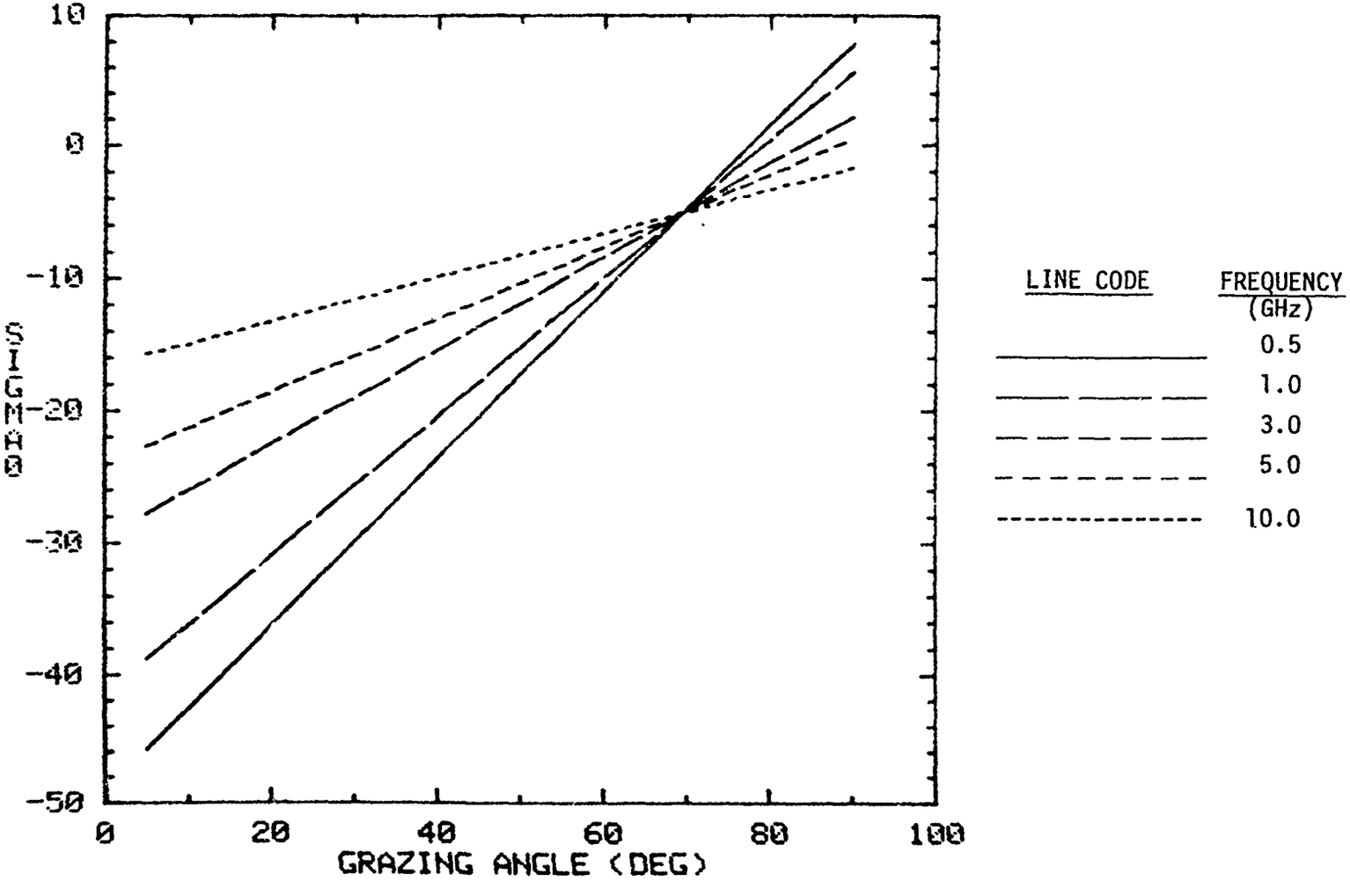

Figure 8a. Forest, $\bar{\sigma}^{\circ}$ versus Grazing Angle

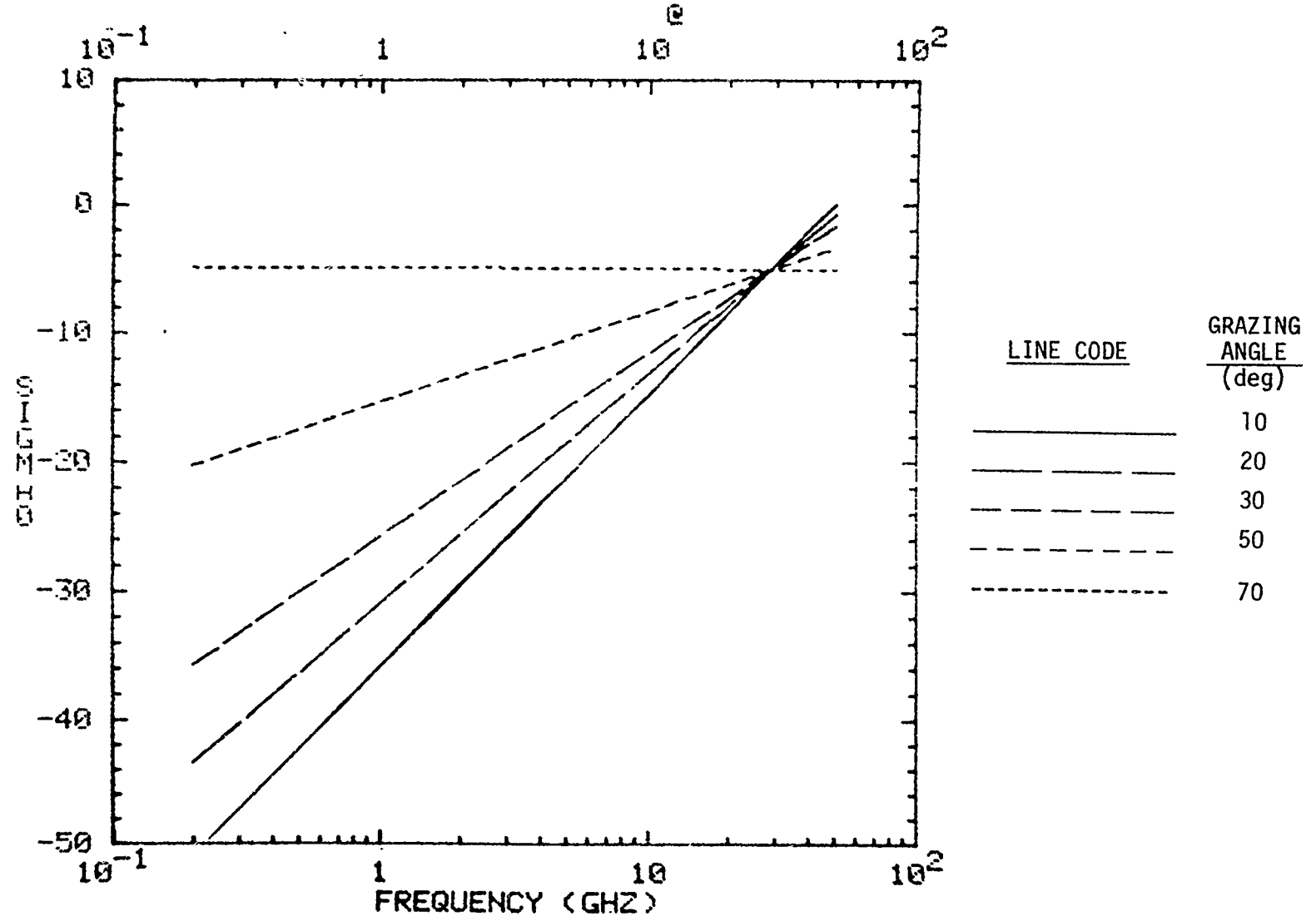

Figure 8b. Forest, $\bar{\sigma}°$ versus Frequency

$$\bar{\sigma}^\circ = -30.24 + 0.173\theta + (8.82 - 0.015\theta) \log F \qquad (3\text{-}7)$$

$$\delta = 1.02 \text{ dB}$$

This is plotted in Fig. 9a,b. The data show that $\bar{\sigma}^\circ$ continues to decrease as θ decreases. However, due to the specular scattering phenomenon and shadowing, data from mountains and hills tend to have a very large variance. This could mean that the clutter could actually be more severe a problem as the grazing angle decreases.

3.2.5 Snow and Ice

Snow and ice covered terrain is of great interest in the planning and analysis of SBR early warning systems since the northern perimeter surveillance fence covers arctic regions. There exists a fairly large amount of data on ice and snow.

There was a high degree of variance in the data from the different sources so the rms deviation from the fit is larger than in the previous examples, being 5.01 dB. The fitted parameters were

$$\bar{\sigma}^\circ = -32.97 + 0.340\theta - (1.797 + 0.035\theta) \log F \qquad (3\text{-}8)$$

$$\delta = 2.9 \text{ dB}$$

with $\bar{\sigma}^\circ$ plotted in Fig. 10a,b.

One curious feature of this data is that $\bar{\sigma}^\circ$ decreases with frequency. Again, Kansas, Remote Sensoring Laboratory[1] performed independent fits to their snow data covering grazing angles from 20° to 90° and 1 to 18 GHz. In general, the frequency dependence was weak in their fits; for some categories, $\bar{\sigma}^\circ$ decreased with frequency and for others $\bar{\sigma}^\circ$ increased.

---

[1] R. K. Soofi, et al., ibid.

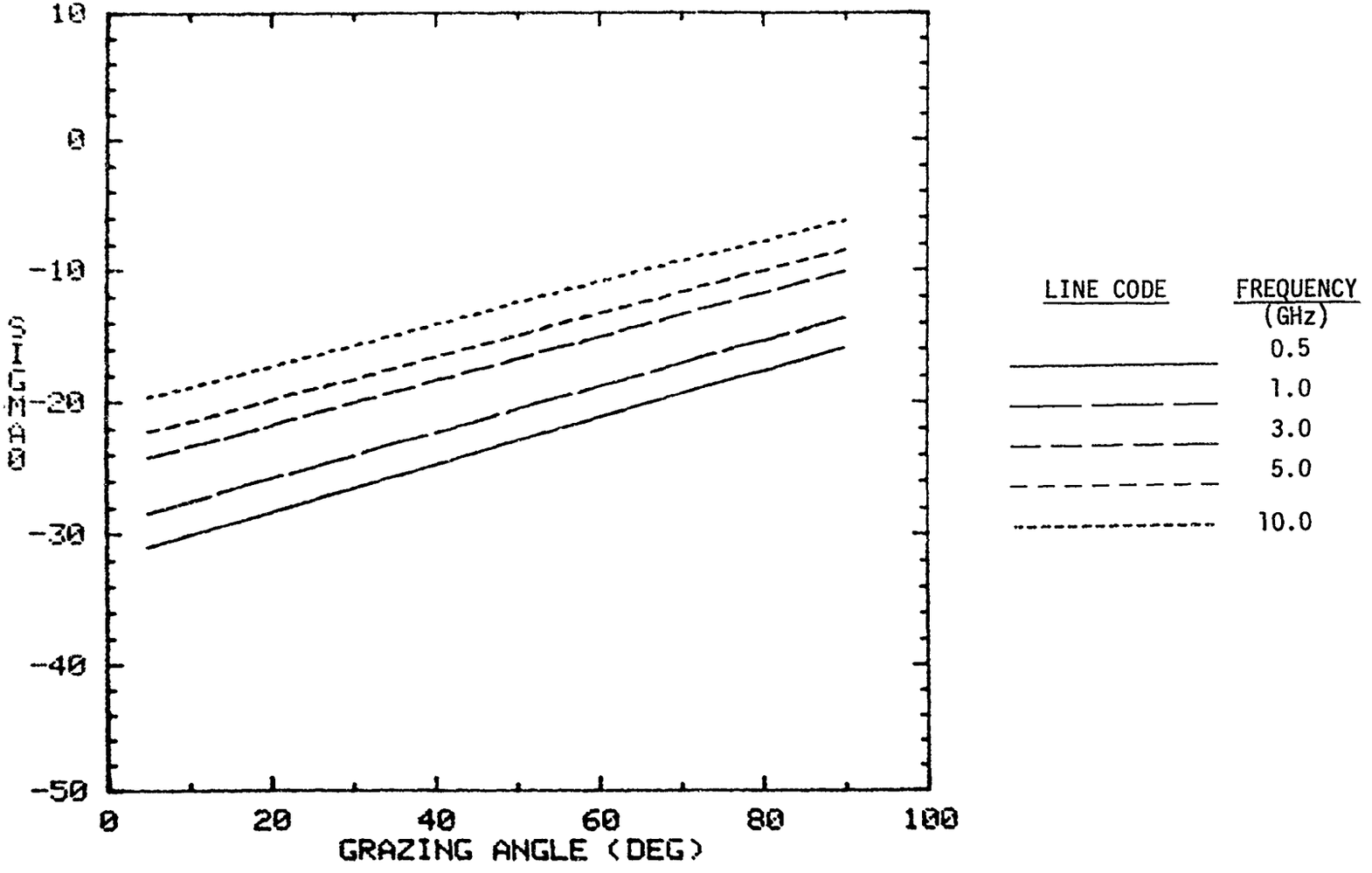

Figure 9a. Mountain, $\bar{\sigma}^{\circ}$ versus Grazing Angle

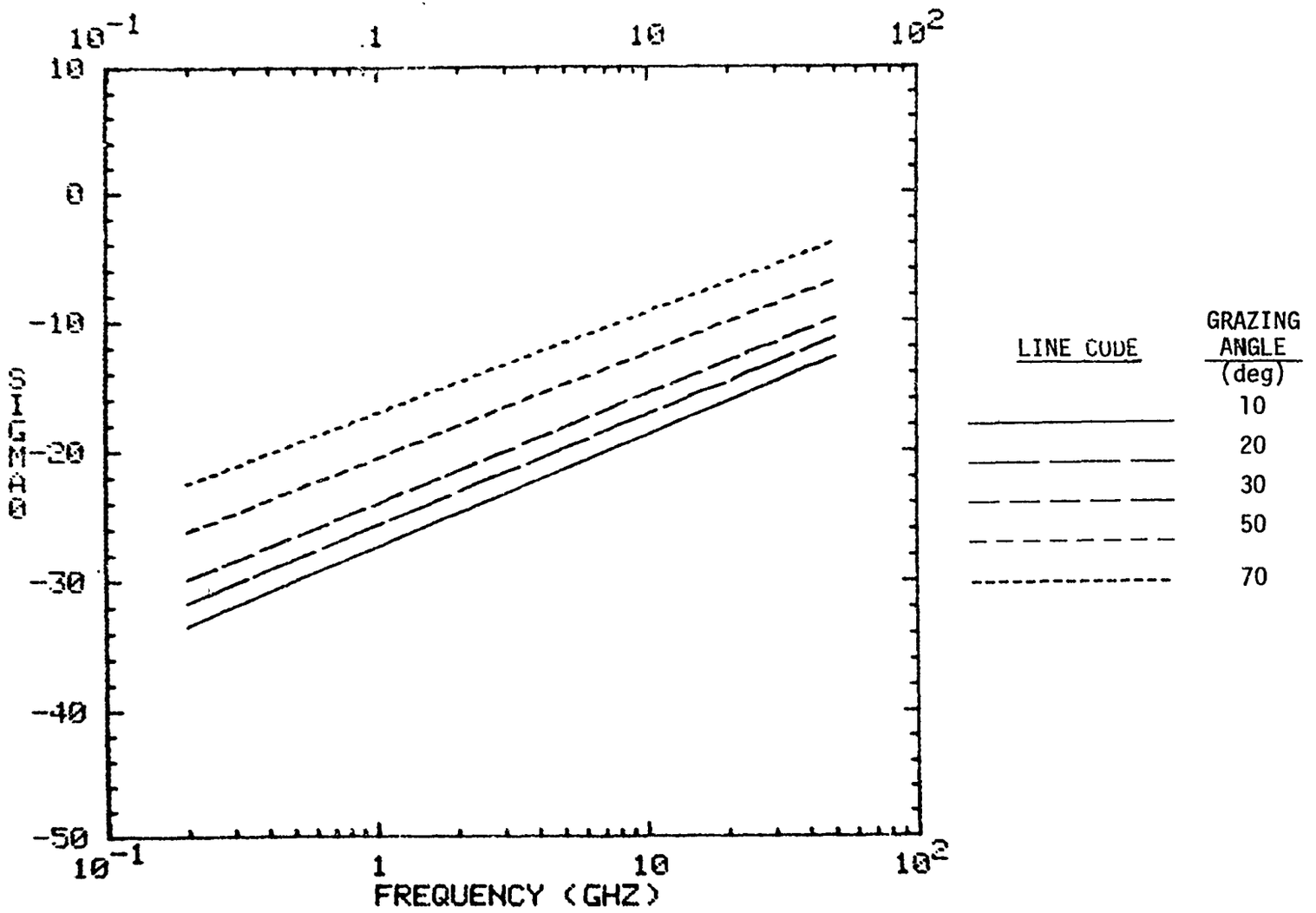

Figure 9b. Mountain, $\bar{\sigma}^{\circ}$ versus Frequency

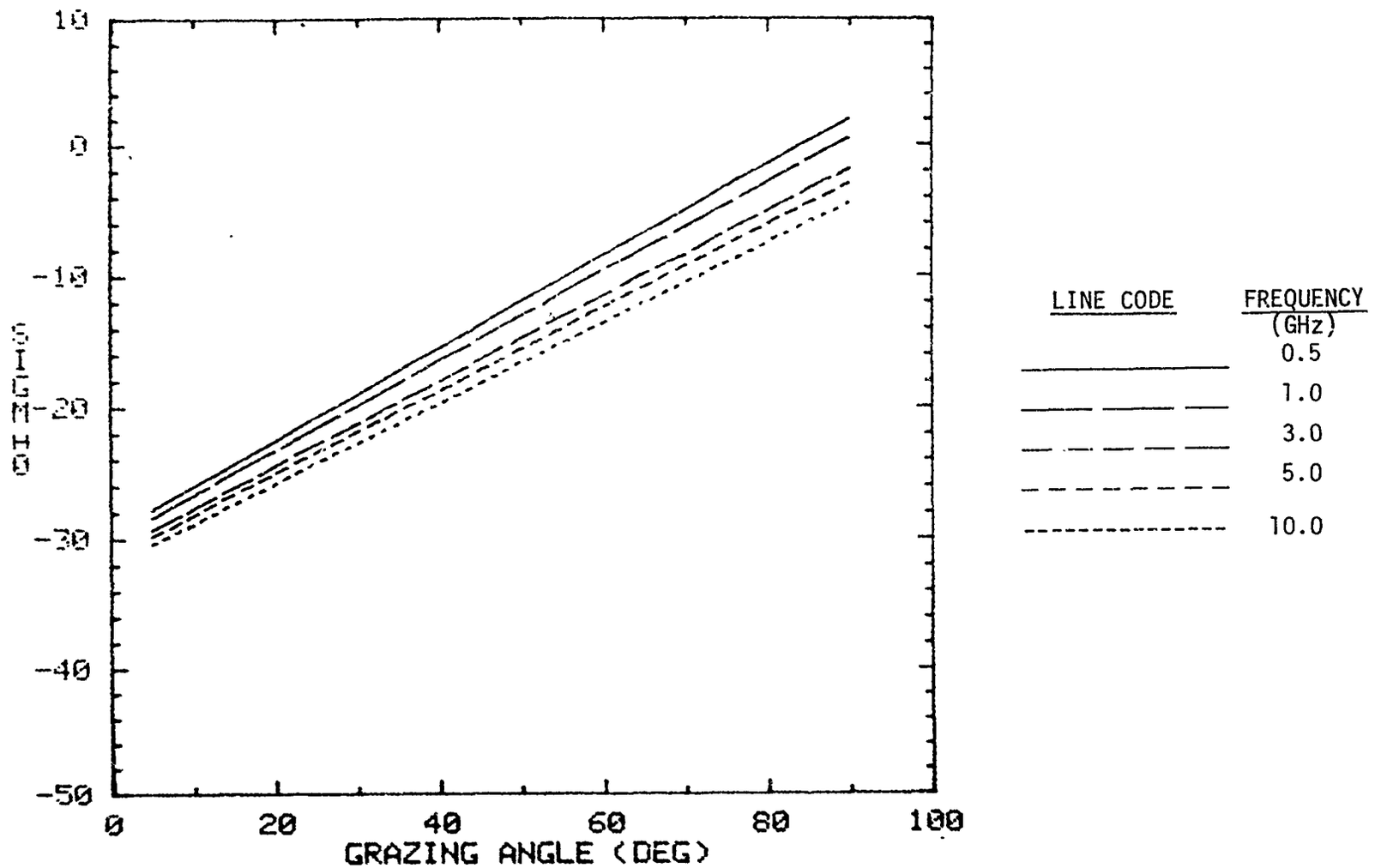

Figure 10a. Snow and Ice, $\bar{\sigma}°$ versus Grazing Angle

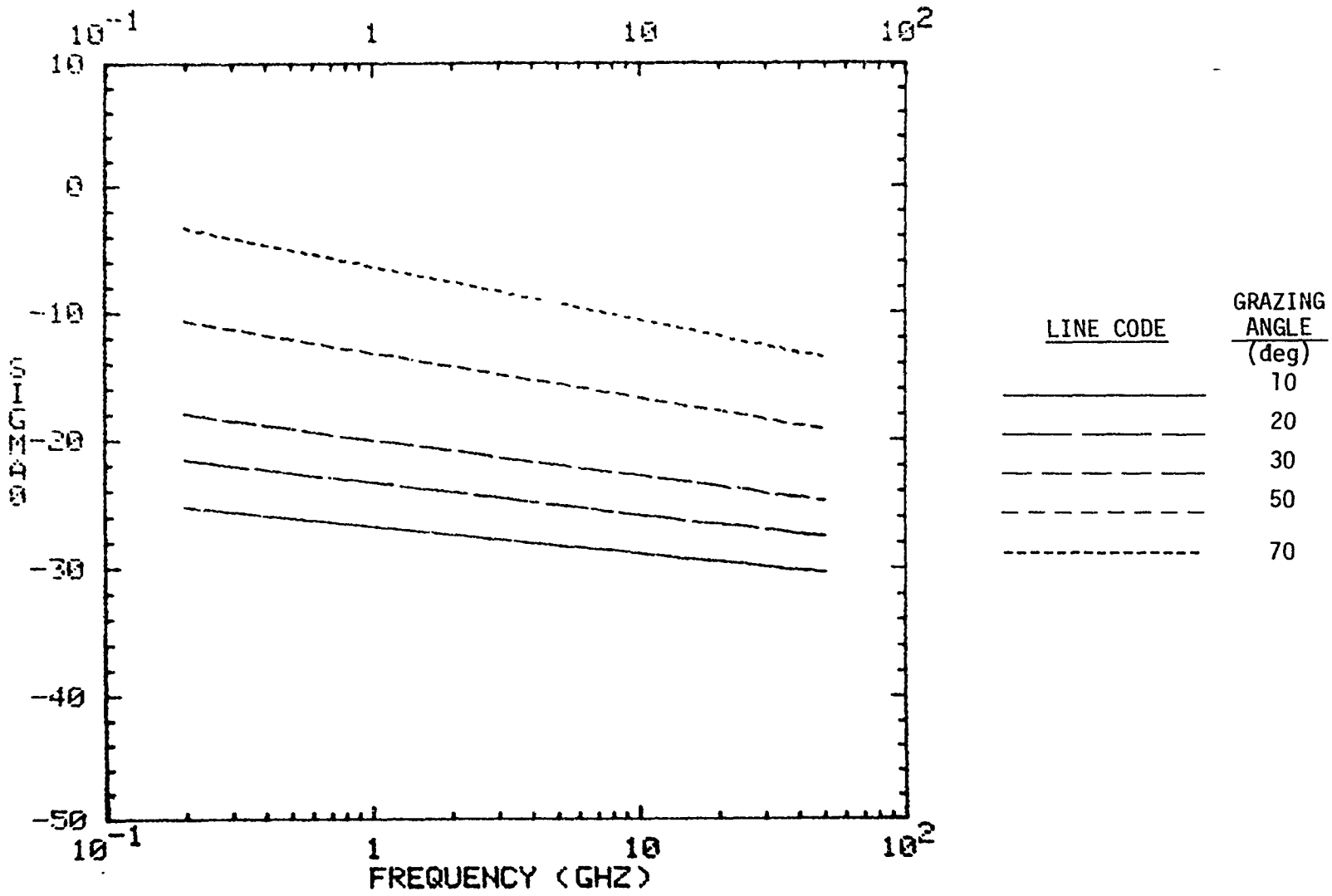

Figure 10b. Snow and Ice, $\bar{\sigma}°$ versus Frequency

3.2.6 Urban Terrain

Urban terrain, which covers cities and residential areas, differs from the other types of terrain in that the reflected energy is probably dominated by that from man-made objects. For this reason, there is a great deal of variability of the data from a given source as well as from one source to the next. For example, data on the city of Phoenix,[1] show a much higher $\bar{\sigma}°$ at $\theta = 8°$ for all frequencies than any other grazing angle. This was excluded from the fit after it appeared to be adversely affecting the θ dependence. Data on the city of Chicago[2] were excluded because the frequency dependence was not monotonic and varied greatly.

In the end, a fit was obtained with an rms deviation of 3.8 dB. The parameters were as follows

$$\bar{\sigma}° = -12.42 - 0.060\theta - (1.79 - 2.07\theta) \log F \qquad (3\text{-}9)$$

$$\delta = 1.65 \text{ dB}$$

This is plotted in Fig. 11a,b.

3.2.7 Sea Clutter

Compared to land clutter, sea clutter is relatively benign. It is very important that a model for sea clutter be included in our SBR clutter model, however, because most of the earth is covered by ocean and one would like to know how small a target can be detected in the sea clutter environment.

Due to the importance of sea clutter to navy radar operations and to theoretical interest, there exists a good deal of data. There is a fairly strong dependence on such factors as wave height and wind velocity all of

---

[1] J. C. Daley, et al., Ibid.

[2] W. Ament, "Radar Terrain Reflections for Several Polarizations and Frequencies," Trans. 1959 Symp. Radar Return, Pt 2., May 1959.

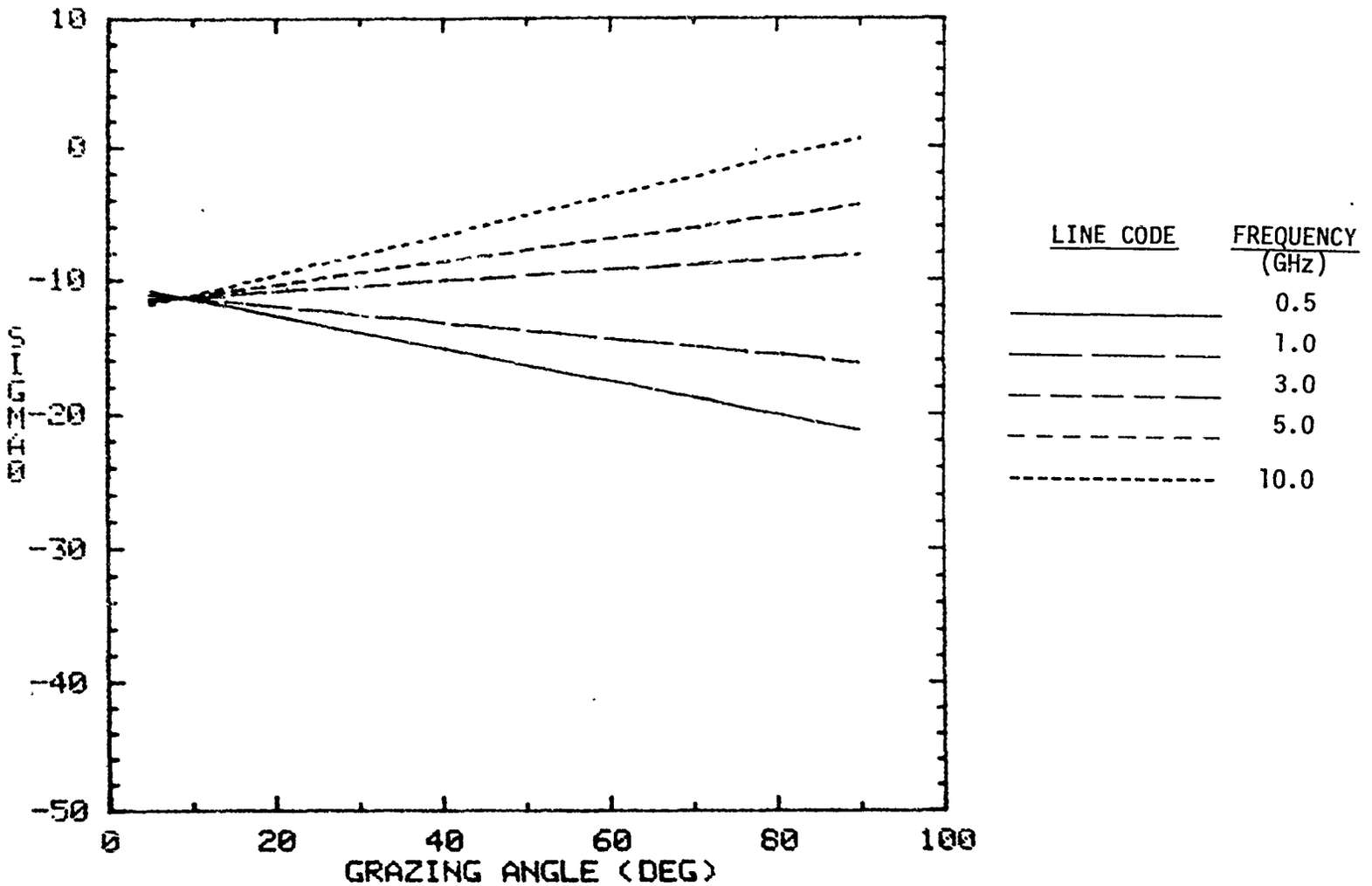

Figure 11a. Urban, $\bar{\sigma}°$ versus Grazing Angle

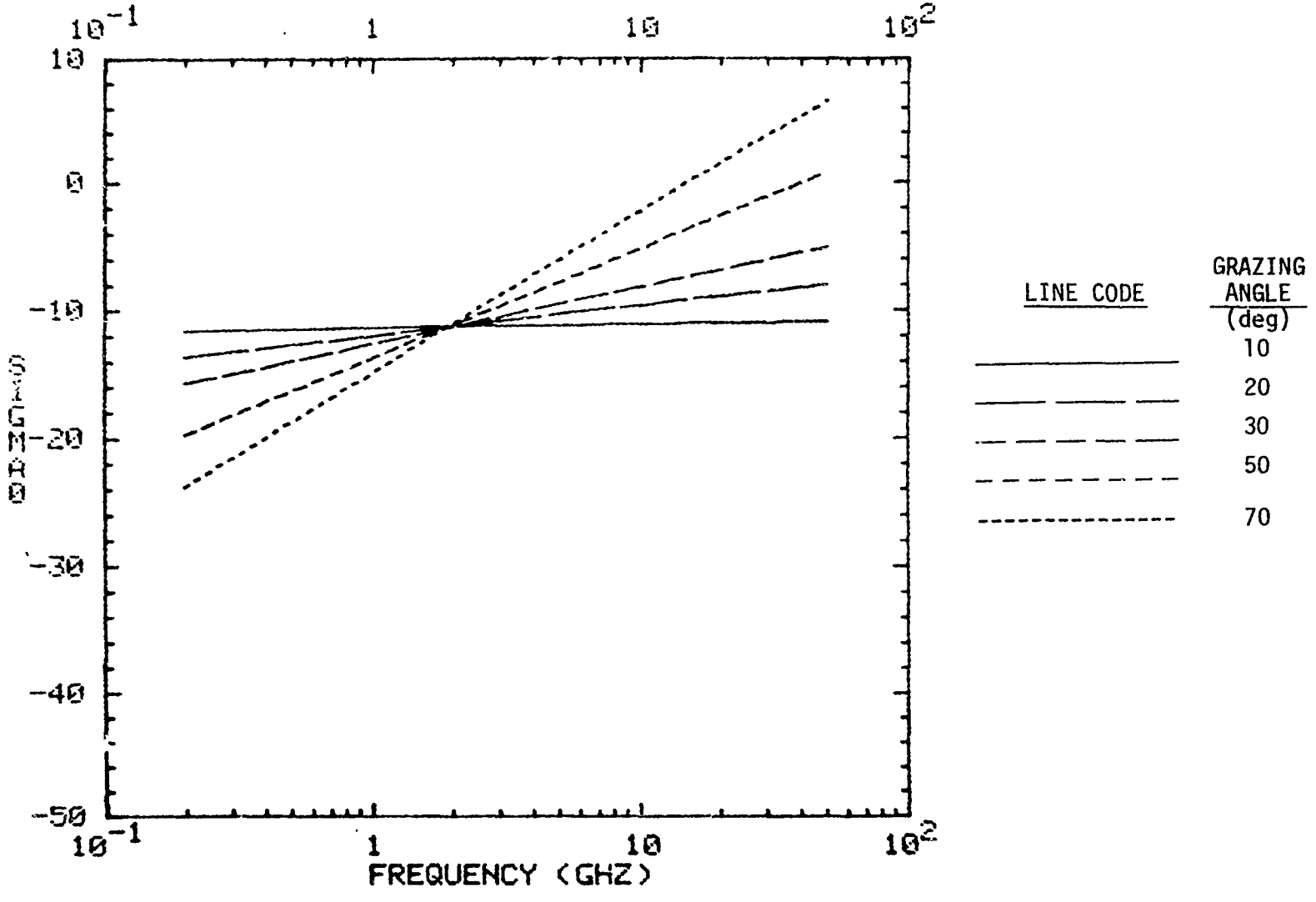

Figure 11b. Urban, $\bar{\sigma}^{\circ}$ versus Frequency

which are not independent. There is also a stronger polarization dependence than in the case with land clutter. For these reasons, we have segregated that data into four categories based on wind speed and polarization. These are as follows:

Category	Polarization	Wind Speed (kts)
1	like	>15
2	like	$\leq$15
3	cross	>15
4	cross	$\leq$15

For a single sea clutter model, category one is the preferable choice since like polarization is more common and high winds are prevalent in northern seas. Sea clutter tends to drop sharply at low grazing angles and for this reason better fits resulted when the θ dependence was proportional to log θ instead of θ. The results of the fits are given below for each category.

Category 1. (like polarization/high wind)

$$\overline{\sigma^\circ} = -58.9 + 19.5 \log \theta + 1.19 \log F + 3.60 \log \theta \log F$$

rms deviation = 5.3 dB

δ = 3.2 dB (3-10)

Category 2. (like polarization/low wind)

$$\overline{\sigma^\circ} = -65.5 + 21.96 \log \theta + 6.68 \log F = 1.45 \log \theta \log F$$

rms deviation = 6.9 dB

δ = 5.5 dB (3-11)

Category 3. (cross polarization/high wind)

$$\bar{\sigma}^\circ = -59.8 + 12.3 \log \theta + 1.43 \log F + 0.88 \log F \log \theta$$

rms deviation = 1.5 dB

$$\delta = 0.25 \text{ dB} \qquad (3\text{-}12)$$

Category 4. (cross polarization/low wind)

$$\bar{\sigma}^\circ = -58.8 + 9.62 \log \theta + 5.68 \log F - 7.69 \log \theta \log F$$

rms deviation = 2.2 dB

$$\delta = 0.56 \text{ dB} \qquad (3\text{-}13)$$

These are plotted respectively in Figs. 12a through 15b.

Summary

The fitted parameters for the model as well as the rms deviations and δ, the factor which compensates for fitting $\bar{\sigma}^\circ$ rather than σ° are presented in Table 1. In general we feel that these fits provide a fair description of the collective clutter data available at this time.

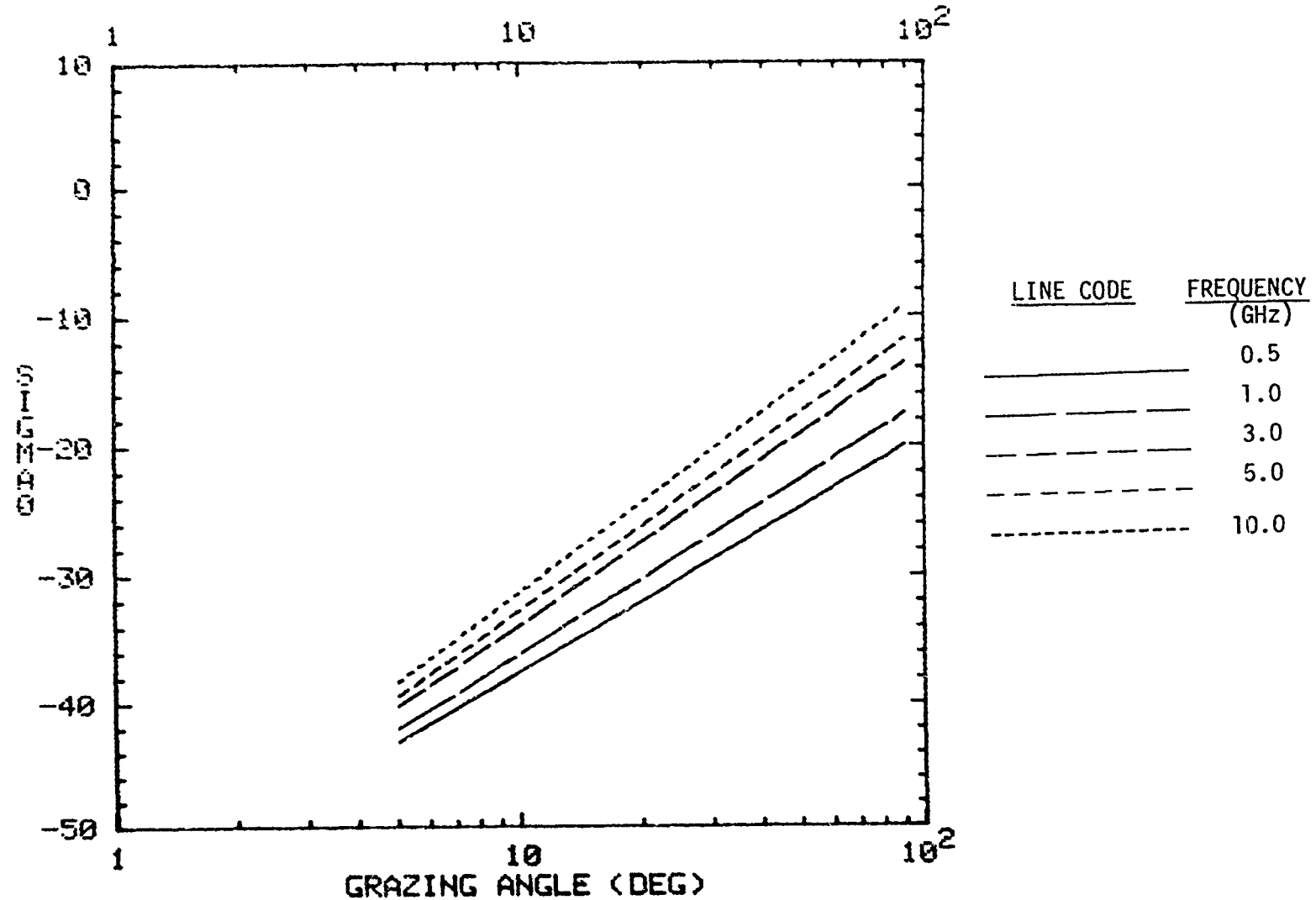

Figure 12a. Sea. Like polarization, high wind speed, $\bar{\sigma}°$ versus grazing angle.

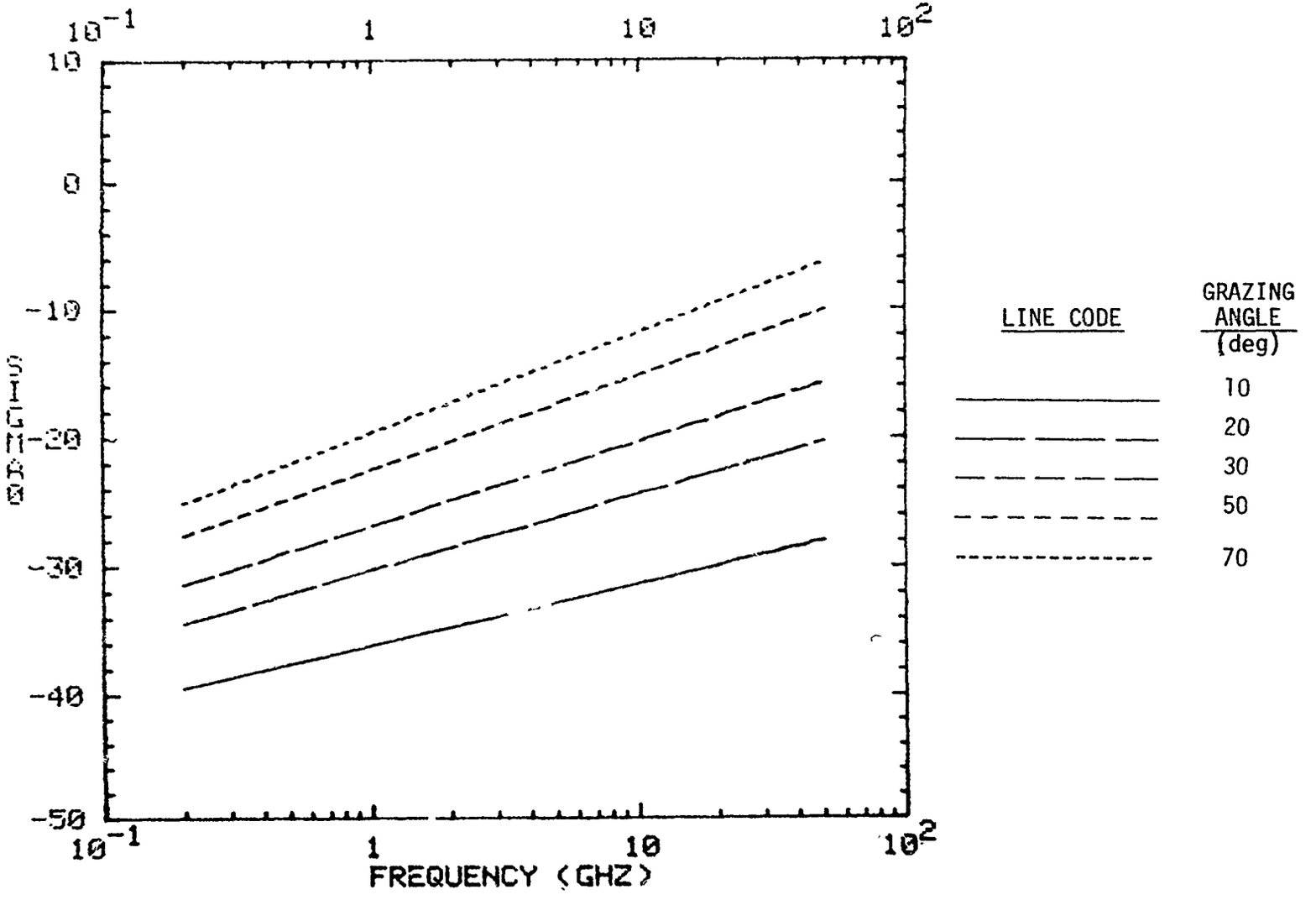

Figure 12b. Sea. Like polarization, high wind speed, $\bar{\sigma}^{\circ}$ versus frequency.

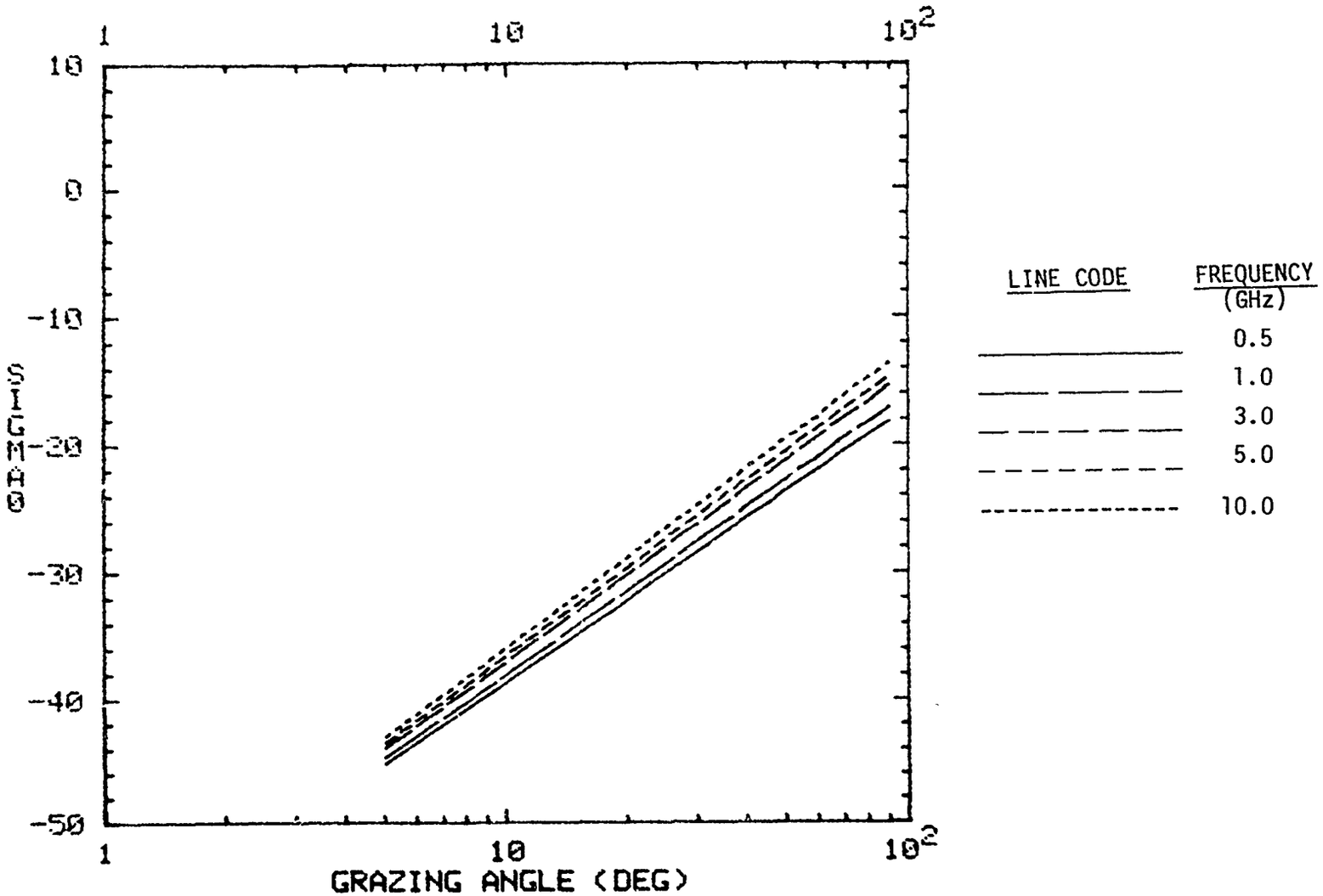

Figure 13a. Sea. Like polarization, low wind speed, $\bar{\sigma}°$ versus grazing angle.

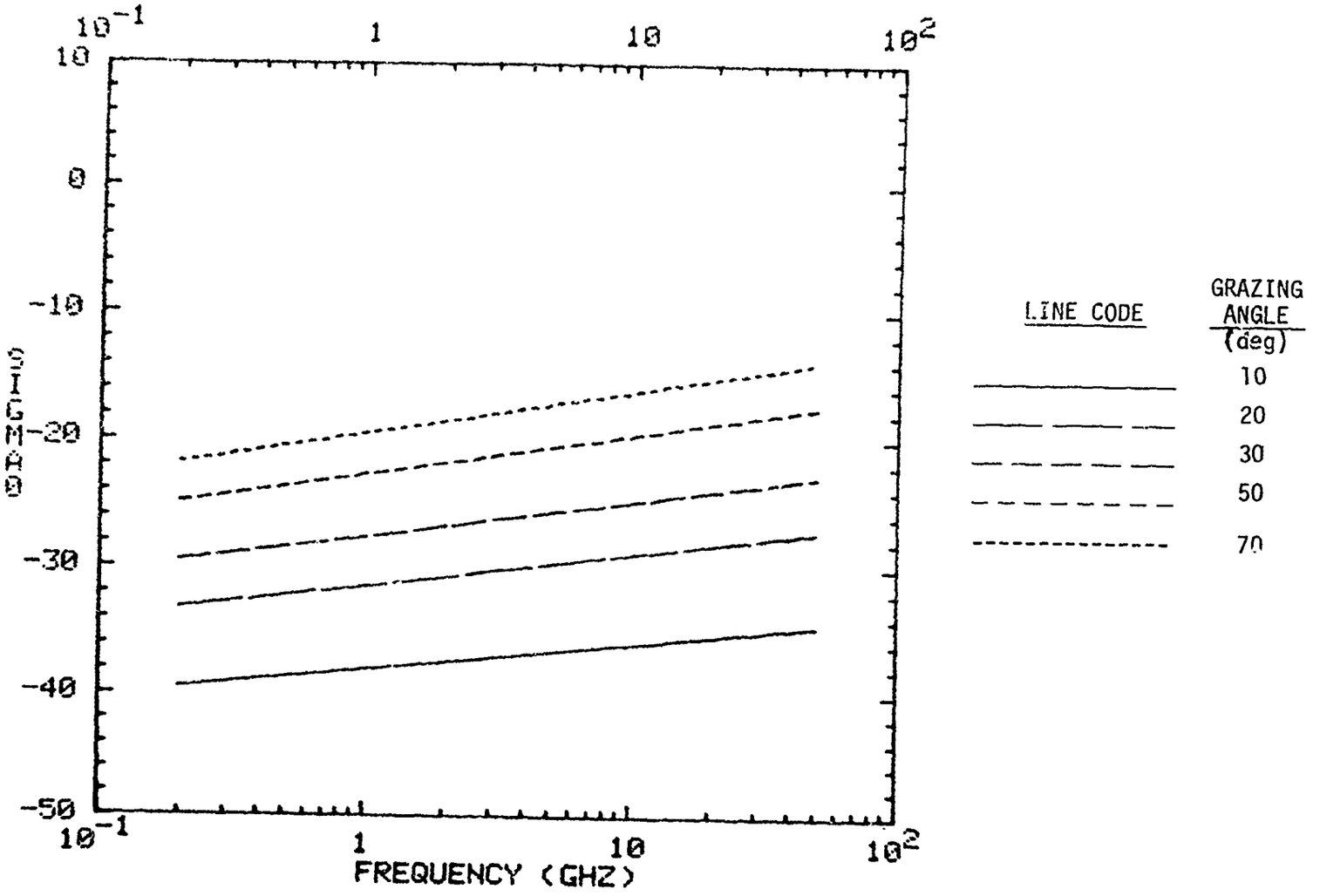

Figure 13b. Sea. Like polarization, low wind speed, $\bar{\sigma}^{\circ}$ versus frequency.

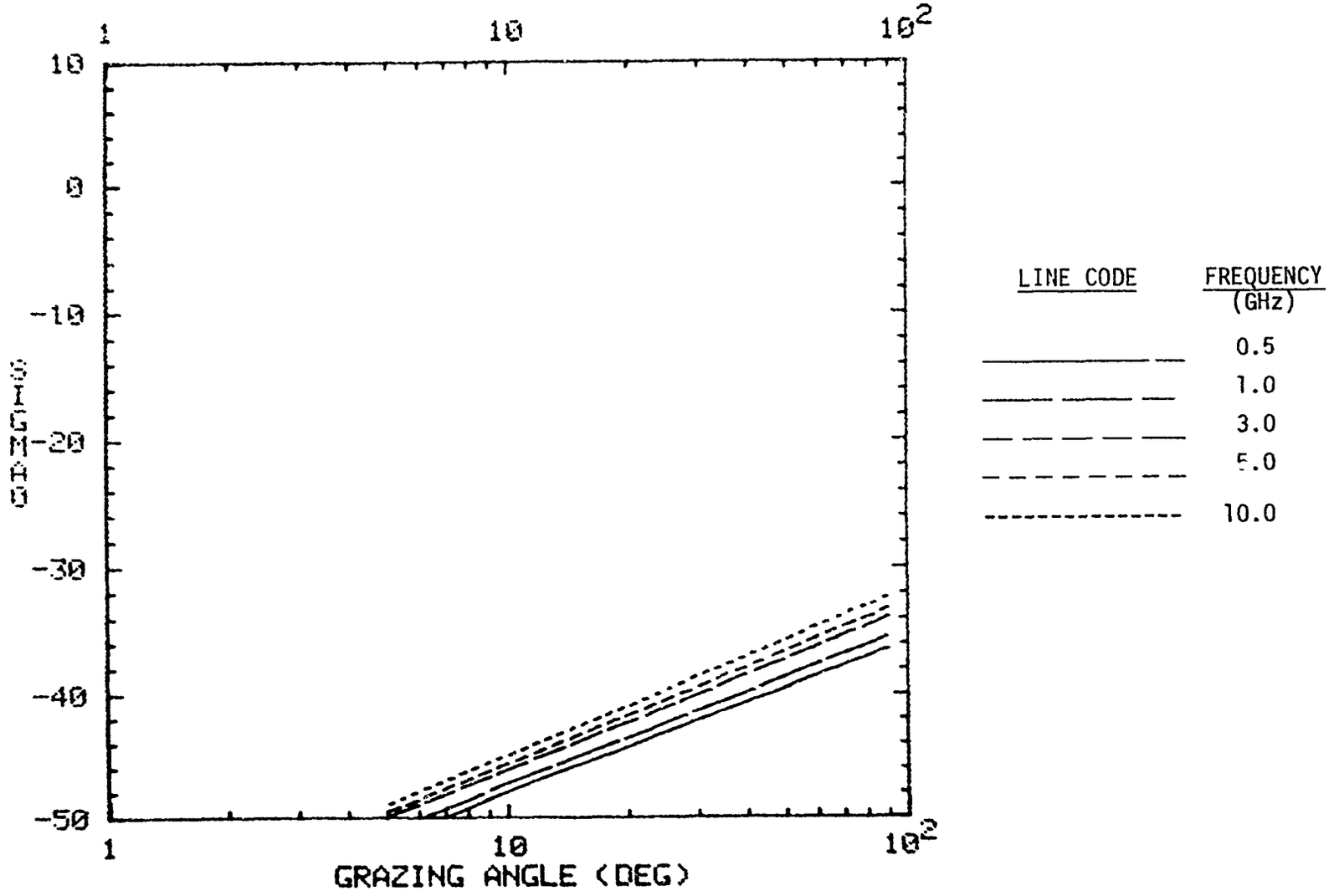

Figure 14a. Sea. Cross polarization, high wind speed, $\bar{\sigma}°$ versus grazing angle.

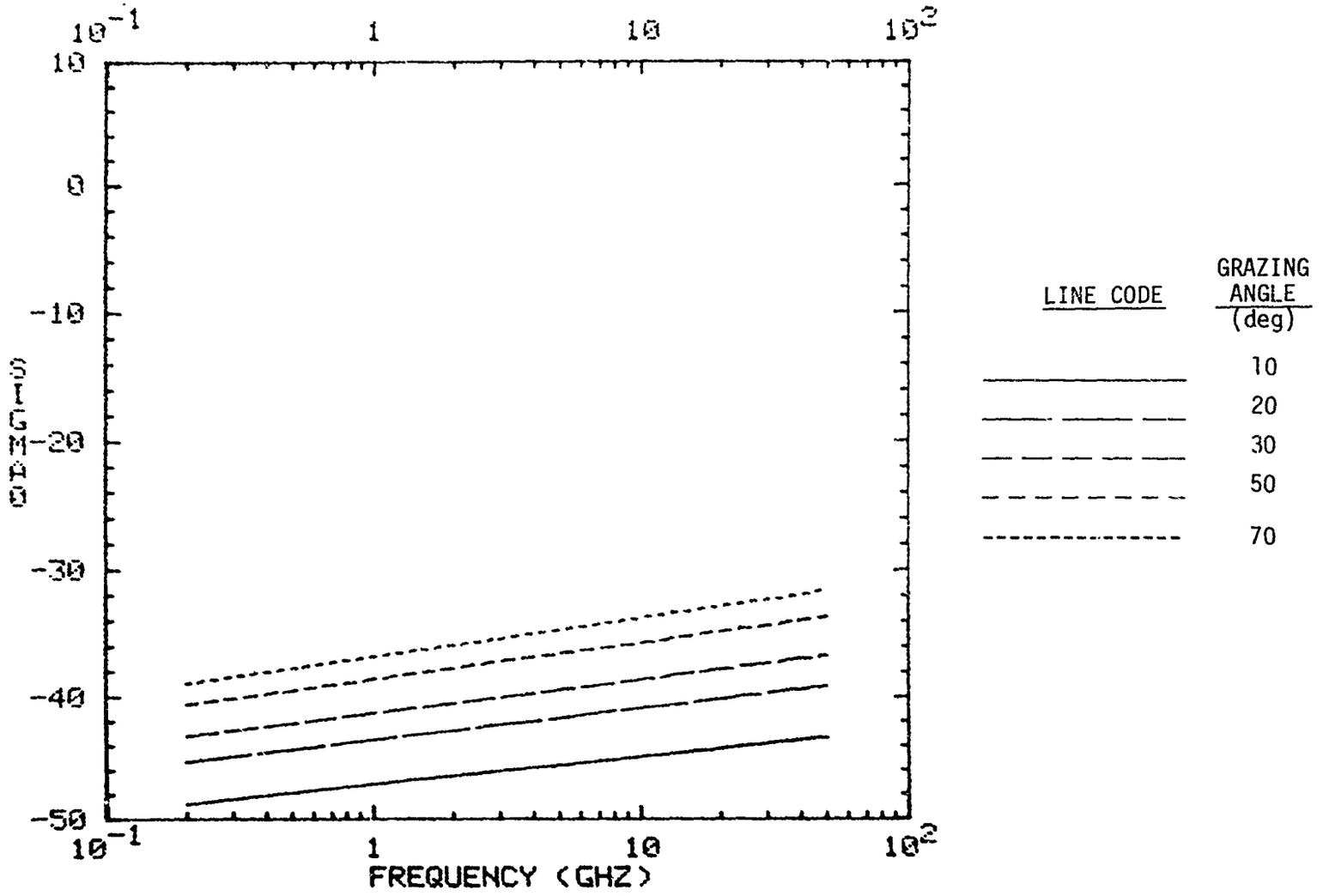

Figure 14b. Sea. Cross polarization, high wind speed, $\bar{\sigma}^{\circ}$ versus frequency.

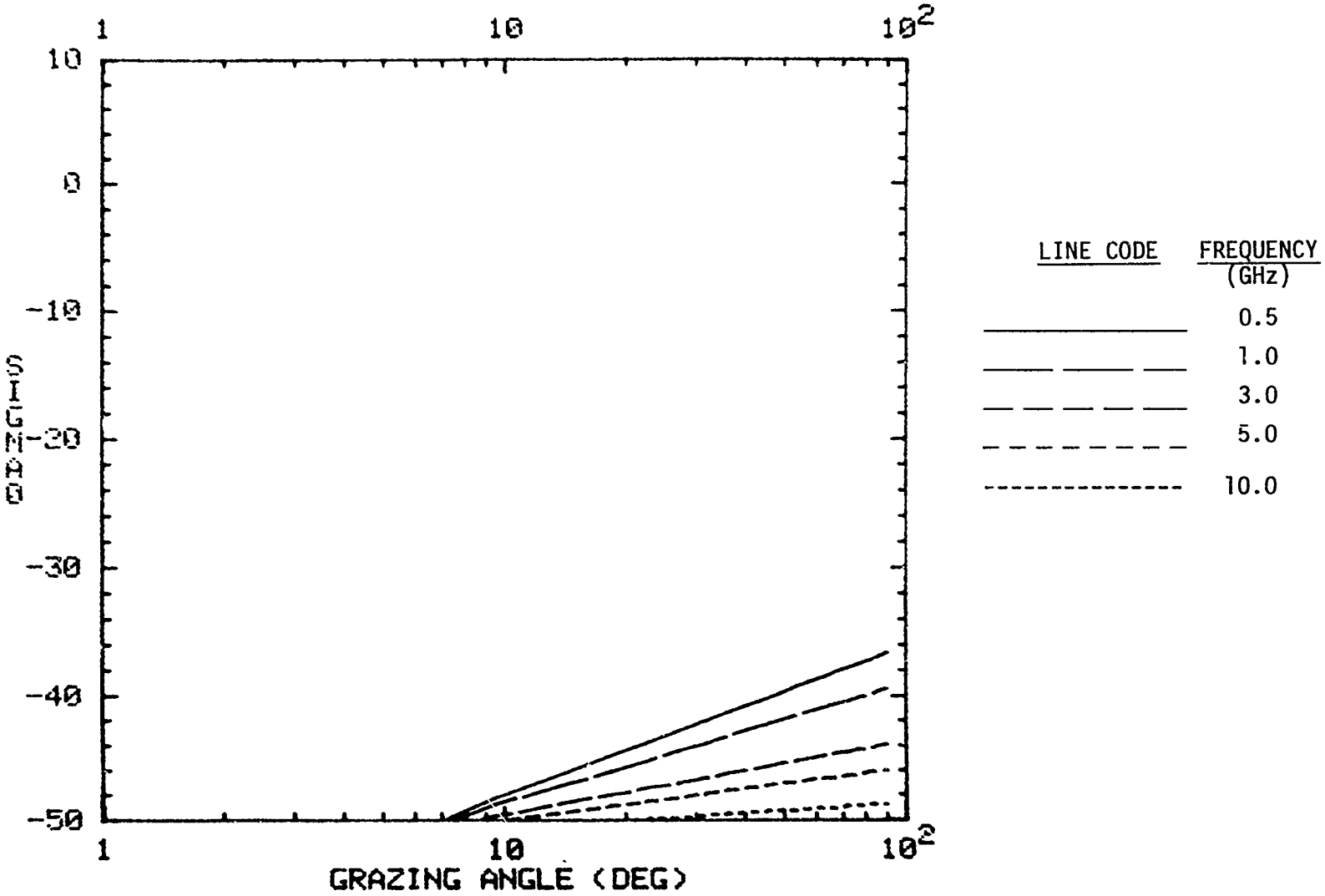

Figure 15a. Sea. Cross polarization, low wind speed, $\bar{\sigma}^{\circ}$ versus grazing angle.

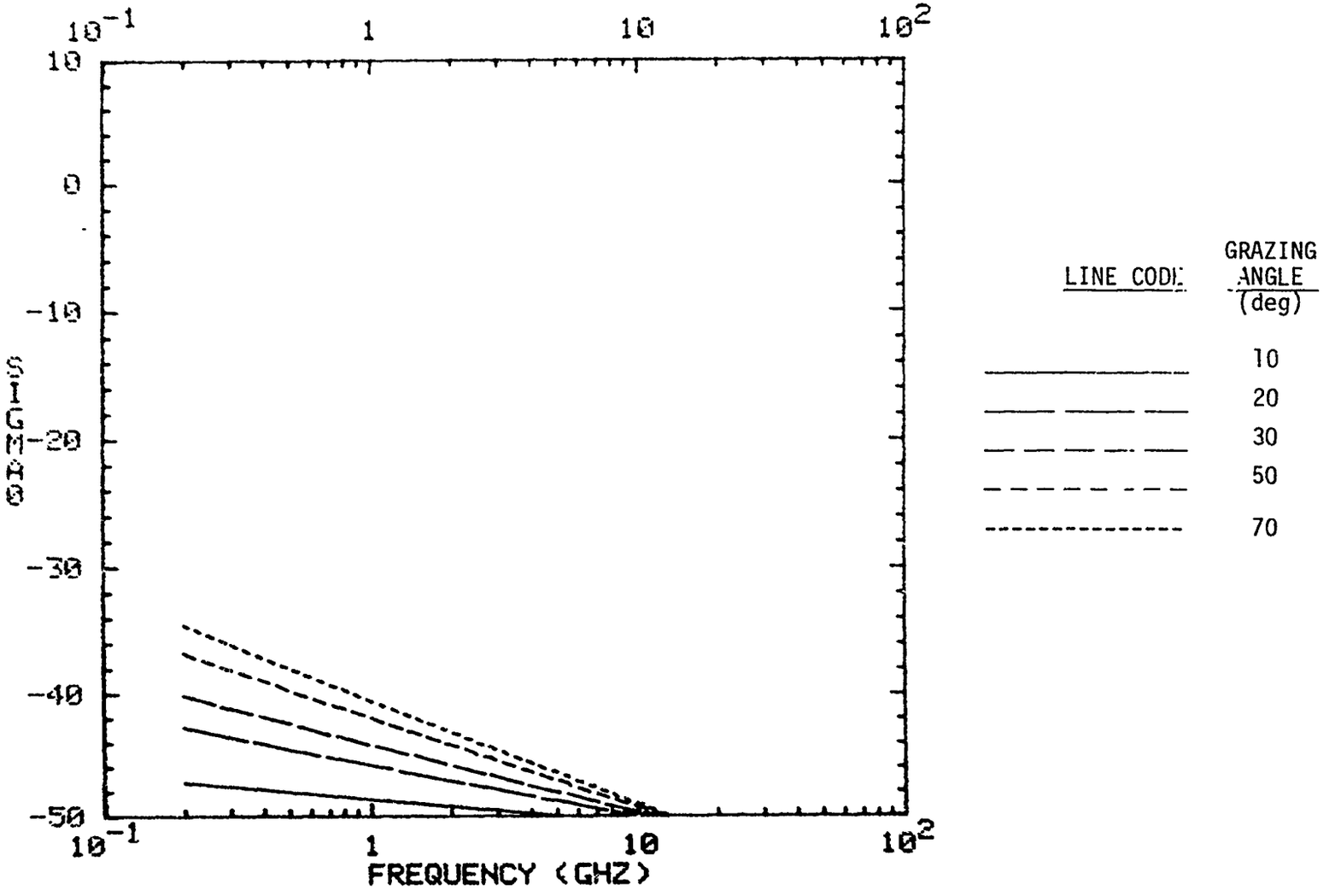

Figure 15b. Sea. Cross polarization, low wind speed, $\bar{\sigma}^\circ$ versus frequency.

TABLE 1

FITTED PARAMETERS IN REGRESSION ANALYSIS

TERRAIN TYPES		A	B	C	D	δ (dB)	rms deviation (dB)
Desert		-34.15	0.163	8.69	0.0093	1.16	3.20
Rural		-23.61	0.0994	3.53	0.091	0.79	2.62
Forest		-42.36	0.520	24.93	-0.358	0.91	2.81
Mountains		-30.24	0.173	8.82	-0.015	1.02	2.98
Snow and Ice		-32.97	0.340	-1.797	-0.035	2.9	5.01
Urban		-12.42	-0.060	-1.79	2.07	1.65	3.8
Sea	*1	-58.9	19.5	1.19	3.60	3.2	5.3
	2	-65.5	21.96	6.68	1.45	5.5	6.9
	3	-59.8	12.3	1.43	0.88	0.25	1.5
	4	-58.8	9.62	5.68	-7.69	0.56	2.2

*Note A, B, C, D, are defined differently for sea clutter. See Eqs. 3-1 and 3-2.

4.0 PROBABILITY DISTRIBUTION OF CLUTTER σ°

Of primary importance in assessing the impact of clutter on detection is not the average clutter cross section but the probability that it will exceed a critical threshold. This notion can be derived from the probability density function (pdf) for RCS. For example, most theories of detection model the noise contribution to the in-phase and quadrature components as Gaussian. This implies that its amplitude is Rayleigh distributed

$$P(V) = \frac{2V}{V_o} \; e^{-V^2/V_o} \tag{4-1}$$

in the probability that the amplitude V is between V and V + dV. Likewise the power n is exponentially distributed

$$P(n) = \frac{1}{N_o} \; e^{-n/N_o} \tag{4-2}$$

where

$$N_o = V_o^2$$

$$n = V^2$$

Thus, the probability that noise of mean N_o will exceed n is given by

$$P_c(n) = e^{-n/N_o} \tag{4-3}$$

These statistics also apply in theory to the reflections from a few ideal clutter types, such as

1. An infinite number of scatterers in each resolution cell (like chaff).

2. Any number of scatterers in the resolution cell if their amplitude distribution is Rayleigh.

In each case, the phase must be random and uniformly distributed, and the amplitude and phase of each scatterer must be independent.

A Rayleigh distribution is very convenient since P, the probability density function, contains only one parameter. Then, if the pdf describing the target statistics likewise has only one parameter, the mean RCS (e.g., nonfluctuating, Swerling I, II, III, IV), the detection statistics are completely determined by the singal-to-interference ratio.

Unfortunately for the detection problem, ground and sea echos do not always obey Rayleigh statistics, thus complicating the theory and making detection in general more difficult. The probability distribution of clutter amplitude has received a significant amount of attention, both theoretically and experimentally, in the past. Nevertheless, there is still a great deal of uncertainty and misunderstanding. The fact is that variability in the clutter reflectivity is very difficult to define, much less to predict or to measure.

In this section we shall attempt to define clutter statistics which are relevant to the SBR detection problem, identify factors which contribute to clutter variability, and show how one might use the model to predict the probability that clutter will exceed a given threshold. Throughout, the size of the resolution cell will be stressed as a crucial parameter. In the case of SBR, we are primarily interested in large resolution cells.

4.1 DEFINITION

First, we shall define what we feel to be the problem of most interest in detection in clutter. Generally, one is interested in the number of

false alarms per unit time or false-alarm rate. Given the number of resolution cells per second this implies a false alarm probability. Most modern radars contain constant-false-alarm rate, CFAR, capability which makes use of a local average to set the detection threshold which preserves the false alarm rate. The CFAR must take into account the variability in the clutter return from this local sample. The variability of clutter in a given scene is important in determining how flexible the CFAR must be in processing a single scene, and finally the variability from scene to scene is also important. By scene we mean a batch of data upon which detection decisions are made. Typically, a scene would include all the data within the beam footprint.

4.2 CAUSES

We shall list a number of factors which influence clutter variability and the scales over which we feel the influence is most prominent. We shall discuss each in more detail.

4.2.1 Mutual Interference Effects

Mutual interference effects are responsible for the so-called Rayleigh statistics encountered in chaff and most distributed clutter. The pdf is well known and is given by the Rayleigh theory

$$P(\sigma^\circ) = \frac{1}{\mu} \, e^{-\sigma^\circ/\mu} \tag{4-4}$$

where μ is the mean value of σ°. It applies only to cases where the individual scattering center themselves are Rayleigh or for an infinite number of scatterers.

4.2.2 Man-made Objects

We can use urban data to determine the cross section per unit area of man-made objects by assuming the urban clutter is dominated by man-made objects. The difference between urban clutter and rural clutter, for example, is 10 dB at low grazing angles and decreases as the grazing angle increases (Section 3.2). If one assumes that a fraction ρ of resolution cells contain all man-made objects then the fraction ρ will be 10 dB higher than the others.

As resolution cells increase in size, every resolution cell will contain part natural and part man-made clutter, and the variance will be smaller. Taken to the limit of very large resolution cells, perhaps several miles square, one might expect every resolution cell to contain a fraction ρ of man-made clutter. Then the variance should reduce to essentially zero.

4.2.3 Variation in Terrain Type

In a given scene (or even resolution cell), there may be more than one terrain type. For instance, forest and fields or rural and urban terrains often coexist. For land clutter, the difference in σ° among terrain types is about 20 dB, the difference between urban clutter and desert or snow. Again the actual variance is a function of resolution cell size with the same argument as given in 4.2.2.

4.2.4 Variation in the Slope of Terrain

In cases where the terrain is not flat and the period of undulation is large compared to resolution cell dimensions, the actual grazing angle will vary from cell to cell. Since clutter reflectivity with few exceptions, is strongly dependent on grazing angle, this leads to significant variance in the observed σ°.

This hypothesis is easy to check. If we approximate the terrain by a series of ridges which have a sinusoidal undulation, Fig. 16, the probability density function of grazing angle and hence RCS can be computed as a function of the ratio of amplitude to period of undulation. A computer program, which included terrain masking effects, was written to do this. Qualitatively, the 0.05 case resembles gentle rolling hills and the 0.1 case resembles very hilly terrain.

Figs. 17 and 18 show the pdf's for the probability that the actual local grazing angle is between θ and $\theta + d\theta$ for nominal grazing angles of 5, 10, 30, 50 and 90° for A/T = 0.05 and 0.1, respectively. For instance, in Fig. 17 we note that for a nominal grazing angle of 30° and A/T equal to 0.05, the actual grazing angles fall between 11° and 48°! Furthermore,

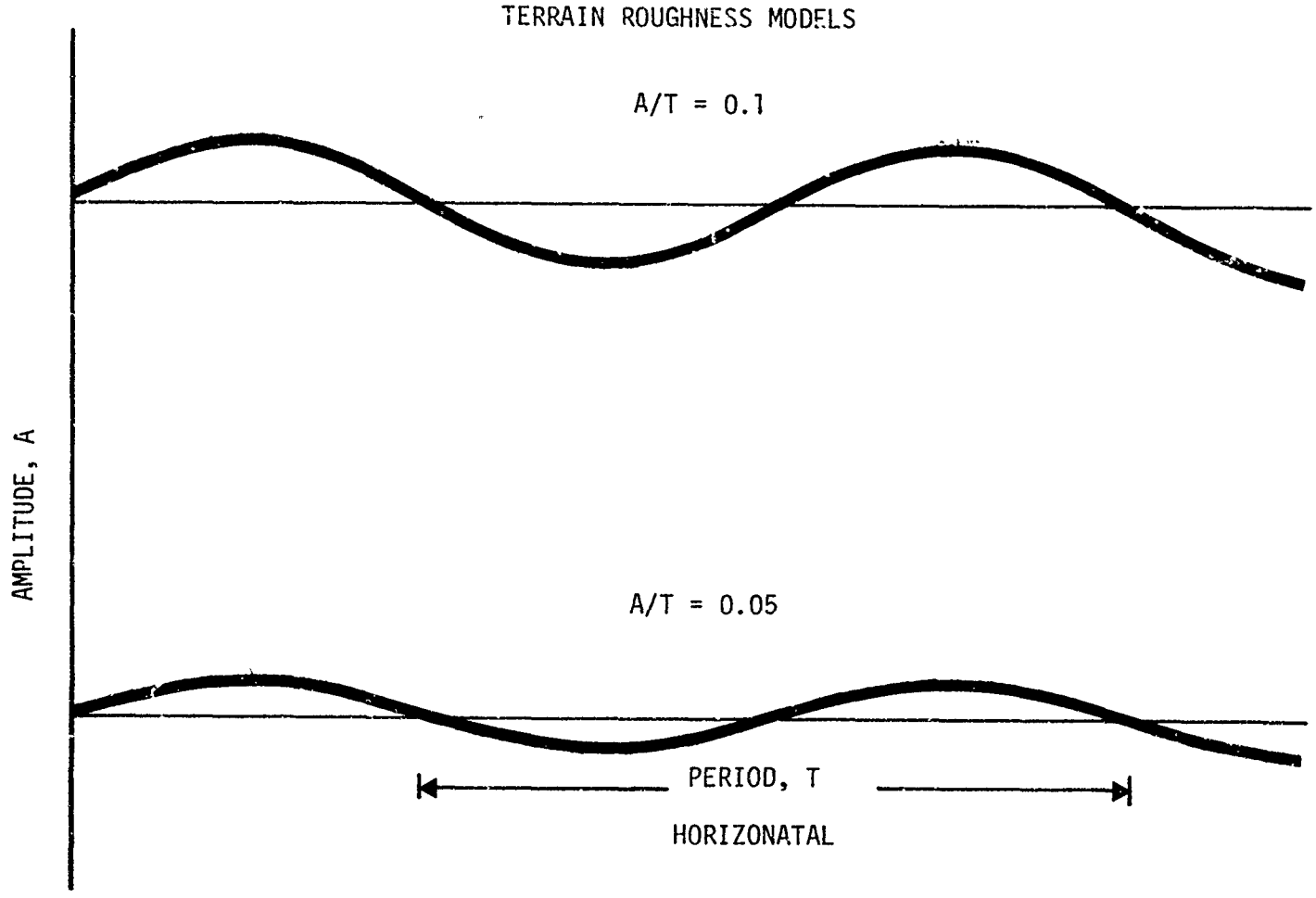

Figure 16. Model for Local Terrain Undulation

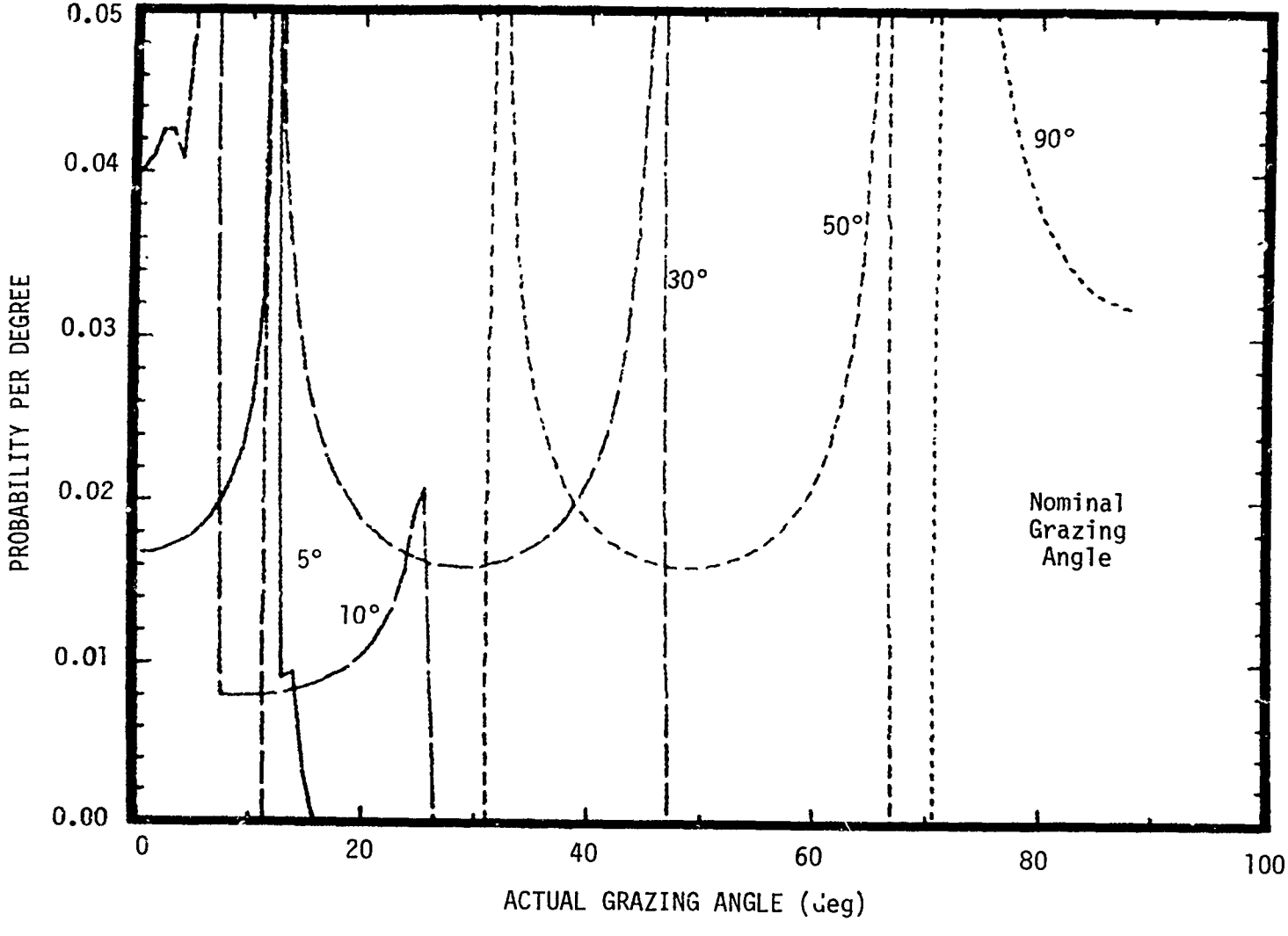

Figure 17. Probability Density Function Versus θ for Undulating Terrain. A/T = 0.05.

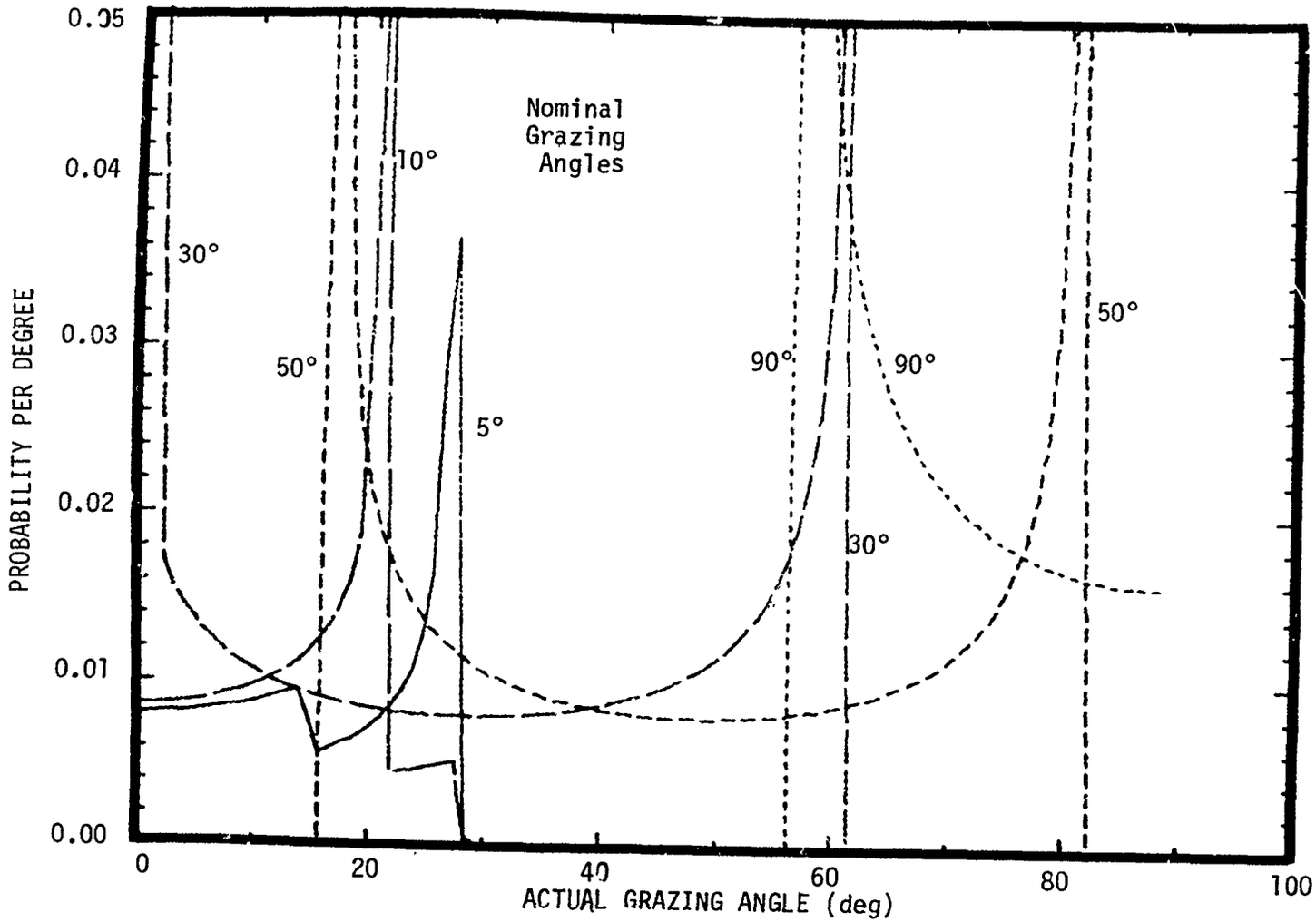

Figure 18. Probability Density Function Versus θ for Undulating Terrain. A/T = 0.1.

values at the extremes of the interval of possible values occur with higher probability.

Given the pdf's for grazing angle it is simple to convert to pdf's for RCS. This is done in Figs. 19 and 20 for rural clutter at 3 GHz. These figures show the probability per dB that RCS will fall between $\bar{\sigma}°$ and $\bar{\sigma}° + d\bar{\sigma}°$. Again, for the 30° nominal grazing angle $\bar{\sigma}°$ falls between -19.6 dB and -14.4 dB with higher probability near the extremes. Table 2 gives the maximum spread in $\bar{\sigma}°$ for each combination of nominal grazing angle and A/T ratio. Note that at low grazing angles there is a lot of shadowing taking place so that there is a higher probability of no clutter at all. All of these results are consistent with the observed phenomenon that the ratio of mean to median clutter increases significantly as the grazing angle decreases.

4.2.5 Variation in Local Conditions

By local conditions, we mean such factors as moisture content of soil, type and density of trees, heights of buildings, etc. Perhaps the best estimate of this variation comes from the variation in observed measurements from highly controlled experiments.[1] From our data base we have have estimated this variation for each terrain type in Table 3.

The University of Kansas, RSL, has collected data to explicitly show seasonal diurnal variations in clutter. These are presented in Figs. 21 and 22. Other data showing variation of $\bar{\sigma}°$ with row orientation relative to radar show large variation at high grazing angles (>50°) but the variation appears to decrease substantially to within the 3 dB estimate given in Table 3 at lower grazing angles. Figure 21 supports a seasonal variation, which might also be interpreted as moisture and crop maturity variation, of about 4 to 6 dB. This figure also supports a variation of about 10 dB with crop type.

---

[1] Soofi, ibid.

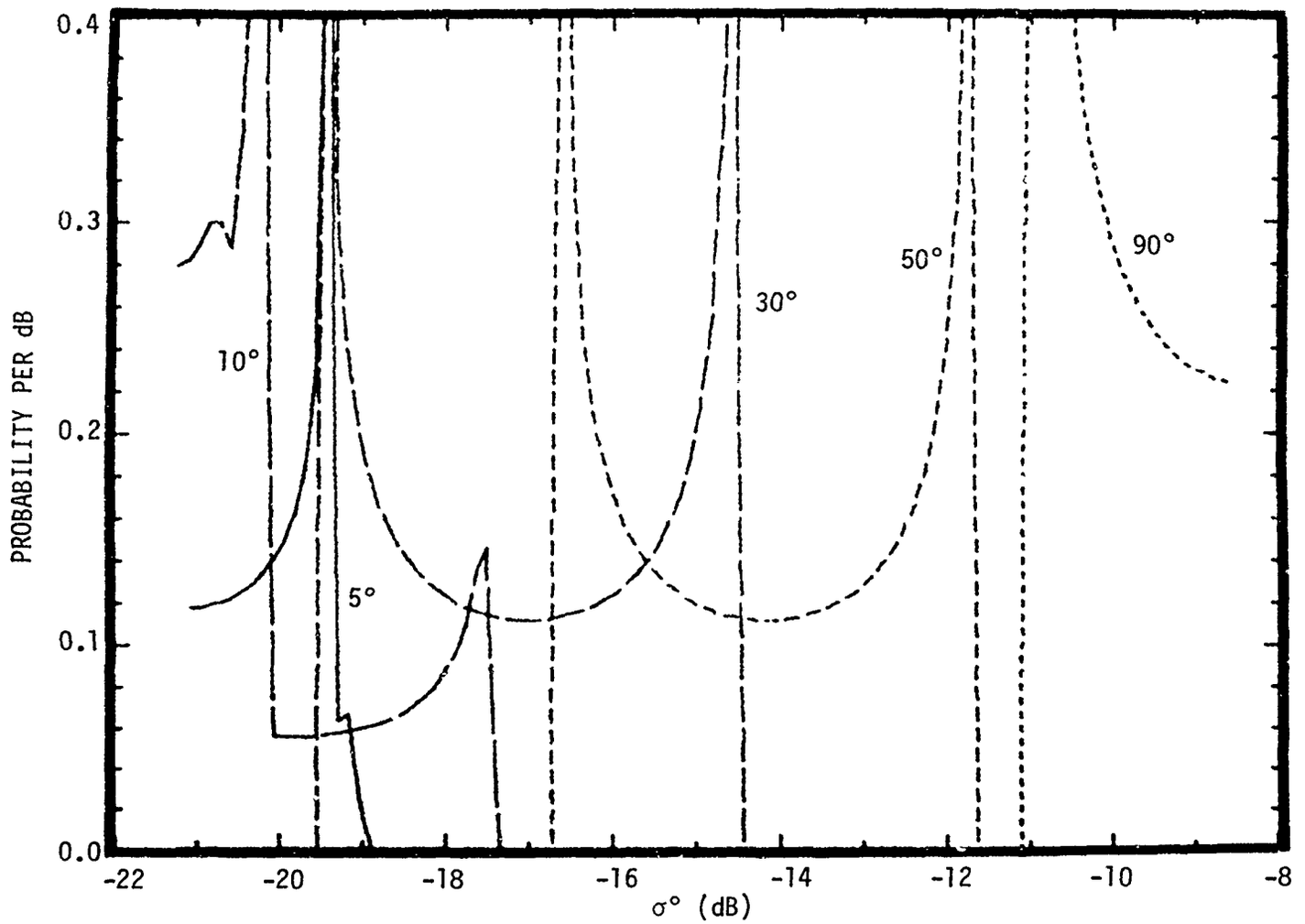

Figure 19. Probability Density Function Versus σ° for Undulating Terrain. A/T = 0.05.

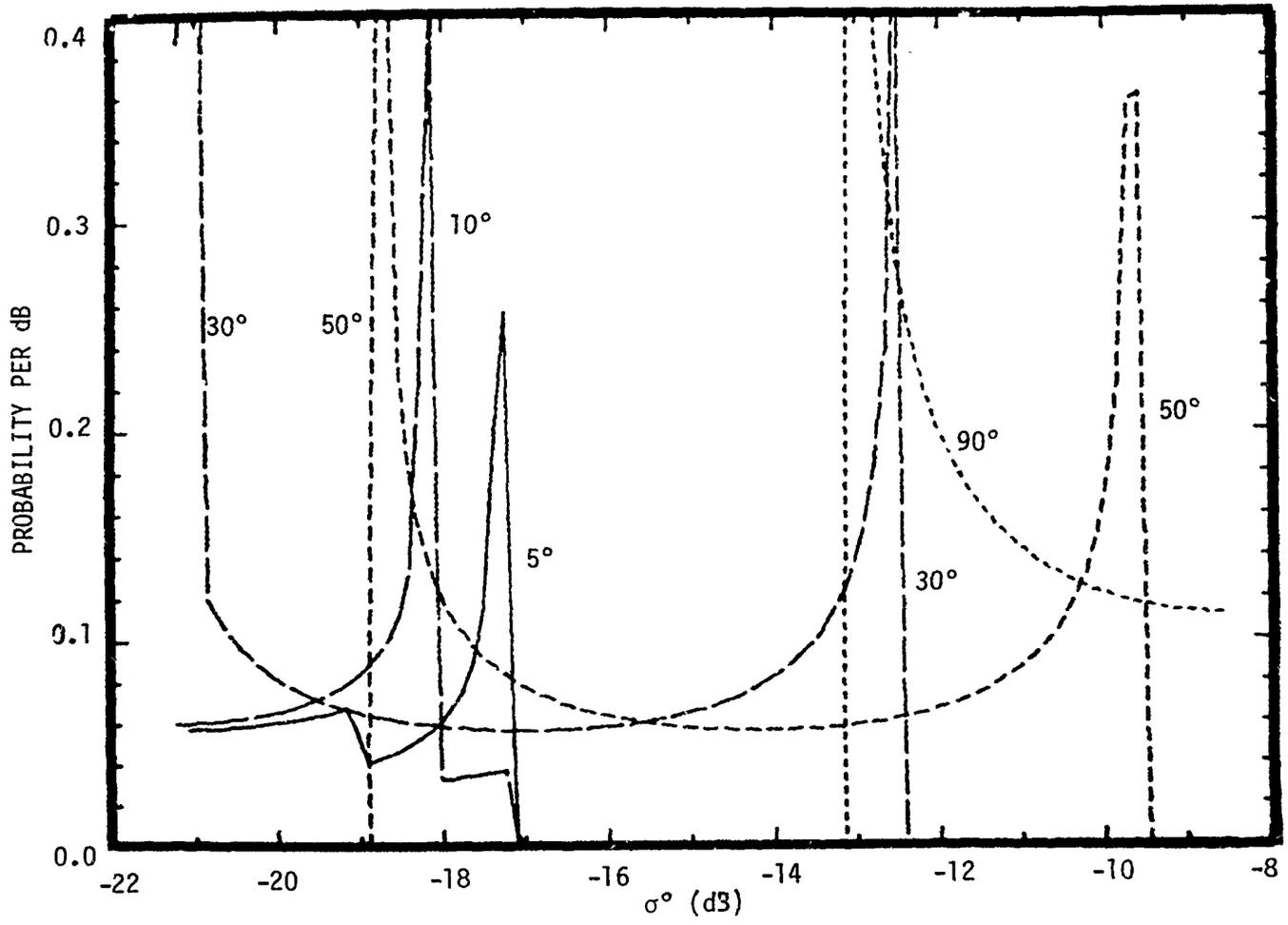

Figure 20. Probability Density Function Versus σ° for Undulating Terrain. A/T = 0.1.

TABLE 2

SPREAD IN $\bar{\sigma}°$ DUE TO UNDULATION OF TERRAIN

MAXIMUM SPREAD IN $\bar{\sigma}°$	A/T	g°
2.3 dB	0.05	5°
3.8 dB	0.05	10°
5.2 dB	0.05	30°
5.1 dB	0.05	50°
2.6 dB	0.05	90°
4.0 dB	0.10	5°
4.0 dB	0.10	10°
8.7 dB	0.10	30°
9.5 dB	0.10	50°
4.6 dB	0.10	90°

TABLE 3

ESTIMATED $\bar{\sigma}°$ VARIATIONS

TERRAIN TYPE	$\Delta\sigma°$
Crops	6 dB
Forest	5 dB
Snow/Ice	2 dB
Urban	7 dB
Sea	3 dB

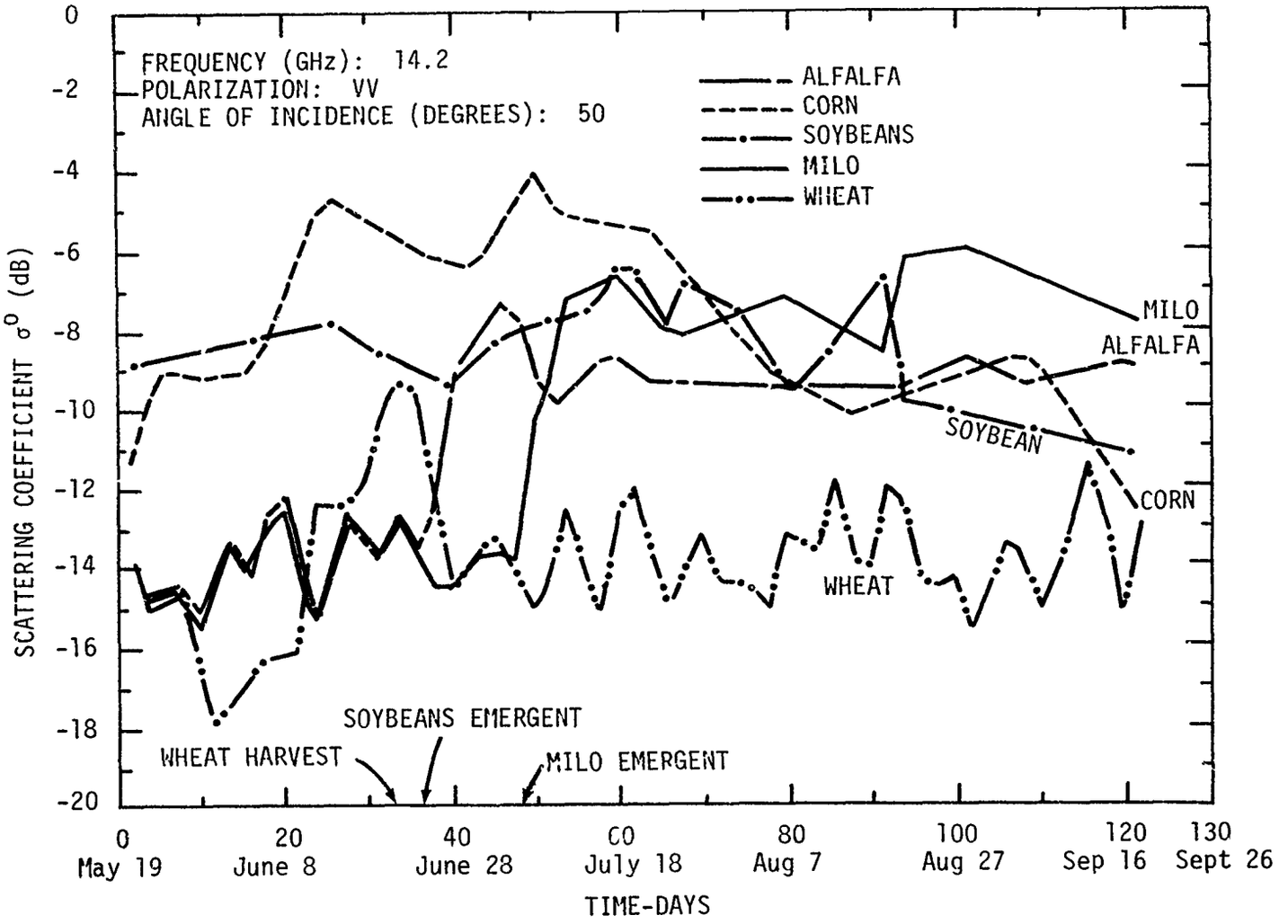

Figure 21. Examples of Seasonal Variation
From W. Simkins, private correspondence

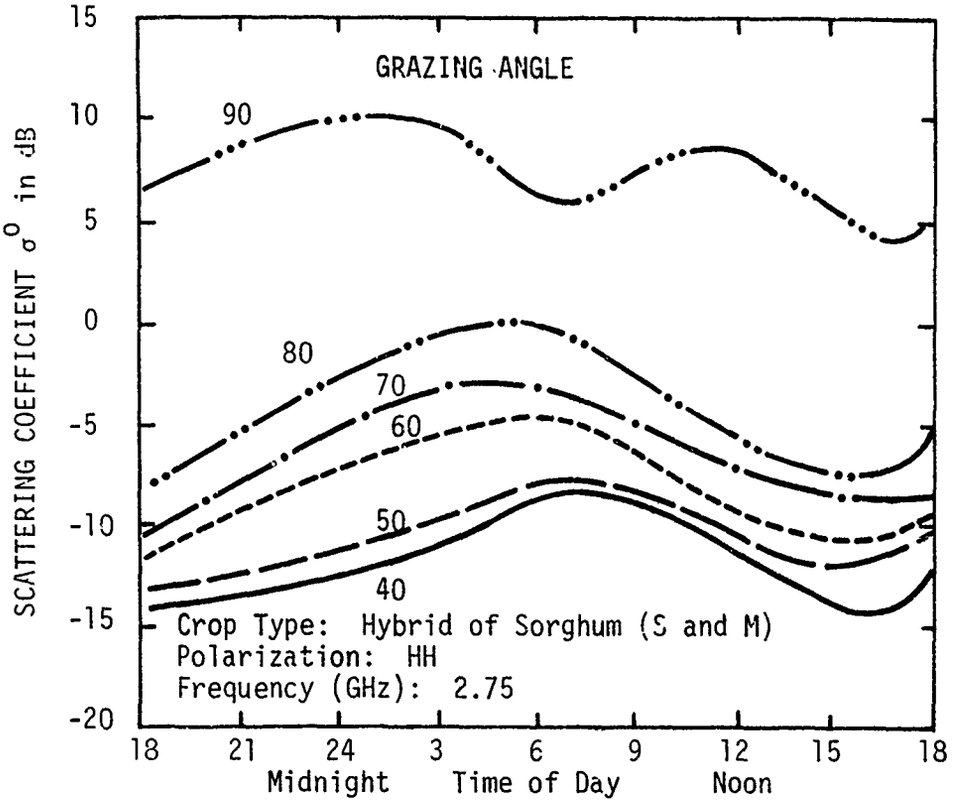

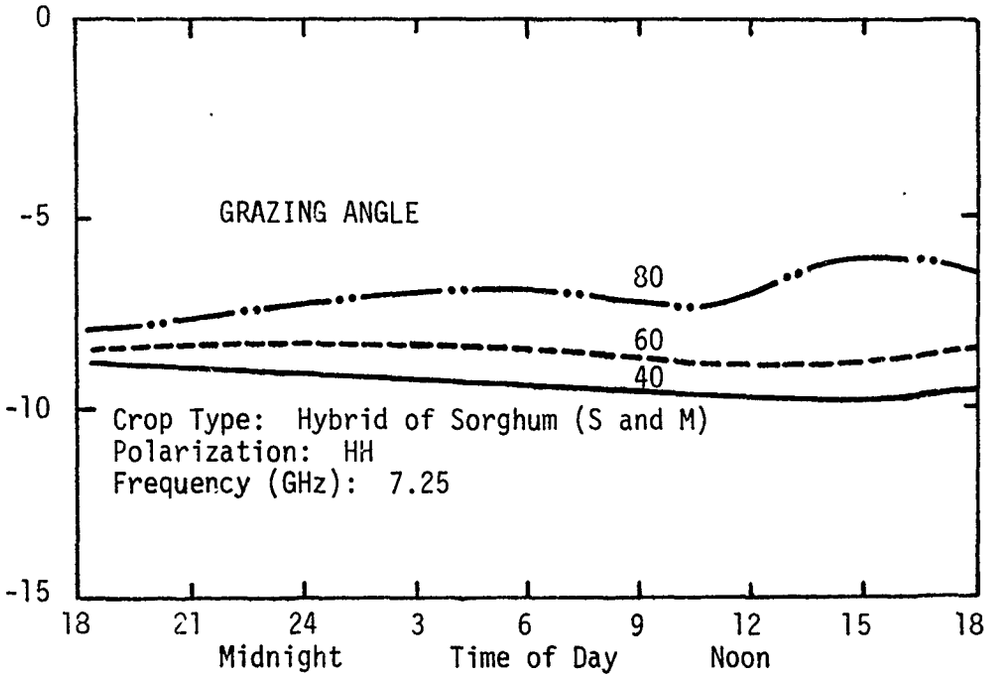

Figure 22. Examples of Diurnal Variation
From W. Simkins, private correspondence.

4.3 CLUTTER AVERAGING AND RESOLUTION CELL SIZE

It is an established fact that for sea clutter, the distribution differs qualitatively and quantitatively as a function of resolution cell size. In particular, if the dimensions of wave height and period are comparable or smaller than the resolution dimensions, the distribution tends to a Rayleigh form.[1] There is experimental evidence to support the same type of trend for land clutter, but the situation for land is complicated by its larger inherent variability compared to sea clutter.

We have a measure of the distribution of RCS in the limit of extremely large resolution cells. This is provided by the University of Kansas RSL[2] who analyzed SKYLAB data over the U.S. and portions of South America. The resolution cell size is 400 to 1000 km^2. This is greater than the correlation length for any local undulation or any local terrain variation. RSL did observe a finite distribution of $\bar{\sigma}°$, however, even after the interference effects were eliminated by incoherent averaging. Two examples are shown in Figs. 23 a and b.

Kansas explained the presence of long tails in the distribution in terms of specular scattering from large lakes and Utah salt flats. At high grazing angles, a specular return results in a large echo producing a tail at high $\bar{\sigma}°$. At low grazing angles, the specular is highly forward, resulting in a low $\bar{\sigma}°$ for backscattering and, hence, a long tail at the lower side. The small but finite width of the central peak in Fig. 23 is due to the variability of the terrain from cell to cell. This small width, in view of the many sources of variability observed for smaller cells, is certain to be due to the averaging effect of the large cells. It is interesting to note the trend in SKYLAB data toward broader distributions with

---

[1] G. V. Trunk and S. F. George, "Detection of Targets in Non-Gaussian Sea Clutter," IEEE Transaction on Aerospace and Electronic Systems, Vol. AES-6 No. 5, September 1970.

[2] S. M. Purduski, "Distribution Tests, 5-Percentile Values, and Autocorrelation Analysis of Skylab S-193 Overland Radar Data," RSLTM 2923-1. (1978)

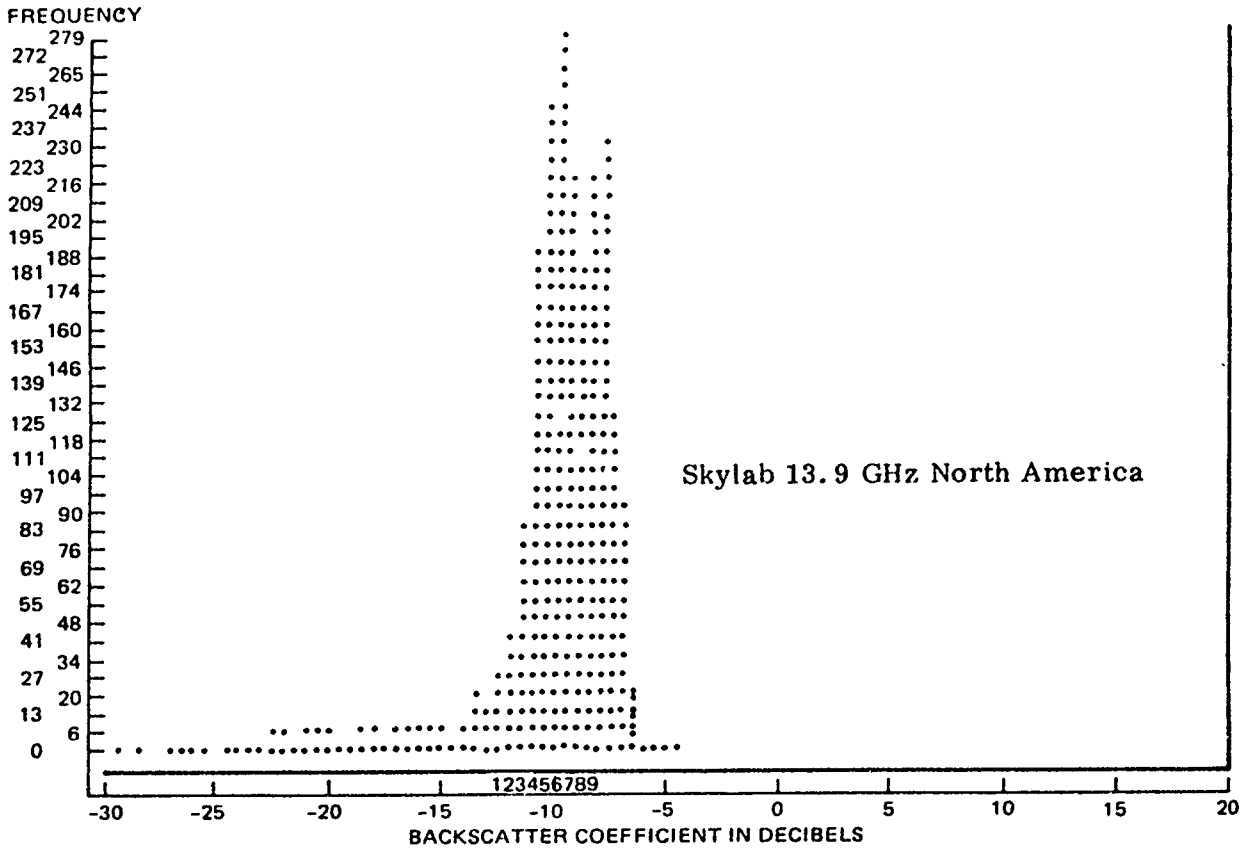

Figure 23a. Histogram of the Scatterometer Backscatter Coefficient, North America, From A. Sobti, "Terrain Repsonse to an Orbiting Microwave Radiometer," Tech RPT 243-10, U. of Kansas Center for Research, Inc., 1975.

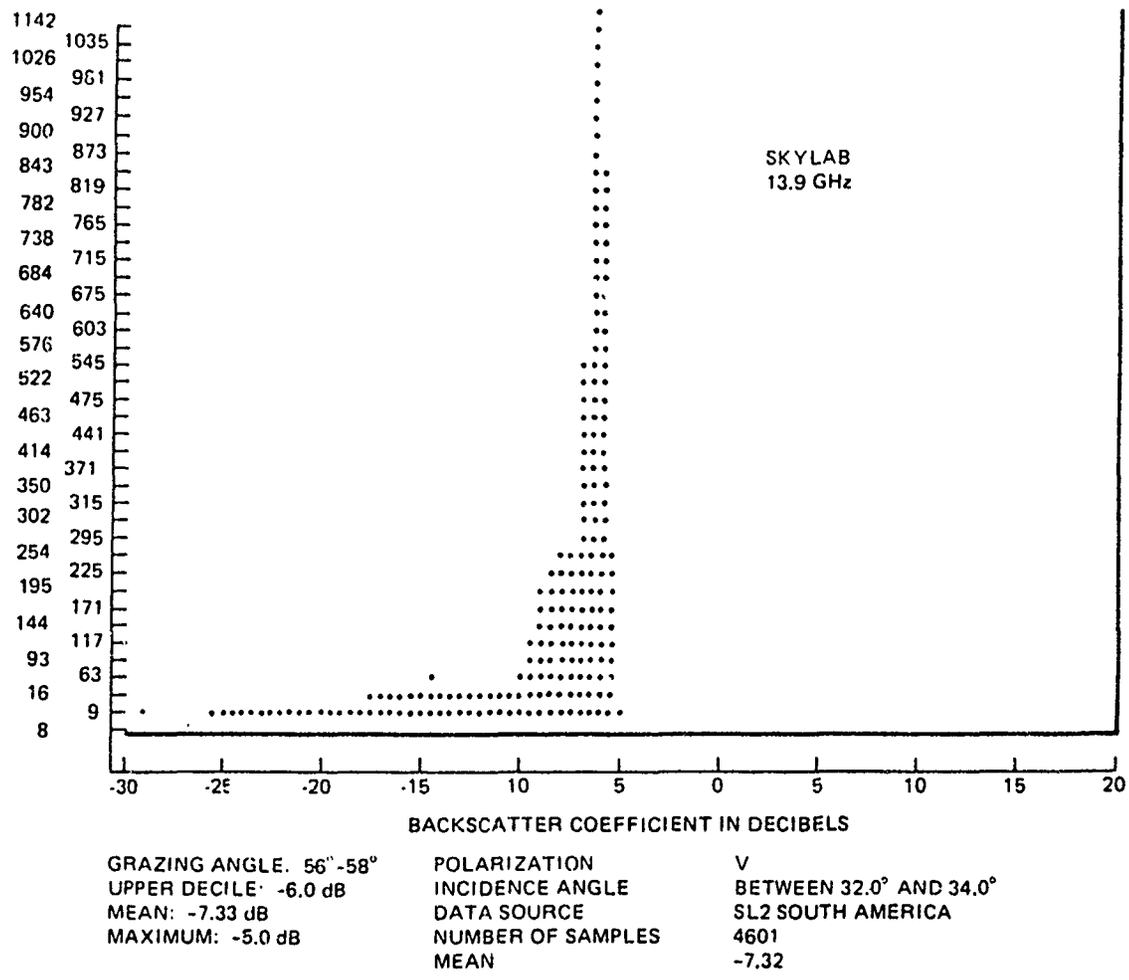

Figure 23b. Histogram of the Scatterometer Backscatter Coefficient, South America; From Sobti, ibid.

decreasing grazing angle, Fig. 24. This behavior is consistent with other data also.

The averaging effect of resolution cell size is complicated by other phenomena which depend on cell size. For example, some terrain may resemble a geometrical shape with a smooth surface. When the resolved areas are smaller than the size of the piece of terrain, the returns are from individual pieces and may appear fairly uniform. However, as the cell size increases the piece of terrain acts as a single scattering center and the distribution of observed RCS is qualitatively different. An example of this is the specular parts of the SKYLAB distribution discussed above. Another hypothetical example is terrain made up of flat areas randomly oriented with respect to the radar. Each facet has a radiation pattern of the form sin (x)/x where x is proportional to the angle of the radar relative to the facet nominal. Assuming x is a random variable, the distribution which results resembles lognormal when each facet is sampled separately.

With these complications in mind, we present other distributions. First there are synthetic aperture radar (SAR) data[1] measured by the Environmental Research Institue of Michigan (ERIM). The SAR technique is used normally for high-resolution imaging of the ground. Figure 25 shows X-band data for mountains, crops, and a city, for two resolution sizes, 10' x 10' and 20' x 20'. These cells were obtained by incoherently adding even higher resolved cell size.

Another example involves a RADC study of the Seek Igloo Radars.[2] These are ground radars whose beams can be directed at nearby clutter. RADC measured probability distributions by setting thresholds and counting

---

[1] ERIM, private communication.

[2] W. L. Simkins, et al., Seek Igloo Radar Study, Rome Air Development Center, RADC-TR-77-338, (October, 1977), A047897.

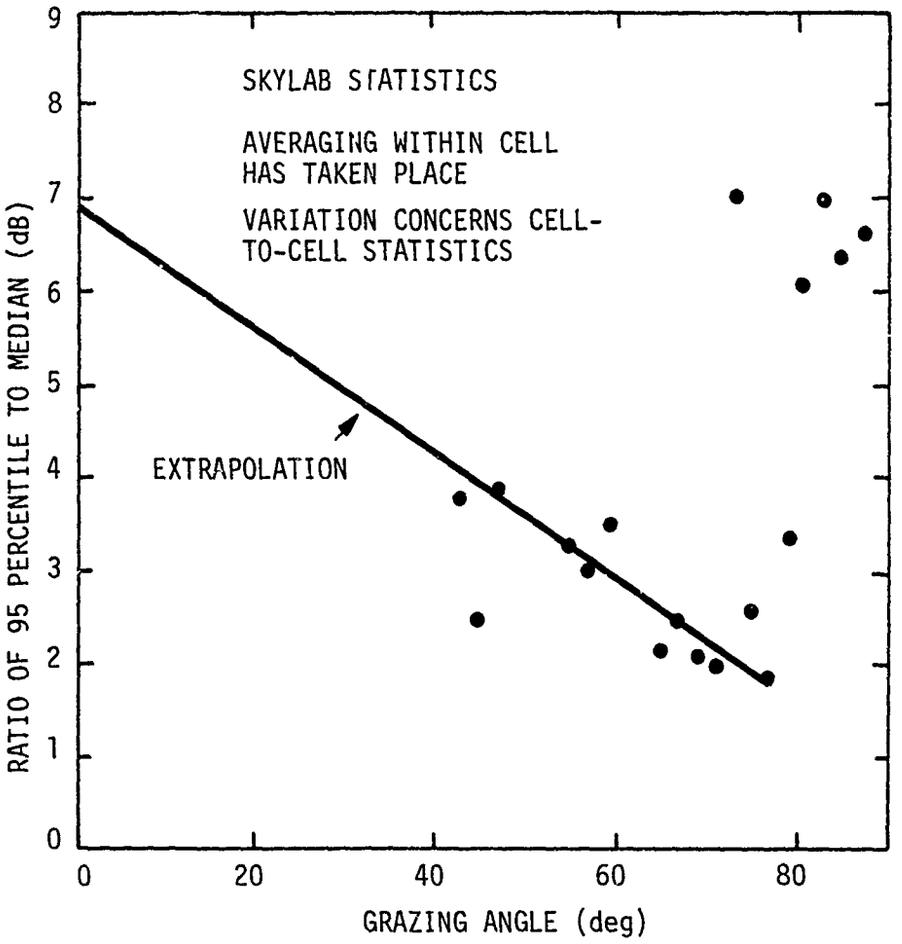

Figure 24. Distribution of SKYLAB Data versus Grazing Angle

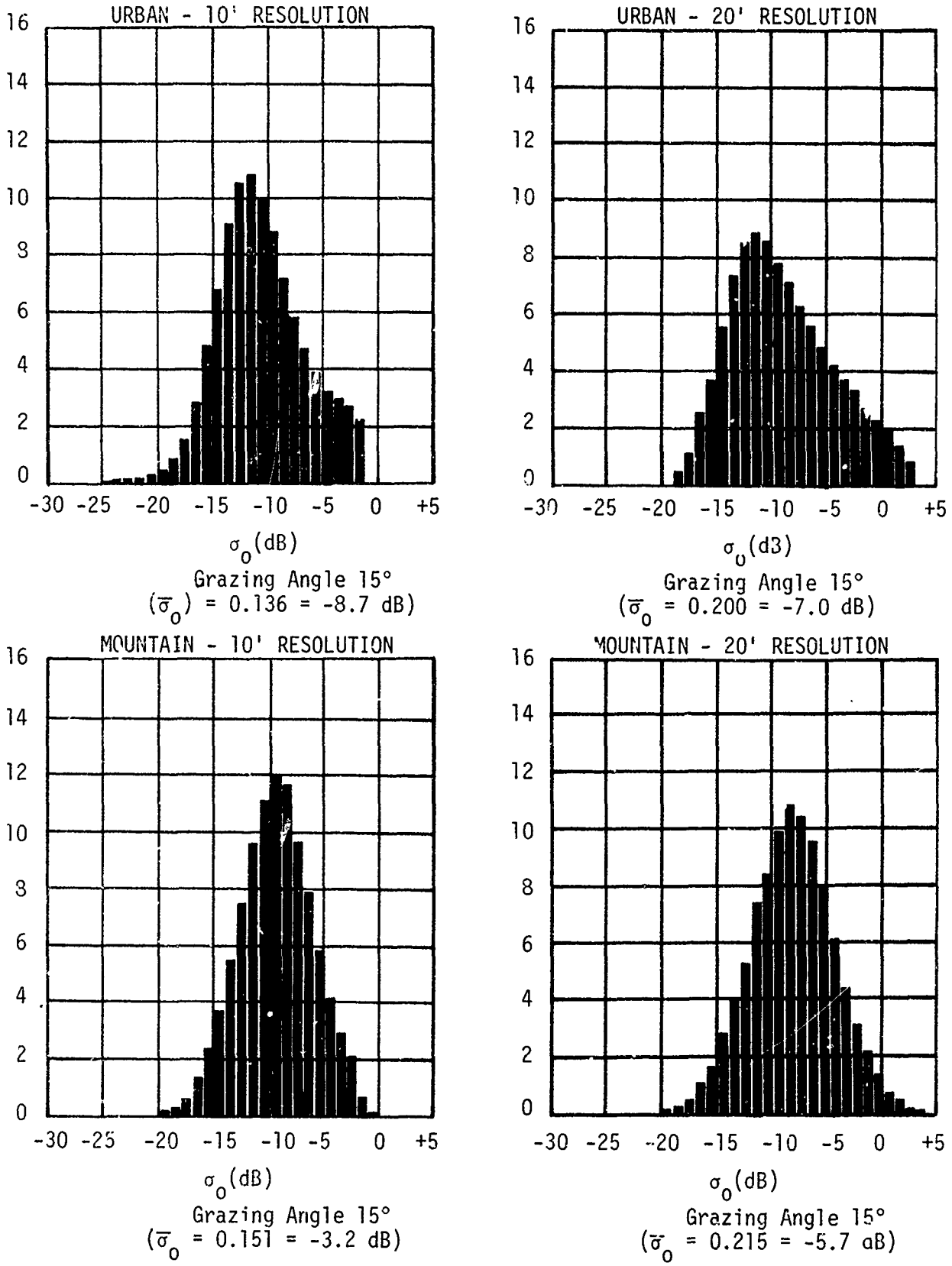

Figure 25. ERIM X-band SAR Histograms (Pol = HH)

false alarms. Presumably, Rayleigh-type interference effects are included. Additionally there is a greal deal of terrain masking due to the low grazing angles. Resolution cells are quite large and were varied by changing the range resolution (or pulse width τ). Several terrain types were observed. Most were hills and mountains but some swamp land was also included. Examples from the RADC report are shown in Figs. 26 and 27. In general, the distribution from hills and mountains is much broader than the swamp land. Also in almost every case the probability of exceeding a high value of $\bar{\sigma}^\circ$ is smaller for the larger resolution cells (e.g., Fig. 26) indicating that an averaging is taking place. The extremely broad distribution for hilly terrain should probably be replotted with the terrain-masked areas eliminated. This is shown in Fig. 28; for curve 20 in Fig. 27, note that this distribution is much more in line with what one would estimate based on the variability factors we have discussed above, and with other data.

4.4 MANY SCATTERER THEORY

We have discussed clutter distributions so far in a very general way, avoiding until now an analysis of its impact on threshold settings, detection, and false alarms. We feel that too much has been made of the shapes of distributions and curve fitting to predict detection statistics and false alarms. The reason is that, for acceptable false alarm rates, the signal-to-clutter ratio must be very high; therefore only the extreme tails of the distribution are of real interest. There is no data at this extreme so that predictions are usually based on excessive extrapolation.

Our model is based on the idea that the expected values of σ° can vary due to the various factors listed above, and that one can estimate and predict a distribution of mean σ°.

Let us define amplitude A as $\sqrt{\sigma^\circ}$. The problem reduces to predicting amplitude and phase of the combined echos

$$Ve^{i\phi} = \sum_{j=i}^{N} A_j \, e^{i\varphi_j} \qquad (4\text{-}5)$$

CURVE NO.	PLACE	DATE	τ usec	TERRAIN TYPE	AREA NO.
13	TATALINA	25 AUG	6.0	SWAMP	7
16	TATALINA	25 AUG	3.0	SWAMP	7
21	TATALINA	25 AUG	1.0	SWAMP	7
23	TATALINA	25 AUG	0.5	SWAMP	7

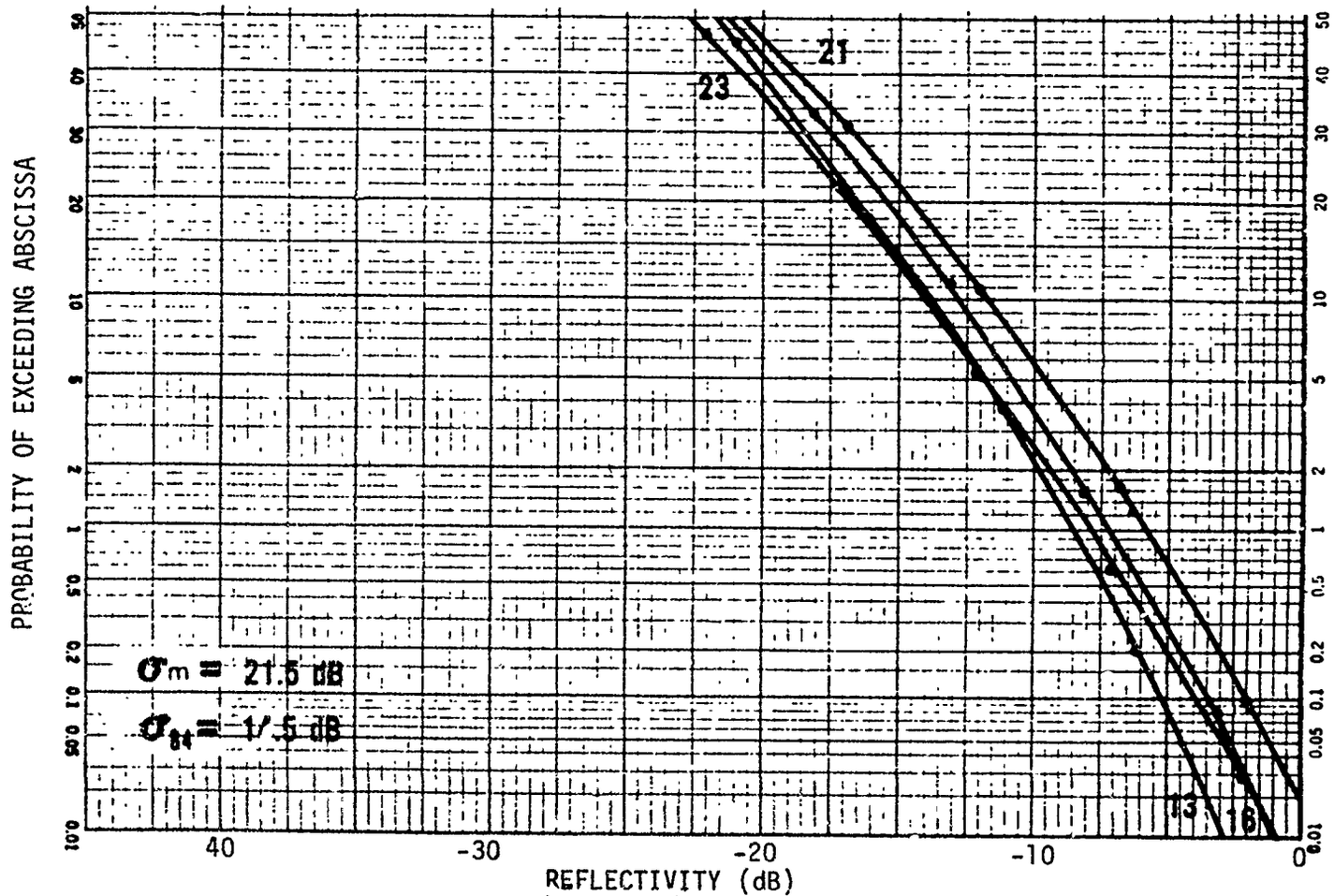

Figure 26. Swamp (Tatalina), from W. Simkins et al.

CURVE NO.	PLACE	DATE	τ usec	TERRAIN TYPE	AREA NO.
19	TATALINA	25 AUG	1	MOUNTAINS	9
20	TATALINA	25 AUG	1	HILLS	6
21	TATALINA	25 AUG	1	RIVER BEDS & SWAMP	7

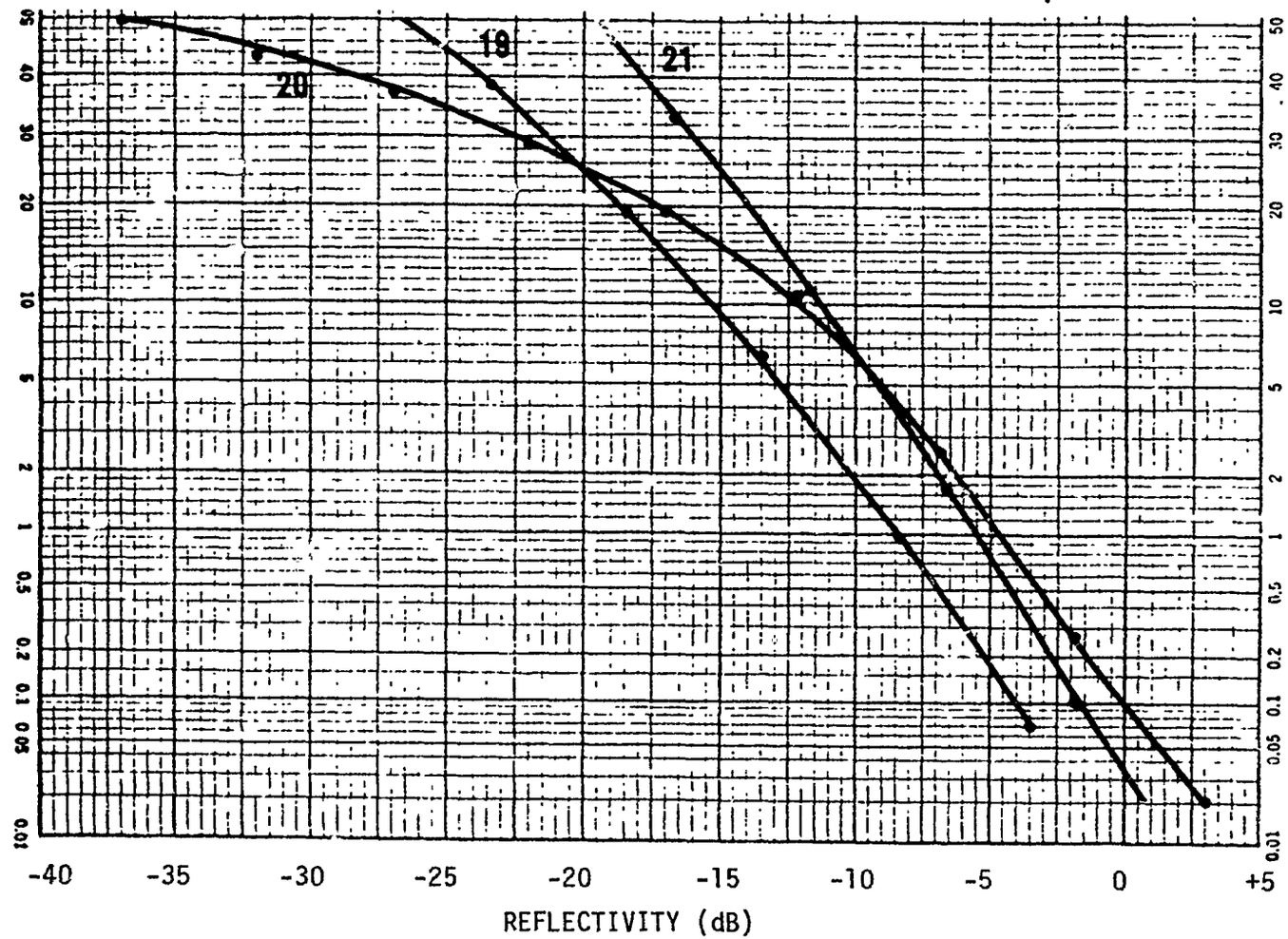

Figure 27. Comparative Distributions (Tatalina), from W. Simkins, et al.

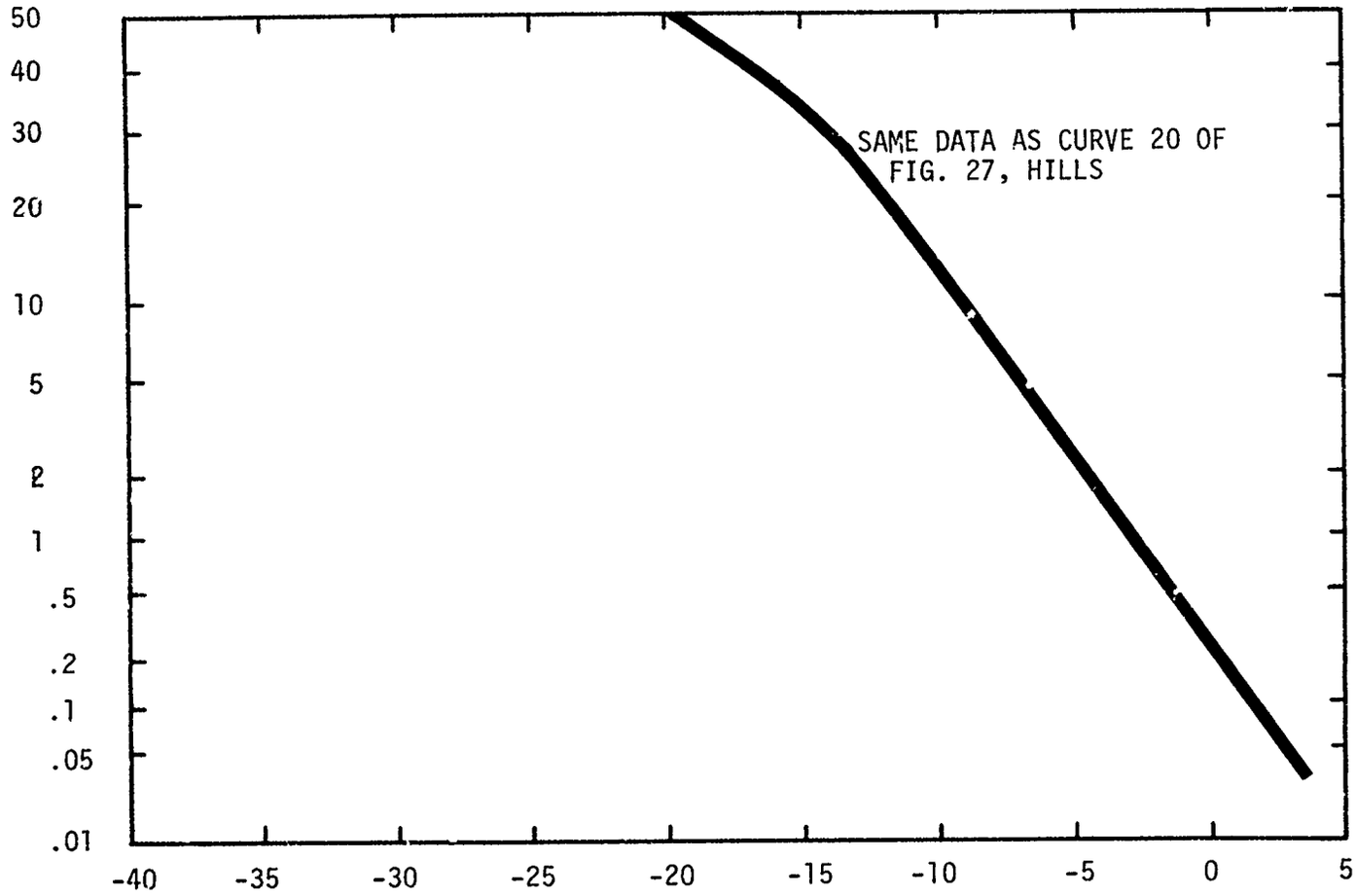

Figure 28. pdf of Non-Shadowed Part of Hilly Terrain

Assuming A_j and Φ_j are statistically independent and Φ_j is uniformly distributed over a full period. Beckmann[1] has shown that to order N^{-1} where N is the number of independent scatterers the pdf of V is given by

$$P(V) = \frac{2V}{I_o} e^{-V^2/I_o} \left\{ 1 + \frac{3}{8N} \left[\frac{E(A^4)}{E^2(A^2)} - 2 \right] \left[\frac{V^4}{2I_o^2} - \frac{2V^2}{I_o} + 1 \right] \right\} \quad (4\text{-}6)$$

where $I_o = NE(A^2)$ and E(x) denotes expected value. Therefore, defining $\sigma = V^2/I_o$, the probability of exceeding any given value σ is given by

$$P_c(\sigma) = e^{-\sigma}(1 + \beta[\sigma^2/2 - \sigma]) \quad (4\text{-}7)$$

where

$$\beta = \frac{3}{8N} (\alpha - 2)$$

and

$$\alpha = E(\sigma^2)/E^2(\sigma) = E(A^4)/E^2(A^2)$$

This tells us exactly how the averaging process of large cell sizes influences the probability distribution. For example, assuming a correlation length ℓ, N approximately equals A_R/ℓ^2 where A_R is the resolution cell area. Eq. 4-6 shows that as A_R approaches infinity, P(V) approaches Rayleigh.

In the limit, where resolution cells are small, N is small so that each cell may contain a different clutter of a different expected amplitude. In the case of N = 1, then obviously

$$P(V) = P(A)$$

[1] P. Beckmann, Probability in Communication Engineering, New York: Harcourt, 1967.

Note that the parameter β in Eq. 4-7 is actually a measure of how closely the clutter pdf resembles a Rayleigh distribution. For $\beta = 0$ the distribution is Rayleigh. Also note in the definition of β in the line below Eq. 4-7 that a small value of β can occur for either of two reasons: large number N of independent scatterers in the resolution cell, and $\alpha = 2$ which occurs if the underlying pdf of individual scatterers is Rayleigh.

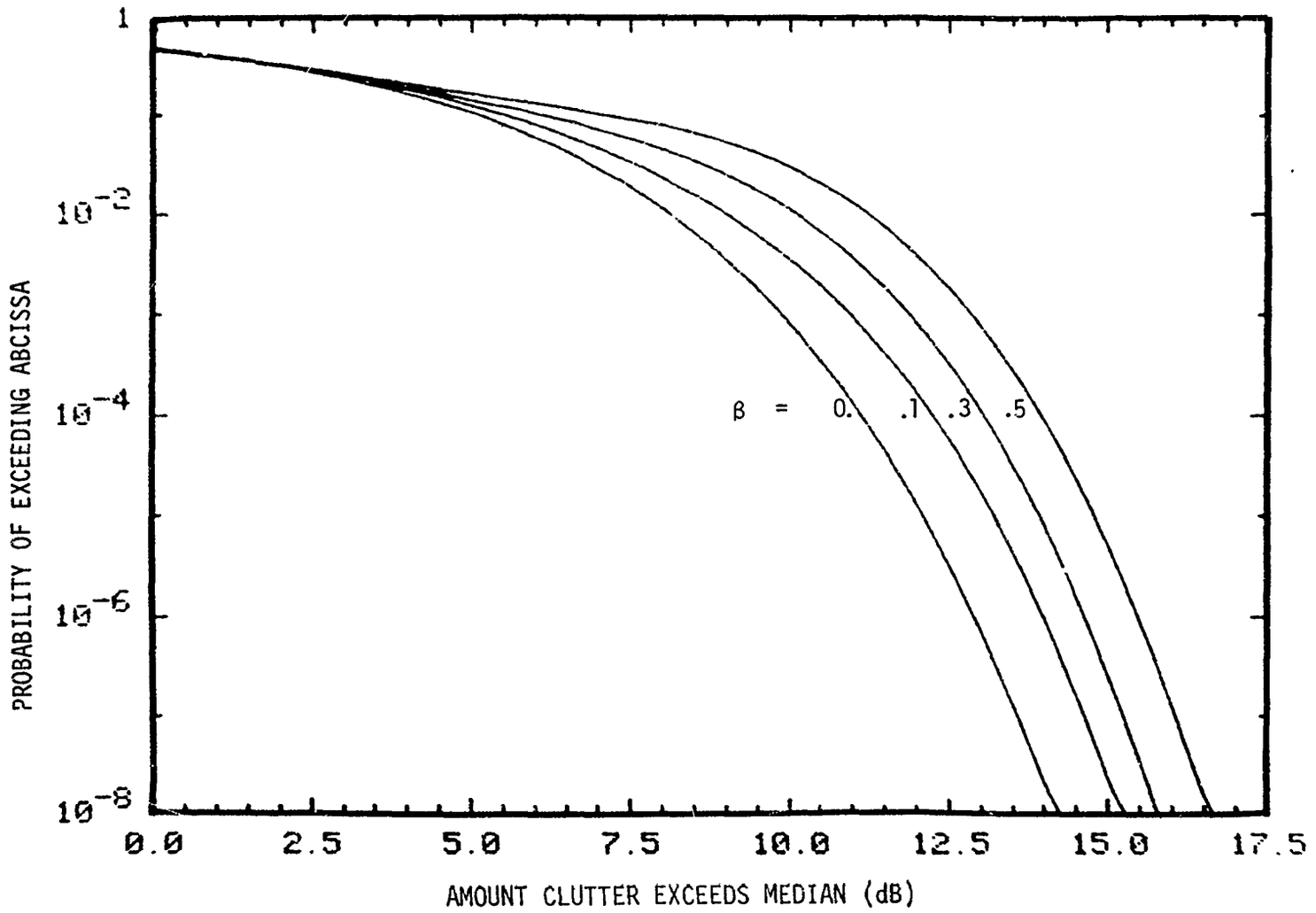

Figure 29. Probability of Exceeding Median Versus σ

$$\text{BETA} = \frac{3}{8N}\left[\frac{E(\sigma^2)}{E^2(\sigma)} - 2\right]$$

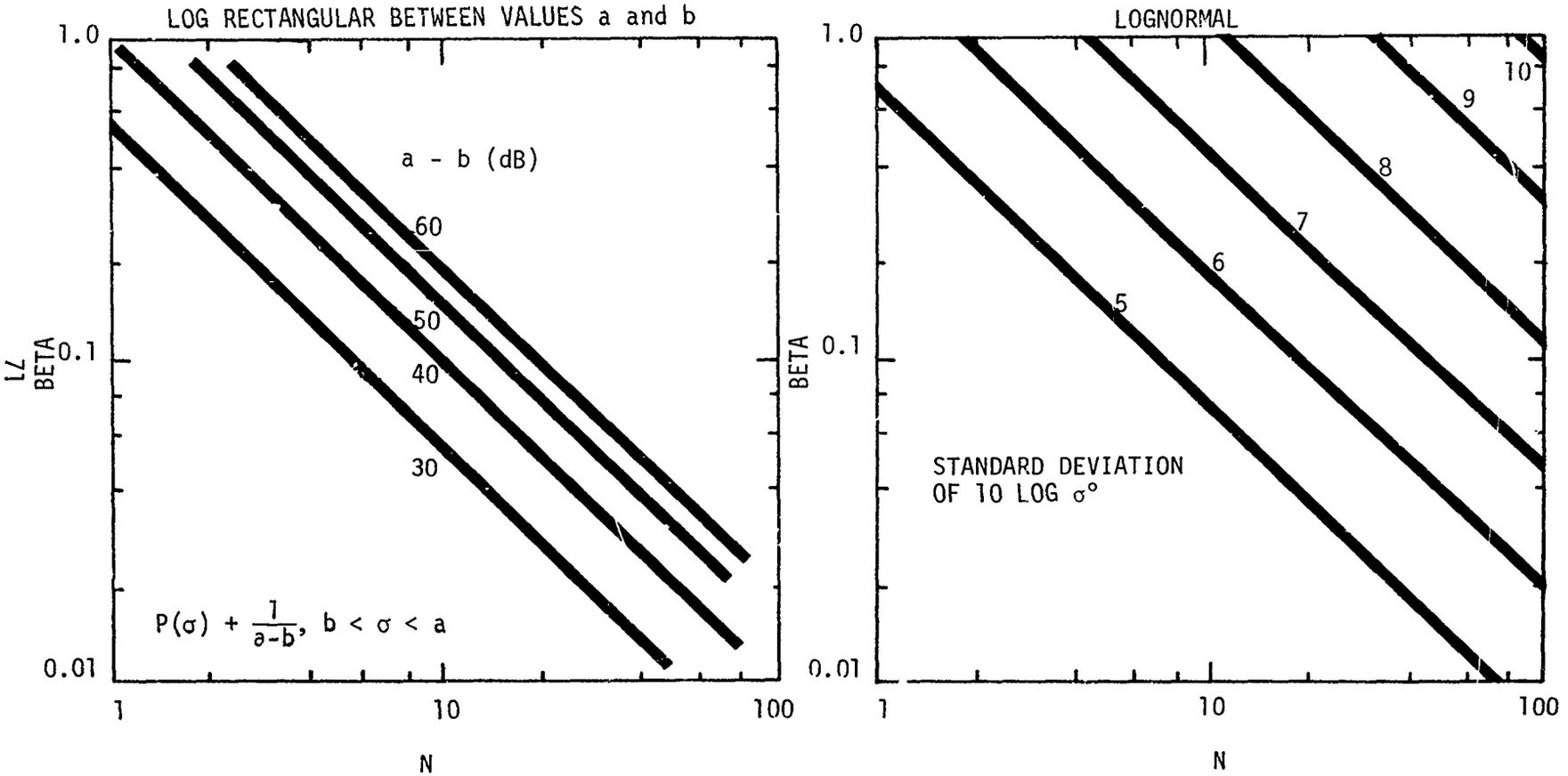

Figure 30. Plot of BETA versus N for Lognormal and Log Rectangular

The fact is that there is no single number such as correlation length which can completely describe the effect. For example, there is a correlation length associated with terrain undulation, another associated with changes in vegetation, another associated with major variations in terrain type, etc.

The Skylab data[1] shows that some of these correlations lengths may be very large. There, the resolution cells were very large, 400 to 1000 square kilometers. Yet there is a variation of about five dB in the mean $\bar{\sigma}^\circ$ from cell to cell. This is an indication of either the variation in scattering properties of the clutter, or a failure to average enough samples within each cell to remove the Rayleigh effects.

On the other hand, there is a component which has a very short correlation length, namely discretes. In general, one could probably estimate the most important correlation lengths by looking at contour maps or (even better), SAR radar images.

Some experimental data has been gathered by IIT[2] to determine the autocorrelation function of clutter. To be meaningful, the Rayleigh effects should have been averaged out and the resolution of the experimental radar should be less than the correlations of interest.

The question which now arises is how to estimate the number of independent scatterers, N, and $P_A(A)$ from which to compute $E(A^4)/E^2(A^2)$. Logically these should be obtained from single-look experimental pdf's and autocorrelation functions where the experimental resolution is fine enough to resolve individual scatterers. The IIT results are based on a 100 ft^2 resolution area and some of the Rayleigh effects are averaged out. If $P_A(A)$ is based on many-look samples, and does not include the Rayleigh spread, one can define $P_{A'}(A')$ and redefine β' as

---

[1] S. M. Purduski, ibid.

[2] S. Kayel et al., Extensions to the ORT Clutter Model, IIT Technical Report under Contract No. F33615-69-C-1387 (1971).

$$\beta' \doteq \frac{3}{8N} \frac{E(A^4)}{E^2(A^2)} \tag{4-9}$$

If not all of the Rayleigh effects have been averaged out, the error which results from redefining β in this way makes the analysis slightly conservative. Also, in general, $N' < N$ since averaging tends to smooth the terrain return resulting in a longer correlation length.

The effective value of N' is obtained from the autocorrelation function $\Gamma(x)$. We derive N' from Γ in the following manner:

For independent samples, the ratio of the variance of the individual samples, δ^2, to samples of ensemble averages of N samples each, δ_N^2, is just N. Thus

$$N = \frac{\delta^2}{\delta_N^2} \tag{4-10}$$

If they are not independent, we compute δ_N^2 and define the effective N as in the above equation. In order to do this, it is convenient to confine ourselves to the variable component of the clutter return. The total clutter return is given by

$$C(X) = V(X) + \mu$$

where

$$\int_{-\infty}^{\infty} V(x)\, dx = 0 \tag{4-11}$$

Therefore the following discussion is simplified by considering a function of mean zero, V(x).

If V(x) is sampled at a large number of x values and averaged within an interval δx, the variance of the averages is given by

$$\delta_N^2 = \frac{2\delta^2}{x\delta} \int_0^{\delta x} \Gamma(x)\, dx \qquad (4\text{-}12)$$

where $\Gamma(x)$ is defined as the expected value of the product

$$V(x' + x)V(x')$$

divided by $E[V^2(x)]$ and is computed by taking the autocorrelation of V(x)

$$\Gamma(x) = \frac{\int V(x' + x)V(x')\, dx}{\int V^2(x)\, dx} \qquad (4\text{-}13)$$

IIT computed the autocorrelation functions of the variable component of σ° for four terrain types. These are shown in Fig. 31. These are only experimental approximations to the true autocorrelation functions which should be smooth. Our approximations to the true values based on IIT's experimental evidence is shown in Table 4.

Note that δx is a strip of continuous clutter. If there are ambiguous range strips spaced more than about 2 nmi apart, each strip contributes additional independent samples.

Thus, the effective values of N for each clutter type is given below from Eq. 4-10, for N_{amb} ambiguous ranges:

	N (effective)
Desert	$(\delta x/0.79) \times N_{amb}$
Farms	$(\delta x/0.72) \times N_{amb}$
Mountains	$(\delta x/0.24) \times N_{amb}$
Cities	$(\delta x/1.12) \times N_{amb}$

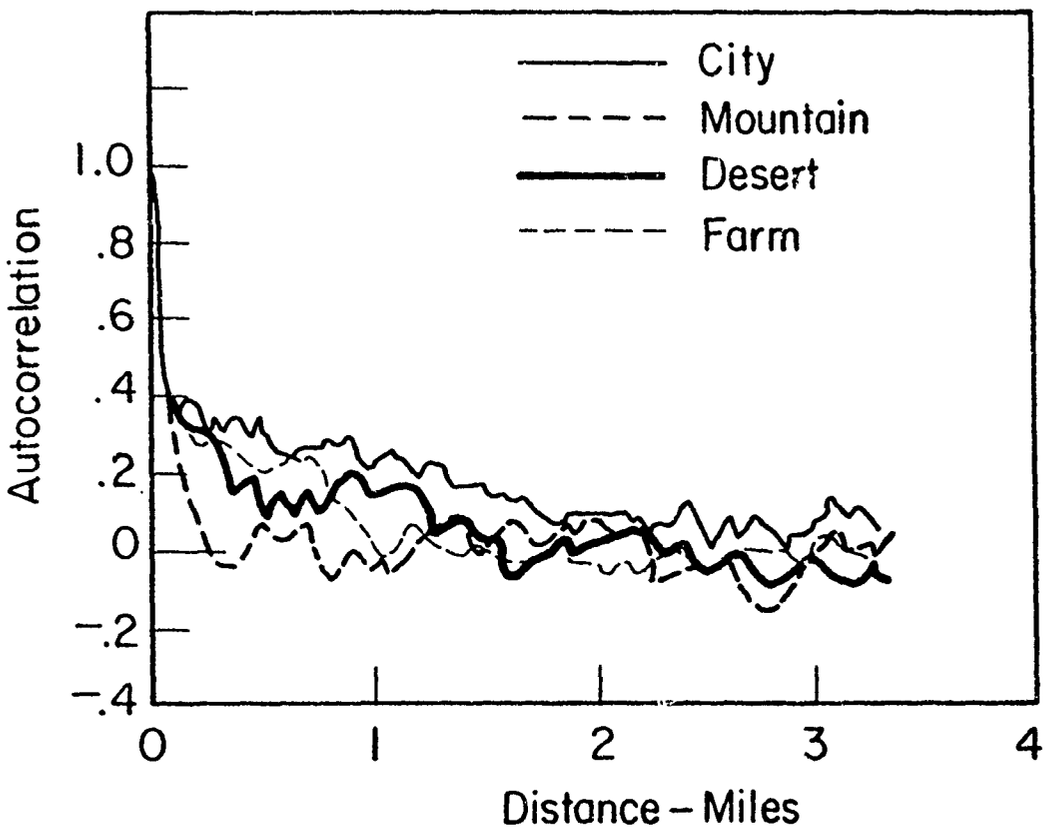

Figure 31. Autocorrelation of Variable Component of Several Terrains, from S. Kazel et al.

TABLE 4

AUTOCORRELATION FOR FOUR TERRAIN TYPES

TYPE 1. $r(x) = a\, e^{-x/C} + b \quad x \leq x_0$

$= 0 \quad x > x_0$

	a	b	c (nmi)	x_0 (nmi)
Desert	0.8	0.2	0.18	1.25
Farm	0.75	0.25	0.18	0.9
Mountain	1.0	0.0	0.12	∞

For cities the form is slightly different:

TYPE 2. $r(x) = 0.6\, e^{-x/0.27} + 0.4(1 - x/2) \quad x \leq 2$ nmi

$= 0 \quad x > 2$ nmi

IIT did not compute $\Gamma(x)$ for woods, but a correlation length of 1 nmi, based on other terrains, seems a reasonable and conservative estimate. Therefore, we estimate for woods,

$$N_{eff} = (\delta x/1) \times N_{amb}$$

4.6 EXAMPLES AND PREDICTIONS FOR FIVE TERRAIN TYPES

This section describes a procedure for predicting the threshold settings, above median clutter, required to achieve a given false alarm probability. It is based on experimental data and the distribution suggested by Beckmann. Examples are worked out, based on the SAR data of IIT.[1] This data was analyzed expressly for the purpose of clutter modeling. Five terrain types were considered: desert, woods, farms, mountains and cities. Grazing angles were not reported.

We shall begin with a review of the theory of Sec. 4-4 in order to set the requirements for RCS and scattering. It states that if amplitude and phase are independent and the pdf of amplitude, P(A) is independent and uniformly distributed, then the pdf of the power resulting from the sum is given by Eq. 4-6 or 4-7 with β replaced by β' of Eq. 4-9 if Rayleigh effects have been eliminated by averaging.

The pdf's for desert, woods, farm, mountain, and city, are shown in Fig. 32. For desert, woods, and mountain, the distributions are nearly lognormal. For farms the distribution is approximately the sum of two normal distributions or contaminated lognormal. For cities it is well described by breaking the region into two sections and performing straight-line fits (on log-log paper) in each sector. The resulting parameters are given in Table 5. IIT could not calibrate the data, so the mean values of these distributions are meaningless in themselves.

---

[1] S. Kazel et al., ibid.

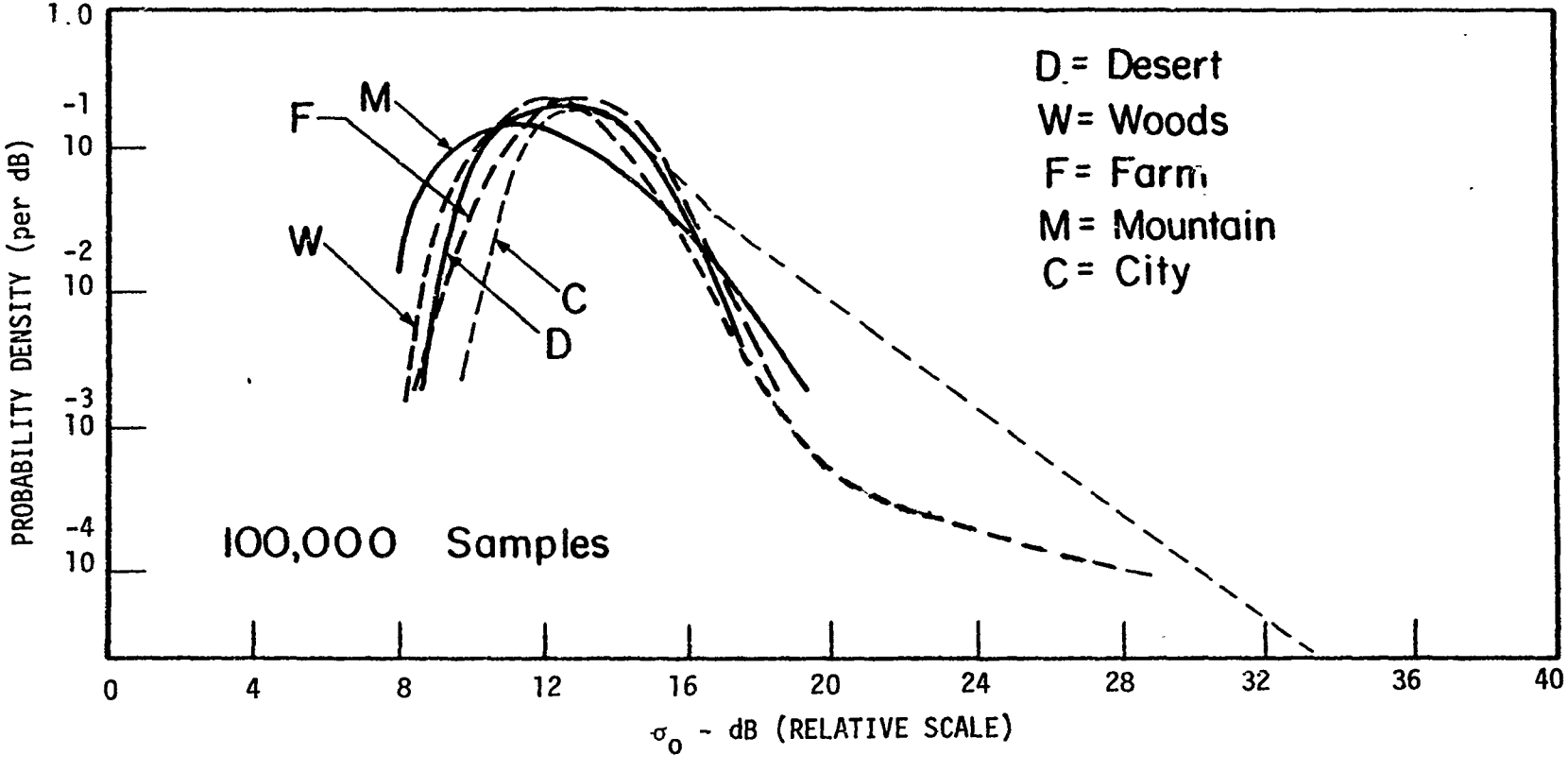

Figure 32. Comparison of Probability Density Function for Various Terrains from S. Kazel et al.

TABLE 5

PROBABILITY DENSITY FUNCTIONS

1 and 2. Desert and Woods

$$P(u) = \frac{1}{\sqrt{2\pi}\ \sigma}\ e^{-u^2/2\sigma^2}$$

$$u = 10\ \log_{10}(A^2)$$

$$\sigma = 2.1\ \text{dB}$$

3. Farms

$$P(u) = \frac{.98}{\sqrt{2\pi}\ \sigma_1}\ e^{-u^2/2\sigma_1^2} + \frac{.02}{\sqrt{2\pi}\ \sigma_2}\ e^{-u^2/2\sigma_2^2}$$

$$\sigma_1 = 1.17\ \text{dB}$$

$$\sigma_2 = 8.60\ \text{dB}$$

4. Mountain

$$P(u) = \frac{1}{\sqrt{2\pi}\ \sigma}\ e^{-u^2/2\sigma^2}$$

$$\sigma = 3.02\ \text{dB}$$

5. City

$$P(u) = 3.4 \times 10^{-15}\ u^{11.4} \qquad u \leq 15$$

$$= 9.23\ u^{-1.9} \qquad u \geq 15$$

TABLE 6

SUMMARY OF STATISTICAL PARAMETERS

TERRAIN	pdf	$E(A^4)/E^2(A^2)$	N'	β'	T_1	T_2
Desert	lognormal	1.27	253	0.0019	12.6	14.3
Woods	lognormal	1.27	200	0.0024	12.6	14.3
Mountain	lognormal	1.64	833	0.0022	12.6	14.3
Farms	contaminated lognormal	1.69	278	0.0023	12.6	14.3
Cities	power laws	9.04	178	0.0190	14.3	15.5

Assumptions:

δx = 10 nmi

N_{amb} = 20

T_1 = implies 10^{-6} false alarm probability

T_2 = implies 10^{-8} false alarm probability

From these pdf's we compute the ratio $E(\sigma^2)/E^2(\sigma)$, and hence β' for each terrain type. This was straightforward for all terrain except "city". Here the second moment is infinite unless an upper bound is placed on the highest σ. We chose 36 dB because this is the highest value on IIT's reported pdf. These are presented in Table 6 along with estimated values of effective N'. Also using Fig. 29 or Eq. 4-7 we obtain the appropriate threshold, relative to the median $\sigma°$, required for the given alarm probabilities.

The above is appropriate for a single terrain type in the footprint. If a CFAR is used which operates on local areas smaller than the footprint, it is appropriate for the more general case where each local area is composed of at single type of terrain.

We have considered the case also where there are M areas each having a different type of terrain. Then, there is roughly a log rectangular distribution for P(u) and the number of independent samples is N. The width of the distribution is a most 20 dB. We obtain

$$\frac{E(A^4)}{E^2(A^2)} = 2.3$$

Assuming $N \approx 10$,

$$\beta' = 0.086$$

We conclude from this exercise that there is little cause for concern for high tail clutter returns in a typical pulse-Doppler surveillance SBR. In a SAR mode, however, the fine resolution would greatly reduce the number of independent scatterers and probably require thresholds higher by 1 to 5 dB than those called for by Rayleigh statistics. Over cities, the threshold would have to be 10 to 20 db higher than called for by Rayleigh statistics.

Nevertheless, although the pdf's measured by IIT cover much higher tails than most, it is desirable to examine the high tails more closely to increase our confidence in β'.

5.0 CLUTTER SPECTRA

In addition to the total magnitude of clutter in the resolution cell, the frequency spectra of its radar echos is also critical for moving target indication (or detection), MTI. This is because, in a look-down geometry, the earth reflection will totally dominate most tactical targets. As a result, the Doppler signature must be used to separate moving targets from the stationary earth.

However, a number of factors can cause the clutter to have a finite Doppler spread, resulting in a cut-off velocity for detecting slow targets. These factors include, platform motion and earth rotation, internal motion of clutter, and glint effects.

Platform motion and earth rotation, in addition to producing a finite shift of the center line also cause a spread due to the finite beamwidth. The spread due to platform is given by

$$\frac{2V_p}{\lambda} \theta_\beta \cos \phi \qquad (5\text{-}1)$$

where θ_β is the effective beamwidth, and ϕ is the squint angle.

Earth rotation is usually a much smaller effect but can become comparable to platform motion at high altitude. In general, it can either add to or cancel the spread due to platform motion. In a geosynchronous orbit they cancel exactly.

The internal motion of clutter is usually very small for wind-blown vegetation. It would not be an important consideration unless platform motion effects were eliminated by a displaced phase center antenna (DPCA) and very slow target detection were required.

Other types of clutter with internal motion are weather and land vehicles. Wind-blown weather has a shift relative to the ground and a

finite width. Land vehicles can also be a problem for slow target detection in that they have an RCS of the same order of magnitude as air-vehicle targets and there may be many of them present in each resolution cell. Of course this is less of a problem in the arctic. Table 7 gives some rough order of magnitude velocity spreads from various sources. Figure 33 is an example of a measured clutter spectrum from wind-blown vegetation.

TABLE 7

INTERNAL VELOCITIES OF CLUTTER

Type	Velocity Spread m/sec
Vegetation	0 to 1*
Weather	25
Land Vehicles	30
Civilian Aircraft	200
Birds	18
Boats	10
Sea	5

*Depends upon wind velocity

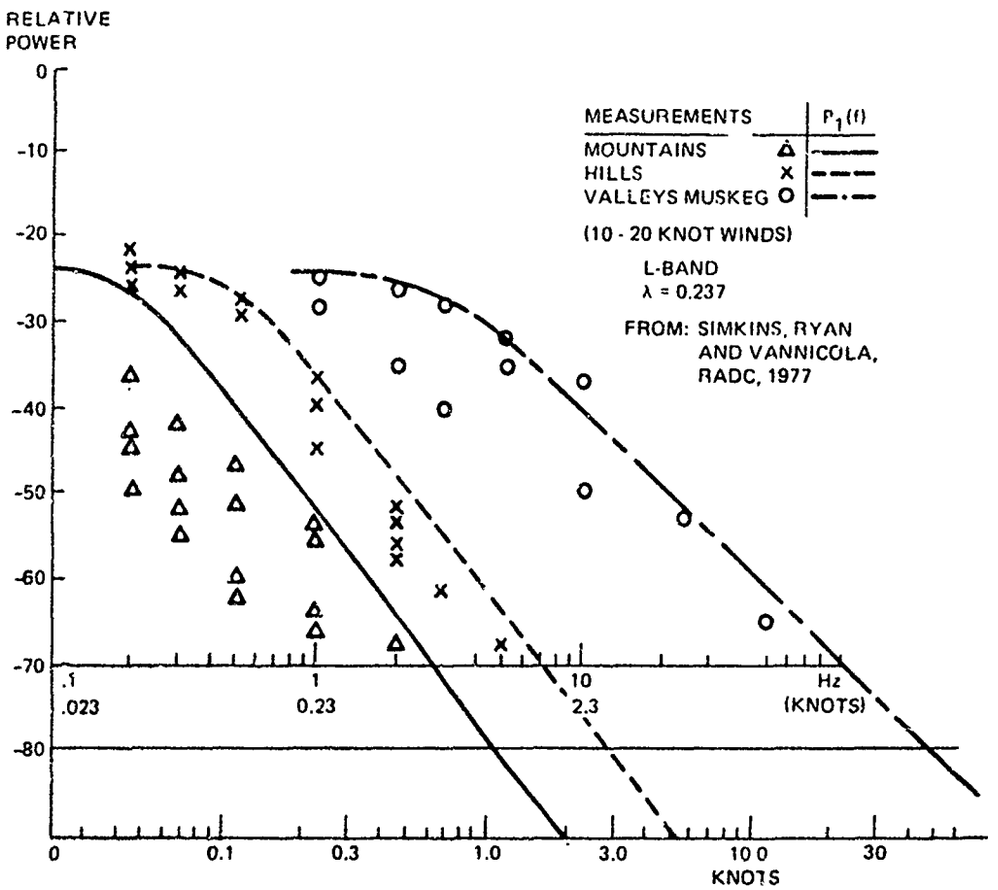

Figure 33. L-Band Power Spectral Density of Alaskan Land Clutter

6.0 RECOMMENDATIONS FOR FURTHER DEVELOPMENT

We feel that about as much meaningful information as possible has been extracted from the present clutter data base. We have performed parametric fits to seven terrain types using two parameters and data from several sources. In addition, the University of Kansas has taken extensive data on crops, snow, sea ice, and forest. They have performed detailed fits in incidence angle and frequency for different polarizations and time of year.

However, there are shortcomings in the present data base which could be improved by further experiment and/or computer synthesis. The following are areas where more information is needed:

1. arctic terrains
2. low grazing angles ($< 10°$)
3. large resolution cells
4. better calibration of data for all frequencies and terrains
5. distributions

Data is needed for arctic terrains because a surveillance fence is required over northern Canada and Greenland against a Soviet attack against CONUS. There are little data for grazing angles less than 10° for any terrain type, and what data there are sometimes contradict each other. It is dangerous to extrapolate from higher angles because the nature of the scattering is qualitatively different for very low grazing angles.

The space radar systems popularly considered at this time have large resolution cells. That is, they are large compared to the resolution of most clutter experiments but small compared to that of SKYLAB. To test the results of our false alarm analysis, resolution cells of the order of 10 miles by 100 meters with a number of range ambiguities is required. There is a need for better calibration; calibration should be a major factor in considering future measurements. Finally, more emphasis should

be put on distributions of RCS about the mean values. It is the fraction of clutter cells which exceed a threshold several dB above the mean which is most important for most SBR missions. The analysis of this report indicates that the distribution is effectively Rayleigh but that remains to be shown experimentally. Most of these requirements point to an actual SBR experiment; however, much could be done as well by an airborne experiment.

Three candidate experiments have been considered:

1. Analysis of the L-band SAR data from SEASAT.
2. Calibration and analysis of L-band and X-band data taken by ERIM over various sites in Canada.
3. An airborne experiment designed by Spectra Research Corporation (SRC) for the purpose of simulating an SBR clutter scenario.

Table 8 summarizes these three experiments with respect to frequency, terrain, grazing angles, and resolution. Of the three, the one which seems most likely to produce information valuable to clutter modeling of SBR is the ERIM data. With SEASAT, the grazing angles are too high and there is only one frequency. Nevertheless, SEASAT data does exist and there are plans by the Defense Advanced Research Projects Agency and Lincoln Laboratory to analyze it with emphasis on large-cell clutter and targets. Although the SRC experiment covers the most relevant scenarios, it has higher technical and financial risk because the required hardware has not been assembled.

There is also the possibility that computer synthesis of data will answer some of the pressing questions at a fraction of the cost of an actual experiment. This would be accomplished by modeling a scene in great detail within a variety of terrain, hills, discretes, etc. The

TABLE 8

SUMMARY OF THREE CANDIDATE CLUTTER PROGRAMS

Candidate Experiment	Frequency	Terrains	Grazing Angles	Resolution
ERIM	L-band X-band	Various terrains in Canada	Choice of 5° to 90°	1.5 m x 1.5 m or larger
SRS/ARIA	L-band S-band	Not specified	0° - 30°	As small as 90 m x 3 km to as large as 900 m x 40 km
SEASAT	L-band (SAR) 1.25 GHz	Sea most of No. America	67 - 73°	25 m x 25 m 25 m x 15 km
SEASAT	K_u-band (SASS) 14.95 GHz	Sea unspecified parts of North America	25° 65°	≤50 km x 50 km

RCS of each scatterer would be estimated from extensive existing data. Then the pdf of clutter magnitude for each scene could be generated as a function of resolution by combining the scatterers, in amplitude and phase, in the computer as they would combine in a radar.

These are a few of the possibilities. It is probably safe to say that clutter will never be understood completely because there are so many different variables to control (e.g., resolution, frequency, angles, season, time of day, etc.).

7.0 SUMMARY AND CONCLUSIONS

In summary, a clutter model has been developed for use in space-based radar analysis. Those aspects of clutter unique to or prevalent in space radar have been identified and discussed. In short, those aspects identified were: large resolution cells, large footprints, range ambiguous mainbeam, high platform velocity, and (except for high resolution SAR) dominance of discretes by distributed clutter.

Existing clutter measurement data were entered into a computerized data base and categorized by terrain type, polarization, frequency, grazing angle, and source for convenient reference and retrieval. Parametric fits were performed on each of the seven terrain types to reduce the data to analytic expressions. These results are discussed in Section 3. In general, the fits agree qualitatively with those performed by other investigators. They differ from others, however, in that they cover data from a variety of sources and in the particular formulation of the models. These results are summarized in Table 1.

In addition to models for average σ°, the variation of clutter echos about the mean, and in particular, the probability of them exceeding the mean by a great deal, is of great concern for detection of targets in clutter. These issues are discussed in Section 4. There the different mechanisms, variation in terrain type, local undulations in slope, man-made objects, variation in local conditions (moisture content, orientation of crop rows, etc.), are discussed and to some extent quantified. A theory is introduced for predicting the pdf of clutter based on the underlying pdf of the individual scatterers, resolution cell size, and spatial autocorrelation function. Based on the theory, examples are worked out for five terrain types and a large footprint SBR geometry of the predicted threshold settings for two values of false alarm probability. These examples show that the thresholds differ very little from those derived from a Rayleigh model. This is not to say that clutter statistics are always Rayleigh or noise-like, but they should be much more so for large resolution cells and/or range ambiguous geometries than for otherwise. This is the first time scattering theory (as opposed to curve fitting) has been applied to statistics of SBR clutter variation.

Clutter spectra and their impact on moving target indication was discussed in Section 4 where it was pointed out that the dominant source of clutter spectral broadening was due to platform motion. This effect is very predictable and there are known signal processing techniques for illuminating it at least in principle. Internal clutter motion is usually smaller but harder to deal with. These are summarized in Table 7.

Finally in Section 6 the current status of our ability to model clutter was reviewed and shortcomings in the present data base were pointed out Given these areas where more data are needed, three candidate clutter measurement programs were analyzed and summarized in Table 8.

In final summary, this report contains a model for clutter as it is encountered in space-based radar systems. It is based on the best experimental data and scattering theory currently available. Many of the approaches, especially in Section 4 are unique. It is hoped that these results will be useful in analyses of detection of targets in clutter in general as a stepping-stone for other modeling efforts.

APPENDIX
SIMULATION OF RADAR SIGNALS

A.1 CLUTTER TAPE GENERATION

DSA has developed a computer model which simulates the time-dependent returns from ground clutter (in digital format) as seen from a space radar system. This process is being utilized to create a data tape used to evaluate candidate signal processing designs for RADC.

The user must specify a number of parameters and option choices. The terrain is defined by a map of the ground clutter as observed by a particular satellite configuration, also specified. The radar parameters define antenna pattern and waveform including beamwidth, pulse width, sampling time, and number of pulses. The beam is divided into a specified number of ambiguous regions. Clearly, the numerous variable parameters make it a versatile program with modeling capabilities in many areas.

The block diagram in Fig. A-1 shows basically how the model combines the parameters to get the desired signal simulation. The backscatter coefficient map will include the different terrain types in the scene along with the model's boundaries and inherent spatial correlations. This map along with the radar's antenna pattern, waveform, and target-sensor geometry are illustrated in Fig. A-2. These parameters in combination with the orbital kinematics which define the satellite's altitude, velocity, and orientation, are input to clutter integration routines to obtain a clutter range, range-rate map. This map contains signals for each ambiguous region folded into an unambiguous Doppler region. A model for the random fluctuation of the clutter is then imposed and these resultant signals are used to generate a received signal for each range strip. The signals from ambiguous range strips are combined and then convolved with a specified single-pulse waveform. Various amounts of implementation error can be added at this point for parametric analysis.

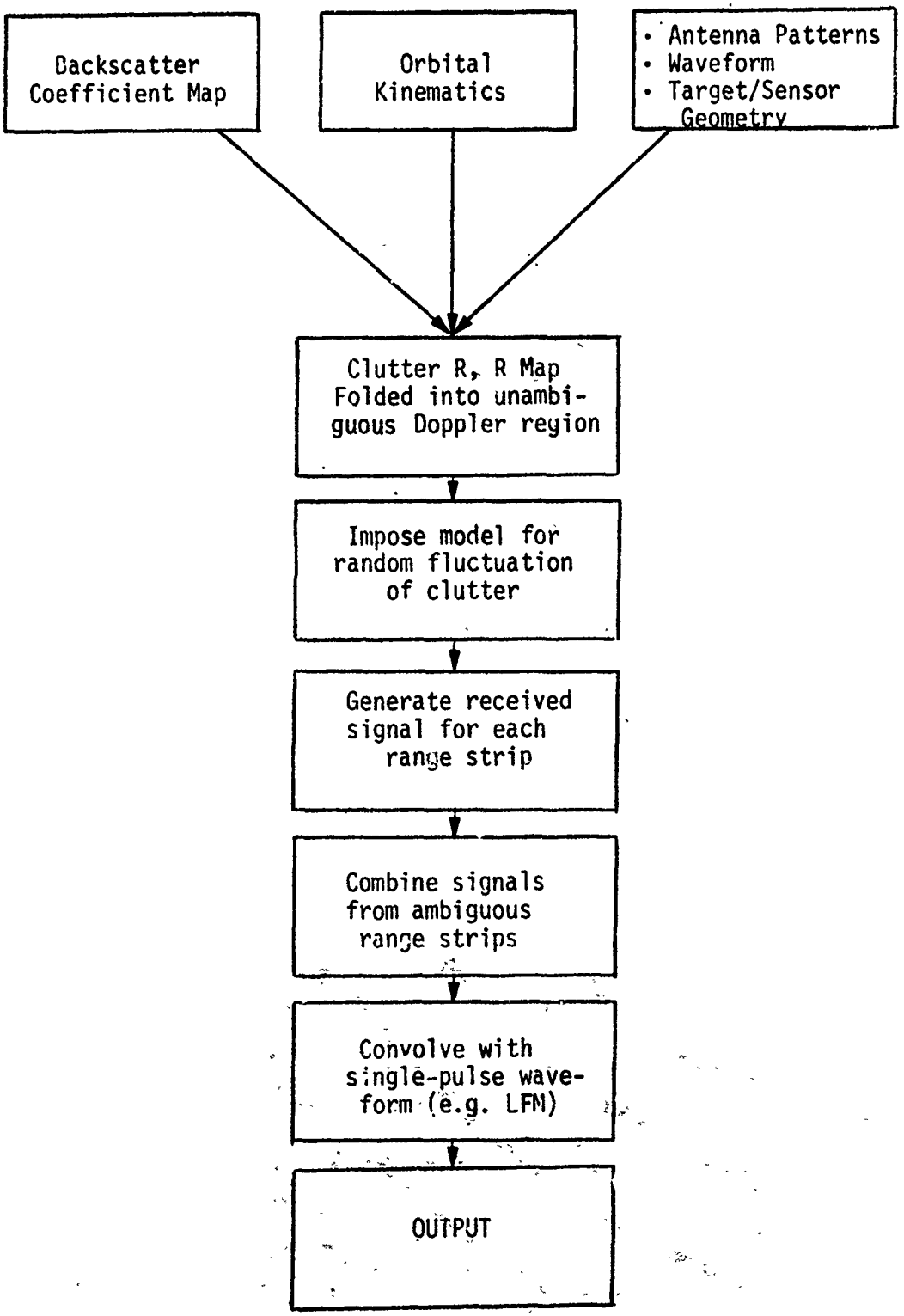

Figure A-1. Block Diagram for Simulation of Time-Dependent Returns From Ground Clutter

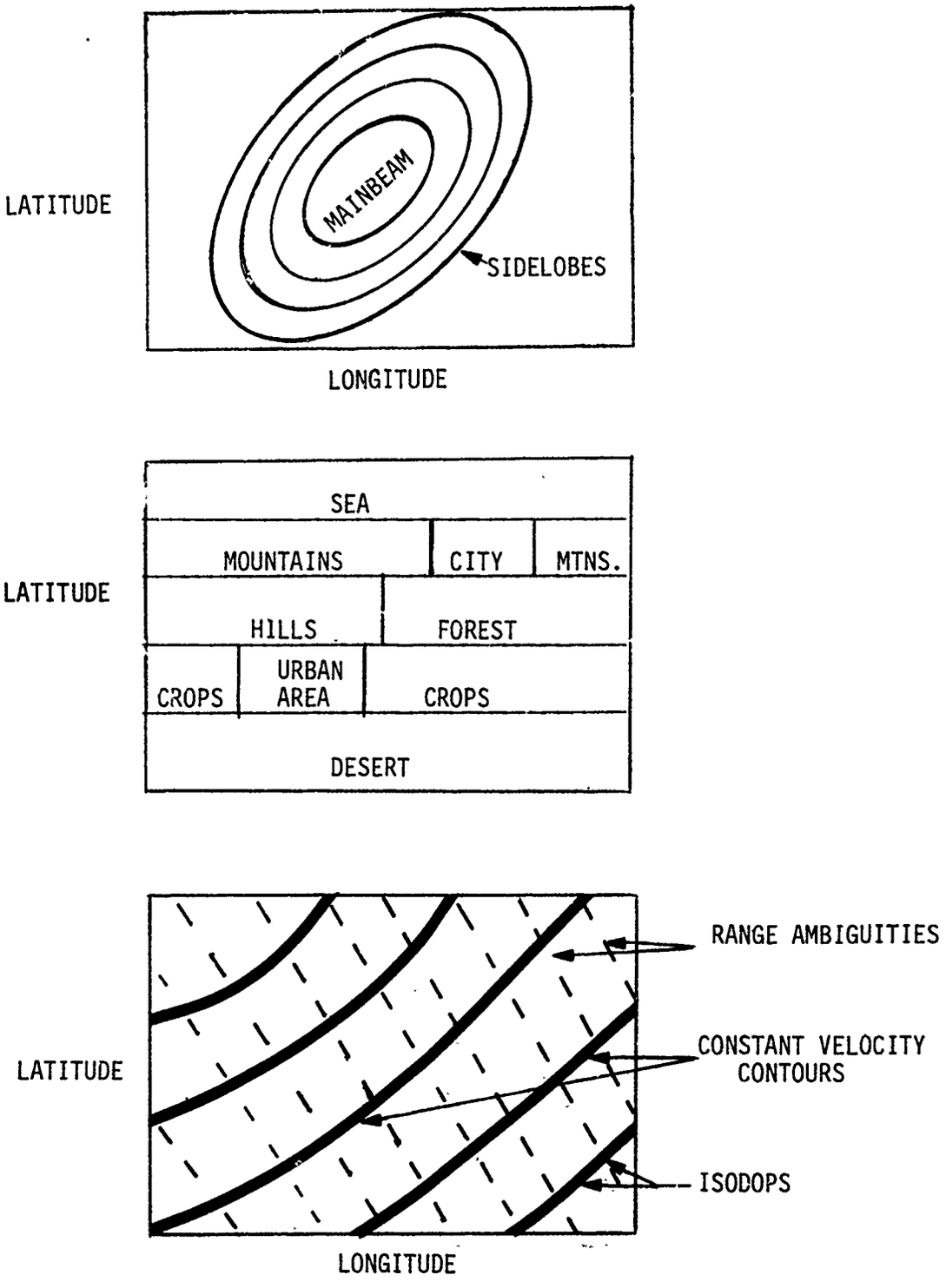

Figure A-2. Clutter Map Inputs

A.2 DOPPLER

The clutter signal as a function of time (t) is given as

$$C(t) = c_0 \int_{R,\dot{R}} A(R,\dot{R}) e^{4\pi j t\dot{R}/\lambda} \, s(t - 2R/c) dR d\dot{R} \qquad \text{(A-1)}$$

where $s(t)$ is the waveform, c_0 is a complex constant, λ is the wavelength, R is the range, c is the speed of light, $\dot{R}$ is the range rate, $j = \sqrt{-1}$, and $A(R,\dot{R})$ is the complex reflection coefficient of clutter whose expected value $E|A(R,\dot{R})|^2$ is the clutter RCS per unit range and range rate. The latter, the clutter RCS density, or "clutter map" is a subject in itself and requires careful modeling to faithfully include effects of viewing geometry and terrain type. It requires antenna patterns, platform and earth motion, and viewing angles. Equally important and least well-defined is the sigma-zero model which is also required. Essentially the radar cross-section per unit area for every point on the earth, could be handled by maps based on actual clutter data, a stochastic model based on probability distributions and spatial correlations of actual data, or a suitable combination of the two. Realistically, the last solution is probably the most suitable in most cases.

For notational simplicity we define the following quantities

$$t' = 2R/c$$

$$v' = 2\dot{R}/\lambda$$

$$W = e^{-2\pi j}$$

$$W_N = e^{-2\pi j/N}$$

Hereafter, j can be used as an index as well as $\sqrt{-1}$ since its meaning should be clear from context.

For the moment consider the waveform to be a weighted train of δ function pulses

$$s(t) = s_0 \sum_{n=0}^{N-1} w_n \delta(t - n\Delta) \qquad \text{(A-2)}$$

where s_0 is a constant, w_n is a set of complex weights and Δ is the interpulse period. The δ-function is defined such that for an arbitrary function g:

$$\int_{-\infty}^{\infty} g(t)\, \delta(t - t')dt = g(t')$$

Substituting (A-2) and (A-1) and integrating yields

$$c(t) = c_0 s_0 \sum_n \int_{-\infty}^{\infty} d\nu'\, A(t - n\Delta, \nu') W^{-t\nu'} w_n \qquad \text{(A-3)}$$

Now suppose that c(t) is sampled at discrete times $t_0 + m\Delta$ for N sample (pulses).

$$\begin{aligned} c(t_0 + m\Delta) &= c_0 s_0 \sum_n \int_{-\infty}^{\infty} d\nu'\, A(t_0 + m - n)\Delta, \nu') W^{-m\Delta\nu'} w_n \\ &= c_0 s_0 \sum_n \int_{-\infty}^{\infty} d\nu'\, A(t_0 + n\Delta, \nu) W^{-m\Delta\nu'} w_{m-n} \\ &= \sum_n c_n(t_0 = m\Delta) - (N - 1) \le n \le N - 1 \end{aligned} \qquad \text{(A-4)}$$

The procedure we use from this point on is:

1. Generate $\sigma(R,R)$, based on a microscopic description of a clutter scene, i.e., you specify $\sigma(X,Y)$ or σ(latitude, longitude) and use the viewing geometry to transform it into $\sigma(R,\dot{R})$.
2. Apply random deviations about the mean to obtain $\sigma'(R,\dot{R})$ where the expected value is $\sigma(R,\dot{R})$. Form $A(R,\dot{R})$ is such that the phase is random and σ' - A*A.
3. By inverse FFT obtain Cn(t) for a large number of pulses. [A pulse is a sample of the discrete series Cn(ti).] Truncate to an N pulse burst.

4. Use Eq. A-4 to form $C(t_0 + m\Delta)$.

We repeat for a large number of range R values and convolve with the single-pulse waveform as described below.

A.3 PULSE COMPRESSION WAVEFORM

This procedure so far is valid only for δ-function waveforms such as Eq. A-2. In general the waveform will be a train of identical pulses of finite length. This is given by

$$s(t) = \int_{-\infty}^{\infty} dt'' \; s_0(t'') \; T(t - t'')$$

where $T(t)$ is a train of δ-function as in Eq. A-3 and $s_0(t)$ is the envelope of the individual pulses.

Equation A-3 now becomes

$$c(t) = c_0 s_0 \int d\nu' \int dt' \; A(t', \nu') w^{-t\nu'} \int dt'' \sum_n \delta(t - t' - t'' - n\Delta) \; X \; w_n s_0(t'')$$

$$= c_0 s_0 \sum_n \int d\nu' \int dt'' \; A(t - t'' - n\Delta, \nu') w^{-t\nu'} w_n s_0(t'')$$

$$= \int c^1(t - t'') s_0(t'') dt'' \text{ where } c^1(t) \text{ is now given by Eq. A-3.}$$

Since the process of convolving a long sequence

$$c^1(t^o + m\Delta)\ t_{min} \le t^o \le t_{max}, m = 0, \ldots, N - 1$$

with a short one such as $s_0(t)$ (the individual pulse length is certainly less than Δ and probably much shorter) is straightforward, it seems appropriate to first compute $c^1(t)$ and then convolve it with $s_0(t)$ by means similar to the FFT convolution algorithm.

A.4 RANGE-WALK

The effect of range walk is a phenomenon which occurs in a high-resolution radar on a fast moving platform. We restrict this discussion to targets whose inherent velocities are small enough so as not to allow additional range-walk in relation to the ground.

The general expression for the clutter reflected from Earth and received by the radar is given in Eq. A-1.

The effect of range-walk is that R itself is a function of $\dot{R}$ and t. In fact the round trip delay t_o equals

$$\begin{aligned} t_o &= 2R\ t/c \\ &\approx 2\dot{R}_o t/c \end{aligned}$$

where R_o is the range rate of targets and clutter in the center of the mainbeam. The approximation obviously does not hold for all clutter, however we are primarily interested in objects in the mainbeam only.

Note that the integral over R is an inverse Fourier transform. Therefore, define for a uniformly spacial (PRI = Δ) train of pulses

$$A'(R,k) = \int d\dot{R}\, A(R,\dot{R})\ e^{4\pi j \dot{R} t_k/\lambda} \qquad \text{(A-5)}$$

where $0 \leq k \leq N - 1$, $t_k = k\Delta$ and N is the number of pulses. For purposes of this discussion we ignore such effects as range foldover as they are not relevant to this discussion.

Now consider the return from the Kth pulse. We make the additional approximation that the range-walk during one pulse repetition interval (PRI) is much less than the range resolution.

$$\dot{R}_o \Delta << \delta R \quad \text{and let } t = t + k\Delta$$

$$C_k(t') = \int dR\, A'(R,k) S_o(t' - \dot{R}_o k\Delta - 2R/c) \tag{A-6}$$

From here on we define $A'_k(R) \equiv A'(R,k)$.

Now, the fact is that the processor is digital and the subpulse waveform is sampled at discrete times. The effect is that corresponding time samples for different pulses (different k) pertain to different clutter.

$$C_k(t') = \int dR\, A'(R + \dot{R}_o k\Delta, k) S_o(t' - 2R/c) \tag{A-7}$$

In the simulation, the above convolution is performed discretely. Define $t'' = 2R/C$.

$$C_k(t'_n) = \delta t'' \sum_m A'_k(t''_m + t^o_k) S_o(t'_n - t''_m) \tag{A-8}$$

where $t^o_k = 2\dot{R}_o k\Delta/c$.

Now the problem is that, in generating $A(R,\dot{R})$, it is not practical to divide the range axis into a grid much finer than the range resolution. The fact that the change in t^o_k from one pulse to the next $(2\dot{R}_o\Delta/c)$ is much smaller than $\delta t'' = 2\delta R/c$ where δR is the range resolution. Therefore, we resort to an interpolation.

The interpolation can be difficult because A' is complex and can vary greatly from one sample to the next. After considering the alternatives available for interpolation, it was decided to base it on the Fourier components of the discrete sample. This is especially attractive since the convolution is to be performed by the convolution theorem so the Fourier components are required anyway. Let

$$a_k(f_\ell) = \sum_i A'_k(t_i)\, e^{-2\pi j f_\ell t_i} \tag{A-9}$$

Then the interpolation gives

$$A'_k(t_i + t_k^o) = \frac{1}{N} \sum_\ell a_k(f_\ell)\, e^{2\pi j f_\ell (t_i + t_k^o)} \tag{A-10}$$

Note that when t_k^o equals an integral number of sampling periods, this interpolation results in a time shift of the original sequence, as it should.

The result of the convolution is

$$C_k(t_i) = \frac{1}{L} \sum_{\ell=1} \left[a_k(f_\ell) e^{2\pi j f_\ell t_k^o} \right] S(f_\ell) \tag{A-11}$$

where $S(f_\ell) = \sum_i S(t_i)\, e^{-2\pi j f_\ell t_i}$.

The net procedure is that the $A_k(f_\ell)$ are multipled by $e^{2\pi j f_\ell t_k^o}$ at the time of the replica multiply before the final inverse Fourier transform.

As we have said this memo addresses only a procedure for range-walk simulation, not compensation. Obviously the perfect way to compensate for range walk in this simulated signal is to reverse the process. This amounts to the following

$$A_k(t_i) = \frac{1}{L} \sum_{\ell}^{\infty} \left[C_k(f_\ell)\, e^{-2\pi j f_\ell t_k} \right] S(f_\ell)\, e^{+2\pi j f_\ell t_i} \qquad \text{(A-12)}$$

where $C_k(f_\ell) = \sum_i C_k(t_i)\, e^{-2\pi j f_\ell t_i}$

This again amounts to interpolating the $A_k(t)$ so that the same targets and clutter appear in the same range samples for every pulse.

MISSION
of
Rome Air Development Center

RADC plans and executes research, development, test and selected acquisition programs in support of Command, Control Communications and Intelligence (C^3I) activities. Technical and engineering support within areas of technical competence is provided to ESD Program Offices (POs) and other ESD elements. The principal technical mission areas are communications, electromagnetic guidance and control, surveillance of ground and aerospace objects, intelligence data collection and handling, information system technology, ionospheric propagation, solid state sciences, microwave physics and electronic reliability, maintainability and compatibility.